The Design of A Compact Integral Medium Size PWR: The CIRIS

by

Koroush Shirvan

Submitted to the Department of Nuclear Science and Engineering in Partial Fulfillment of the Requirements for the Degree of

Master of Science in Nuclear Science and Engineering

at the
Massachusetts Institute of Technology
June 2010

Signature of Author: _____
Department of Nuclear Science and Engineering
April 6, 2010

Certified By: _____
Mujid S. Kazimi, Ph.D.
TEPCO Professor of Nuclear Engineering
Thesis Supervisor

Certified By: _____
Pavel Hejzlar, Sc.D.
Thesis Reader

Accepted By: _____
Jacquelyn C. Yanch, Ph.D.
Chair, Committee on Graduate Students

The Design of A Compact Integral Medium Size PWR: The CIRIS

By
Koroush Shirvan

Submitted to the Department of Nuclear Science and Engineering on January 15, 2010, in partial fulfillment of the requirements for the Degrees of Master of Science in
Nuclear Science and Engineering

Abstract

The International Reactor Innovative and Secure (IRIS) is an advanced medium size, modular integral light water reactor design, rated currently at 1000 MWt. IRIS design has been under development by over 20 organizations from nine countries, led by Westinghouse. IRIS has a standard Westinghouse PWR core, but is an integral reactor, which means the reactor vessel contains all pumps, steam generators, pressurizer and control rod drive mechanisms. This work assesses possible improvements of the plant economics by the allowable power in the IRIS vessel, while maintaining the same or better safety limits, through increasing the power density in the core and heat exchangers.

IRIS was designed with 8 Once-Through Helically coiled Steam Generators (OTHSG), located in an annulus near the vessel in the region above the core. The unit size dictates the vessel diameter, or limits the core size for fixed vessel diameter, and thus the reactor power rating. The Printed Circuit Heat Exchangers (PCHE) of HEATRIC^{TM} are compact heat exchangers that can provide high power density along with low pressure drop. They are proposed here as replacement for the OTHSG. The PCHEs experience is mostly for single phase heat transfer. A model is developed for the two phase fluid heat transfer in the small horizontal PCHE flow channels. The PCHE performance under IRIS conditions was modeled by a one dimensional nodal code. For the same power output, the PCHEs are found to safely reduce the IRIS vessel diameter by as much as 1.5 m and reduce the pressure drop in the SG by 30 %.

The Internally and eXternally cooled Annular Fuel (IXAF) had been investigated as part of MIT's Advanced Fuel Project. It was found to maintain the current operating MDNBR margin under steady state IRIS conditions at 150% of nominal power density when the flow rate can be proportionally increased. The MDNBR in the inner channels was sensitive to flow changing flow conditions. A complete RELAP5 model of the IRIS reactor, along with PCHE and IXAF design representation, was developed. The PCHE RELAP model was first benchmarked against the stand-alone code and their agreement was demonstrated successfully. The short and long term responses of IRIS with PCHE and IXAF were analyzed for a Loss Of Flow Accident (LOFA) and a Loss Of FeedWater Accident (LOFWA). Under LOFA the MDNBR margins were found to be acceptable with added inertia to current IRIS pumps configuration.

Therefore, the pressure vessel size can be reduced by implementing the PCHE instead of the OTHSG, and IXAF instead of solid fuel rods in addition to increasing the power rating of the reactor by 50% for the same vessel size. The results indicate that a large potential exist to reduce the cost per kilowatt and increase the attractiveness of the IRIS reactor design.

Thesis Supervisor: Mujid S. Kazimi
Title: TEPCO Professor of Nuclear Engineering and
Professor of Mechanical Engineering

Acknowledgements

I would like to thank Prof. Mujid Kazimi for providing me with the opportunity to work with him, Dr. Pavel Hejzlar for his continuous support and help throughout my thesis, the MASDAR Institute and Prof. Shatilla for providing the funding for the project and Bo Feng for providing me with many files on previous work on Annular Fuel.

Also, I want to thank all my family for all their support and encouragement and especially my uncle, Prof. Samim Anghaie for providing me the passion for nuclear energy as well as life to succeed.

Table of Contents

List of Figures

List of Tables

Chapter 1 Introduction

1.1 Motivation

Over the remainder of this century, the need for viable clean sources of energy will be getting more important, as billions of tones of carbon based fuel is being burned, contributing to global warming through green house gas emission and depleting valuable resources for future chemical industry. Nuclear power can be one of the options for emission-free large scale electricity production in the US and other countries. However, in order for nuclear power to be viable, it has to be competitive with other options. Currently in the US, the nuclear power electricity production cost is very competitive with other means of production, such as coal and natural gas power plants. The main reason for this is that the capital cost of the nuclear plants has been already paid and the operating costs are dominated by the O&M and the fuel cycle costs. According to many sources including MIT's "The Future of Nuclear Power" study [Deutch et al., 2009], the capital cost of the nuclear power plants is large and somewhat uncertain compared to coal and natural gas plants. The higher cost along with the uncertainty poses a risk for electric utilities in the US and across the world which has to be considered against the uncertain cost of carbon emissions in the future.

The Small-to-Medium size Reactors (SMRs) have been a hot topic in the nuclear industry in this decade. SMRs can be a more attractive option for developing nations with low electricity demand and grid-size. They can also be used in non-electricity areas such as desalinization and hydrogen production. What defines an SMR size can be debated; typically from 50-600 MWe reactors are considered SMRs. The goals of SMR plants are to have simplified designs that demonstrate safety and show their ability to be economically modularized. Currently, there are

many designs of SMRs being developed by many countries, as referenced in the IAEA 2005 SMRs report:

- Integral type pressurized water reactors targeted for near term deployment: SMART (the Republic of Korea), IRIS (the International Consortium, led by Westinghouse, USA), CAREM (Argentina), mPower (B&W) and SCOR (AREVA-CEA, France);

- Small pressurized water reactors without on-site refueling from Russia: SAKHA-92, ABV-3, ABV-6, KLT-40S (with lifetime core), VBER, RIT (all from OKBM), RUTA-70, UNITHERM, NIKA-70 (from RDIPE), in particular, designed for floating NPPs;

- Direct conversion small light water reactor without on-site refueling ELENA (RRC "Kurchatov Institute", Russia);

- Light water cooled heavy water moderated pressure tube reactor AHWR (BARC, India);

- Light water reactors using coated particle or pebble bed type fuel: PFPWR50 (University of Hokkaido, Japan), VKR-MT (VNIIAM-RRC "Kurchatov Institute", Russia), FBNR (Federal University of Rio Grande Do Sul, Brazil);

- Innovative high temperature gas cooled reactors: PBMR-400 (ESCOM, South Africa), HTR-PM (INET, China), HTR-F/VHTR (AREVA-CEA, France), GT-MHR (GA, USA);

- Lead-bismuth cooled small reactor without on-site refueling SVBR-75/100, targeted for near-term deployment (IPPE and EDO "Gidropress", Russia);

- Innovative lead or lead-bismuth cooled small reactors without on-site refueling: STAR-LM, STAR-H2, SSTAR ("STAR family", ANL, USA), SPINNOR and VSPINNOR (ITB, Indonesia);

- Lead-bismuth cooled compact high temperature reactor CHTR, with HTGR type fuel (BARC, India);

- Molten salt cooled small reactor with pebble-bed fuel MARS (RRC "Kurchatov Institute", Russia);

- CANDLE burn-up concept for small high temperature gas cooled reactors and for small reactors with fast neutron spectrum (RLNR TITech, Japan), Traveling Wave Reactor (Terra Power, US).

In order to find a design that can be used for near term deployment, one must eliminate non-LWR technology as it is still far from realization. Under the LWR category, the first designs considered will be the designs that employ solid cylindrical rods and UO_2 fuel as it is being used across the world and carries the most experience base. This leaves the concepts listed under the first two bullets above as the remaining choices. Since the Russian designs are of typical LWR designs, the amount of improvement is most likely not significant, therefore the concepts under the first bullet remain to be reviewed in more detail.

Table 1-1 shows the detailed description of each design in the first bullet.

Table 1-1 Comparison of current Integral Pressurized LWR designs

General Information						Units
Design Name	IRIS	CAREM	SMART	mPower	SCOR	
Thermal Power	1000	100	330	400	2000	MW
Electrical Power	335	27	100	125	600	MW
Vessel Height	21.3	--	9.8	22	14.67	m
Vessel Outer Diameter	6.21	--	3.96	3.6	5.265	m
Core Information						
Number of Assemblies	89	61	57	69	157	
Assembly Type	17x17	Hex 117	17x17	17x17	17x17	
Assembly Height	4.27	1.4	2	2	3.66	m
Fuel Type	UO2	UO2	UO2	UO2	UO2	
Enrichment	4.95	3.4	Low	<5	--	% U^{235}
Moderator	Water	Water	Water	Water	Water	
Clad	Zirc	Zirc	Zirc	Zirc	Zirc	
Control Rod Material	Ag-In-Cd	Ag-In-Cd	Ag-In-Cd	--	Ag-In-Cd	
Boron	Yes	No	No	--	No	
Core Power Density	51.26	--	62.6	--	75.3	kW/cc
Linear Power	10	10.84	11	11	13.2	kW/m
Reactor Cooling System						
Cooling Mode	Forced	Natural	Forced	Forced	Forced	
Mass Flow Rate	4700	410	1560	--	10465	kg/sec
Operating Pressure	15.5	12.25	15	<14	8.8	MPa
Core Inlet Temperature	292	284	270	--	246.4	C
Core Outlet Temperature	330	326	310	327	285.9	C
Steam Generator						
Configuration	Inside	Inside	Inside	Inside	Outside	
Number of units	8	12	12	12-16	1	
Type	OTHSG	OTHSG	OTHSG	OTHSG	U-Tube	
Rated Power	125	8.4	27.5	--	2000	MW
Secondary Inlet Temperature	224	200	180	--	--	C
Secondary Outlet Temperature	317	290	274	--	237.4	C
Secondary Pressure	6	4.7	5.2	<7	3.2	MPa
PUMP						
Configuration	Inside	NA	Outside	Inside	Inside	
Type	Spool	NA	Glandless canned	--	Coil-type	

Number	8	NA	4	12-16	16	

As seen from Table 1-1, there are many options with integral pressurized water reactors. The hexagonal arrangement of the CAREM reactor makes it less attractive design in terms of licensing in the US. According to a Westinghouse study, the smallest rating of the module to achieve attractive economy is in the neighborhood of 300MWe [Carelli et al., 2009]. Thus, the IRIS is expected to be economically more attractive than the much lower rated SMART and mPower reactors. The SCOR reactor has the steam generator located outside, therefore it is not an integral reactor and the vessel is already very compact. Consequently, the IRIS reactor design is chosen for this project as the most viable option to pursue for near term development. The goal of this analysis is to increase the power density of the IRIS reactor to make it more economically competitive with large traditional reactors such as AP1000 and ABWR as well as the above listed SMR reactor designs.

1.2 IRIS Reactor Design

The IRIS is a medium size, modular light water reactor, rated currently at 1000 MWt. IRIS design has been under development by over 20 organizations from nine countries, led by Westinghouse. IRIS has a standard Westinghouse PWR core, which makes it one of the leading design candidates for medium size reactors. It is an integral reactor, which means the reactor vessel contains all pumps, steam generators, pressurizer and control rod drive mechanisms as seen in Figure 1-1 [Cinotti et al., 2002]. The design is an expansion of 40 years of operating PWR experience and already existing use of passive safety features established by Westinghouse in the NRC certified AP600 plant design.

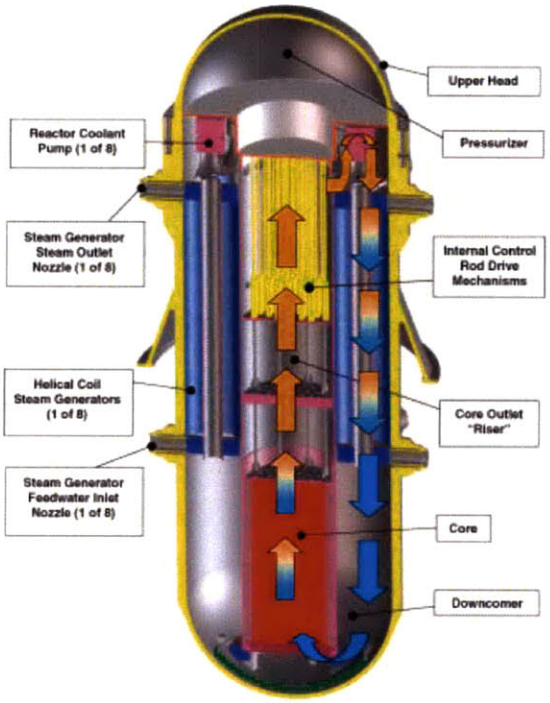

Figure 1-1 IRIS reactor pressure vessel layout (from Cinotti et al., 2002)

The IRIS was designed with 8 Once-Through Helically coiled Steam Generators (OTHSG), located above the core. These OTHSGs are of the family of shell and tube heat exchangers composed of an annulus, where the high pressure fluid flows, and helically coiled tube bundle, in which the lower pressure fluid flows. This geometry can handle thermal expansion and vibration effects which sufficiently lower the probability of steam generator rupture. However, since these steam generators are in the reactor vessel, their size dictates vessel diameter, or limits the core size for fixed vessel diameter, and thus reactor power rating [Cinotti et al., 2002].

The integral design of IRIS reactor uses "safety by design" approach, which means "design the plant in such a way that eliminates accidents from occurring, rather than coping with

their consequences". Furthermore, the design reduces the consequences and/or probability of occurrance of the accidents which could not be eliminated. One of the significant safety features of IRIS compared to a nominal PWR is that safety assessment can ignore the large Loss Of Coolant Accidents (LOCAs), since no large primary coolant loop piping or penetrations exist outside the vessel. The "safety by design" reduces the complexity of the IRIS passive safety systems. Also, the passive safety systems allow for plant simplification, reliability and safety. Such simplifications, along with the elimination of welds for the large pipings, are expected to reduce the construction time.

1.3 PCHE

Public information on the Heatric^{TM} Printed Circuit Heat Exchanger (PCHE) design and performance has been increasing gradually over recent years, due to a rise of interest in the compact design of the PCHEs. For example, University of New Mexico, Kansas state University and MIT along with INL, ANL, KAERI, TITECH have published theses/papers on the subject of using PCHE in nuclear application. The PCHEs are a type of compact heat exchangers that provide high power density along with low pressure drop and maintenance requirements. PCHEs are composed of rectangular plates, diffusion bonded together with semi circular channels, as seen in Figure 1-2. The diffusion bonds in PCHE have proven to be able to withstand pressures much higher than those in nuclear power reactors [Southall, 2009]. The diffusion bonds have also been extensively tested and shown to possess the same strength as the parent material. PCHE channels could be straight or zigzag (Figure 1-2), where the zigzag geometry has the benefit of greater compactness than the straight channel design. The PCHEs are

also proven technology in the oil and gas industries and chemical reactors [Heatric, 2008]. However, no recorded experiment with boiling water through PCHE was found.

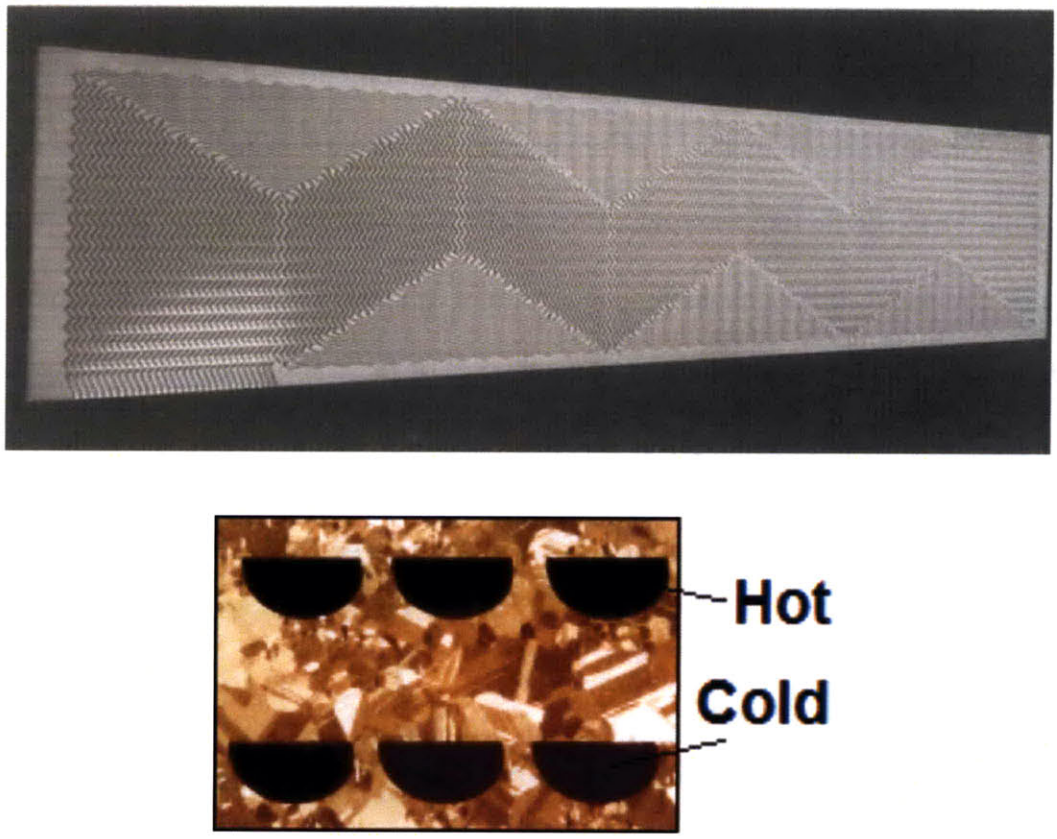

Figure 1-2 A crossection of PCHE from the side and the top view (from Heatric,2008)

Out of all the mentioned list of institutes involved with PCHE only one, ANL, has performed an experiment that has water as a secondary coolant. The rest involve gaseous CO_2 - CO_2 loops. One of the main goals of this work is to analyze the effectiveness of the PCHE performance for water to water heat transfer conditions, whereby the secondary water boils and exits as superheated vapor.

1.4 Annular Fuel

The Internally and eXternally cooled Annular Fuel (IXAF) has been analyzed extensively as part of MIT's Annular Fuel Project. The study has demonstrated that the power density in the core can be up rated by 50% above typical Westinghouse PWR cores. The study has shown that the thermal margins for IXAF are maintained or improved with the 50% up rate, if the flow is also increased by partial blockage of the inner annular region of the fuel rods has also been shown acceptable the MDNBR limits. In terms of neutronic margins, the IXAF has shown reasonable performance compared to typical Westinghouse PWR fuel rods for conditions of a typical four loop plant design [Zhiwen et al, 2007]. The economics of fabrication of annular fuel pellets has also been evaluated by Westinghouse. It was found that only the inner zirconium cladding adds a cost of 0.000002 $/kWhr(e) to 0.005 $/kWhr(e) [Lahoda et al., 2007].

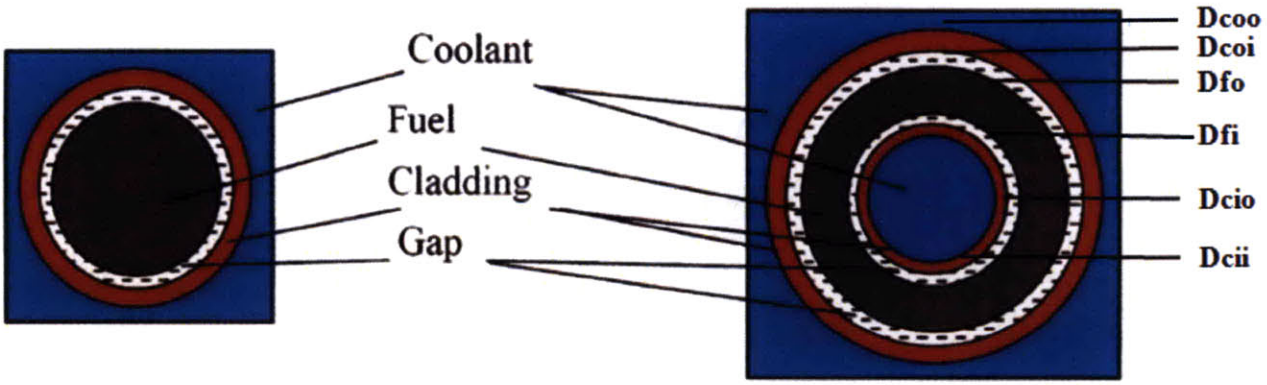

Figure 1-3 Solid and internally and externally cooled annular fuel (from Kazimi et al., 2006)

The MIT study showed there is an incentive for using 13 x 13 annular fuel assembly instead of other combinations in terms of neutronic, thermal hydraulic and economic performance. The 13x13 assembly has 8 guide tubes compared to 24 for a traditional 17 x 17 Westinghouse fuel. The number of control rods in each assembly is also reduced as seen below.

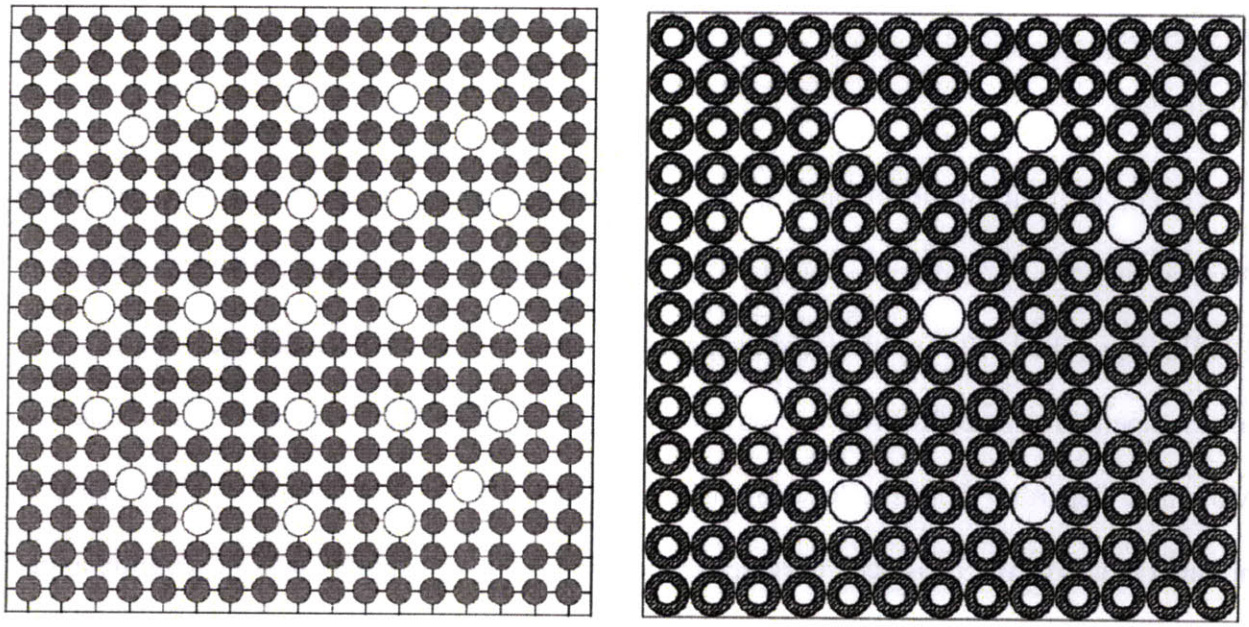

Figure 1-4 Comparison between the 13x13 annular fuel assembly (right) and the reference 17X17 solid fuel assembly (left) (from Kazimi et al., 2006)

1.5 Computational Tools

The main focus of the analysis of IRIS in this work is on thermal hydraulic performance, due to the fact that changing the steam generator has no effect on core neutronics, and the neutronic performance of annular fuel has already been evaluated. The IRIS core is similar to a nominal PWR, so it is assumed that for IRIS the reactivity feedback coefficients, such as moderator temperature and doppler coefficient, and shutdown margin reactivity values for control rods are applicable.

Previously, for PCHE thermal hydraulic analysis, a one-dimensional nodal code that uses various correlations was developed for MIT'S GFR, and benchmarked with TITECH experiments on CO_2 - CO_2 loop [Hejzlar et al, 2006]. The same code is expanded to the use liquids and gas and two phase flows of components available in REFPROP software. The code

is used here to calculate the volume required by the PCHE for given thermal hydraulic parameters.

For analysis of IRIS under steady state and transient conditions, with PCHE and/or Annular fuel, the state-of-art code RELAP5-3D [RELAP5, 2001] coupled to VIPRE-01[Stewart, 1989] is used. RELAP is used to find the general core parameters such as the operating pressure, inlet temperature, mass flow rate and power during a transient. Then VIPRE is used to calculate Minimum Departure from Nucleate Boiling Ratio (MDNBR) during the transient. A RELAP nominal model of IRIS has been developed, however, the input is proprietary. Therefore, a total model of the IRIS reactor along with its main safety systems was developed first, then modified in order to accurately assess the consequences of using PCHE and Annular Fuel for the reactor design.

Since one of the goals of the project is to reduce the vessel diameter, the shielding of the IRIS reactor at a reduced diameter needs to be analyzed. MCNP5 [MCNP5, 2003] was used to assess the dose outside the reactor vessel, taking into account both neutrons and photons. An economic analysis of the fuel cycle cost of the new design was also performed with the aid of CASMO-4 [Edenius et al., 1995] and TK-Solver programs[TK Solver, 2003].

In summary, Chapter 2 will look at the overall OTHSG model developed to be compared to Chapter 3 content on the PCHE model. The Chapter 3, a PCHE model is described and a more detailed analysis and comparison to the OTHSG as given, as there were no publications found with regard to boiling in the PCHE. Chapter 4 will analyze the impact of using the PCHE steam generators and the IXAF core on safety by modeling the IRIS reactor in RELAP. Specifically, the consequences of these changes is shown under loss of flow and loss of feed

water accidents, in addition to showing the long term decay removal capabilities after each accident. Chapter 5 focuses on detailed MDNBR calculation of the IRIS reactor under steady state and transients and shows the MDNBR implication of using PCHE steam generators and IXAF core. Also, it describes the increase of the power from 1000 MWth to 1500 MWth and its MDNBR consequences. Chapter 6 uses the information from all the previous chapters and shows how the new IRIS reactor (the CIRIS) with 50% more power can be successfully and economically designed. Chapter 7 describes the main conclusions and provides recommendations of CIRIS for future work that can be implemented to improve the analysis.

Chapter 2 OTHSG Analysis

2.1 Helical System Generator Model

The current OTHSG in the IRIS design has the primary fluid flowing downward in an annular ring, while the secondary fluid flows upward in multiple helical tubes. OTHSG has been modeled by one dimensional steady state FORTRAN/TK-Solver code. The code modeled an average helically coiled tube and multiplied the appropriate results by the number of tubes.

To estimate the heat transfer coefficient for the primary fluid, the Dittus-Boelter correlation was used:

$$Nu = 0.023\, Re^{0.8}\, Pr^{0.4} \quad and \tag{2.1}$$

$$Nu = h\, D/k, \tag{2.2}$$

where Nu is the Nusselt number, Re is the Reynolds number, Pr is the Prandtl number, D is the tube diameter, k is the thermal conductivity of the fluid.

The hydraulic diameter for the primary side was calculated by estimating from geometric considerations the average flow area seen by each tube. This was done first by estimating the number of rows of helical tube around the annular region of the OTHSG as shown in Figure 2-1. Then the total area occupied by the helical rows is subtracted from the area between the first helical tube and the outside diameter of the SG and then divided by the number of rows to obtain the primary coolant flow average area per helical tube. It is noted that such approximation is only valid for OTHSG such as in IRIS where the tubes are more horizontal than vertical. Therefore, the minimum and maximum diameters that encompass all helical rows are inputs to the code.

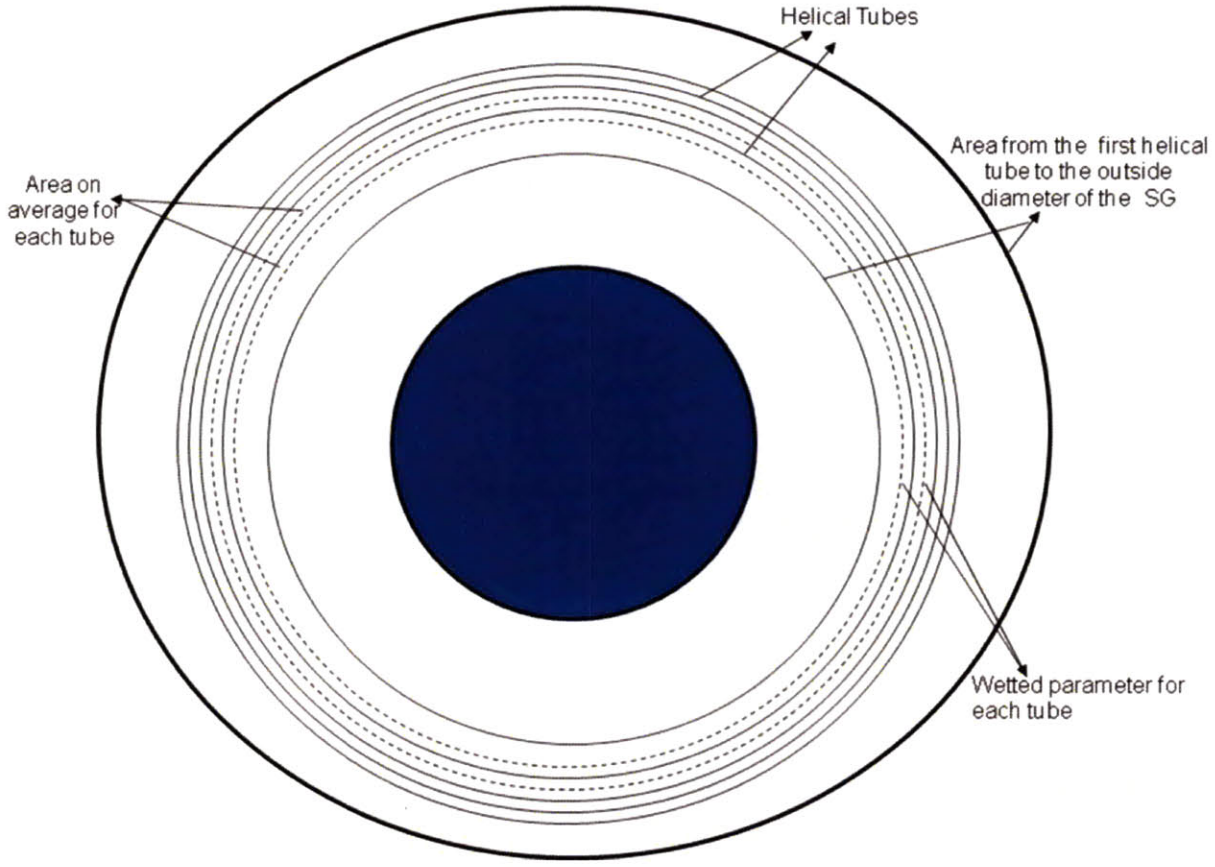

Figure 2-1 OTHSG view from above

Gnielinski's correlation for fully developed turbulent flow in helical tubes, which includes centrifugal effects of the flow in a helical geometry, was considered for the single phase heat transfer coefficient of the secondary side [Gnielinski, 1986]. The Nakayama correlation [Bayless, 1979] for heat transfer also gave very close results compared to the Gnielinski correlation. At the end, it was decided to go with the White correlation and Seban–McLaughlin correlation [Zhao et al, 2003] for single phase pressure drop and heat transfer which also gave close answers to the two correlations above. This correlation was experimentally verified for diameters around the same size and length to width ratio as those of the steam generator of IRIS.

$$fc = 0.08\ Re^{-1/4} + 0.012\ (d_o/D_i)^{1/2}, \qquad (2.3)$$

$$Nu = 0.023\ Re^{0.8}\ Pr^{0.4}\ [Re\ (d_o/D_i)^2]^{0.05}\ \ (6000 < Re < 65{,}600), \qquad (2.4)$$

where fc is the friction factor, d_o is the diameter of tube and D_i is the diameter of the helix as illustrated in Figure 2-2.

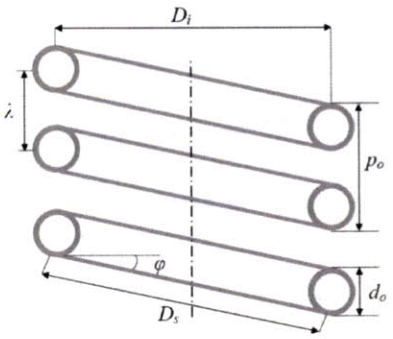

Figure 2-2 Helical Coil Tube

For the two phase region, the straight channel correlation of Chen was used due to negligible effects of the centrifugal force in two-phase flow [Bayless, 1979]. The chen correlation uses a combined boiling and flow heat transfer. For boiling:

$$\alpha_{nb} = \frac{0.00122\,\Delta T_{sat}^{.24}\,\Delta P_{sat}^{.75}\,cp_l^{.45}\,\rho_l^{.49}\,k_l^{.79}}{\sigma^{.5}\,h_{lg}^{.24}\,v_l^{.29}\,\rho_g^{.24}}\ , \qquad (2.5)$$

where α_{nb} is the nucleate boiling heat transfer coefficient, ΔT_{sat} is the difference in wall temperature and saturation temperature, ΔP_{sat} is the difference in pressure at the wall surface and saturation, cp_l is the liquid specific heat, ρ is the density, k_l is the liquid thermal conductivity, σ is the surface tension, h_{lg} is the enthalpy of vaporization, and v_l is the liquid viscosity. The Martinelli parameter is also used:

$$\chi = (\frac{\rho_g}{\rho_l})^{.5} (\frac{\nu_l}{\nu_g})^{.1} (\frac{1-x}{x})^{.27} \quad , \qquad (2.6)$$

where x is the flow quality and ν is the kinematic viscosity. The effective heat transfer coefficient for two phase flow is given by:

$$h = F\, h_l + S\, \alpha_{nb} \qquad (2.7)$$

where h_l is the convection heat transfer calculated based on the flow of the liquid portion in the tube, F and S are defined as:

$$F = 2.35[\frac{1}{\chi} + .213]^{.736} \text{ and} \qquad (2.8)$$

$$S = \frac{1}{1 + 2.53e-6\,\mathrm{Re}_s^{1.17}} \quad , \qquad (2.9)$$

where Re_s is defined as:

$$\mathrm{Re}_s = \mathrm{Re}_l\, F^{1.25} \quad . \qquad (2.10)$$

Additionally, the subcooled region uses the Bergles and Rohsenow equation [Bergles .et al., 1964] to calculate the required wall superheated to have subcooled nucleate boiling as a heat transfer mechanism. Also, the Wong Critical Heat Flux (CHF) correlation [Wong et al., 1990] for horizontal tubes was used to assess the quality at which CHF takes place. This is a conservative assumption as the critical heat flux in helical tubes is greater than that of horizontal tube. Therefore, once the CHF is reached the post-CHF, Groeneveld correlation [Todreas et al., 1990] was used. A listing of the equations of these correlations is given in Appendix D.

For the primary pressure drop, the friction factor of McAdams was used:

$$f = 0.184\ Re^{-.25}, \qquad (2.11)$$

where f is the friction factor and Re is defined for the annulus region. The pressure drop correlations chosen for the secondary side were validated by experimental results from SIET thermo-hydraulics labs in Italy. For Headers and orifices, loss coefficient of 0.2 was used, which is based on experimental results [Santini .et. al., 2008].

The OTHSG model assumes that there is no transfer of heat to the outside of the SG (e.g. zero heat loss). It also assumes that all the helical tubes are identical with the same total mass flow rate and helix diameter. The OTHSG code requires the inlet secondary mass flow rate to one tube, the pressure and temperature for both the hot and cold sides in order to proceed into the calculations. The code first guesses the total length of the OTHSG tube, and then it will divide the length into 80 nodes. Starting with the node at the inlet of the primary side (or outlet of the secondary side), the code calculates the heat transfer coefficient and pressure drop in each node and estimates new length for the individual nodes. The lengths of the nodes are summed up and used to calculate the total transferred power within the OTHSG. This value is compared to the target power value, if it is not within 0.1%, then a new total length is estimated by scaling the previous guess by the ratio of estimated power to desired power. The code also requires the helix pitch and average helical diameter and SG overall desired height for the pressure drop calculations. The input of the loss coefficients for headers is also allowed if it is necessary.

When calculating the parameters for the secondary side, due to the existence of two phase flow, the wall temperature is also used as an iteration parameter. The wall temperature is first

guessed and is used as an input to the Chen correlation, which is used to calculate the heat flux. The heat flux is used to recalculate the wall temperature, which is used again to calculate the heat transfer coefficient, until a numerically stable solution has been reached.

Table 2-1 Sample OTHSG code input

Inputs	Description
125000	power (kW)
15500	pressure - hot fluid - hot end (kPa)
5810	pressure - cold fluid - cold end (kPa)
328.4	temperature - hot fluid - hot end (o C)
223.9	temperature - cold fluid - cold end (o C)
589	mass flow rate on hot side (kg/s)
62.5	mass flow rate on cold side (kg/s)
0.61	hot inner channel diameter (m)
1.62	hot outer channel diameter (m)
0.01324	cold inner channel diameter (m)
0.01746	cold outer channel diameter (m)
1	helix diameter (m)
0.8	helix pitch (m)
0.3	min distance from the first helix to the inner annulus (m)
7.9	HX height (m)
655	number of tubes
0.1	hot header loss coefficient
0.2	cold header loss coefficient
16	thermal conductivity of the plate (W/m-K)
60	# of HX longitude cells
18.0026	wmh - molar mass
18.0026	wmc - molar mass
water.fld	hot fluid id (0 co2 else helium)
Water.fld	cold fluid water
0	if two phase exists 1 else 0
1	two phase side: 1 for hot else 2 for cold
1.0d-5	pressure iteration tolerance

2.2 Benchmarking OTHSG

The result of the OTHSG FORTRAN/TK-Solver code is compared to the results obtained from FLUENT, modeled in Italy [Cioncolini et. al., 2003]. Table 2-2 shows the current IRIS operating conditions and compares the results of the OTHSG code with the calculated parameters.

Table 2-2 Comparison of Parameters for steam generators

Parameters	Italy	MIT	
Power	125	125	MW
Primary side:			
Mass Flow rate	589	589	kg/s
Inlet Temperature	328.4	328.4	C
Oulet Temperature	292	291.9	C
Inlet Pressure	15.5	15.5	MPa
Pressure drop	72	74	kPa
Secondary side:			
Mass Flow rate	62.5	62.5	kg/s
Inlet Temperature	223.9	224.2	C
Oulet Temperature	317	317.5	C
Outlet Pressure	5.8	5.8	MPa
Pressure drop	296	307	kPa
Tube Length	32	32.4	m

As seen from Table 2-2, all the results are very close and consistent with the results of models and experiments from Italy on the prototype IRIS OTHSG. The overall profiles of the temperature and the heat flux from the two models are plotted in Figure 2-3.

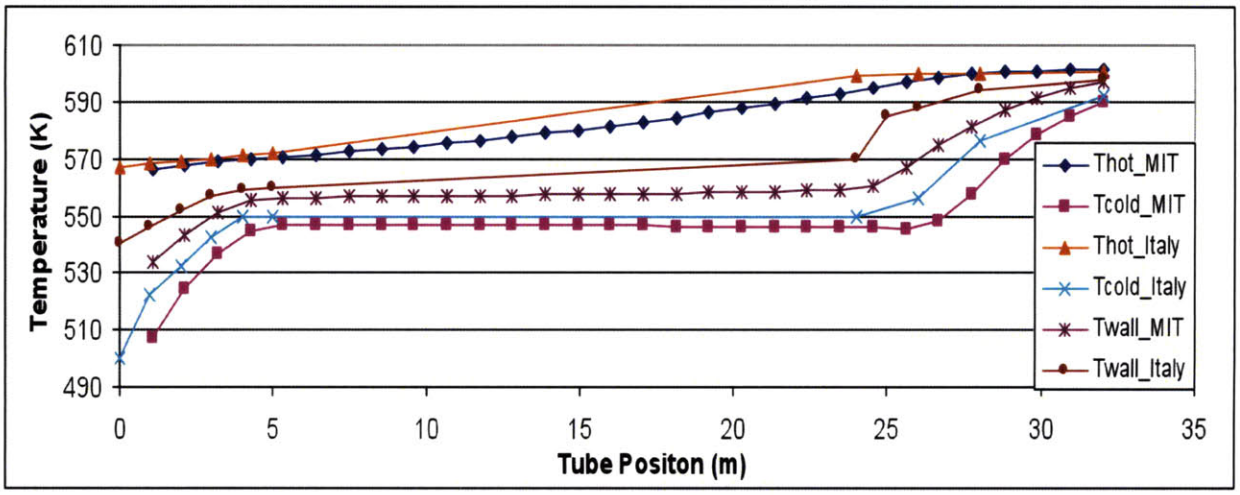

(a)

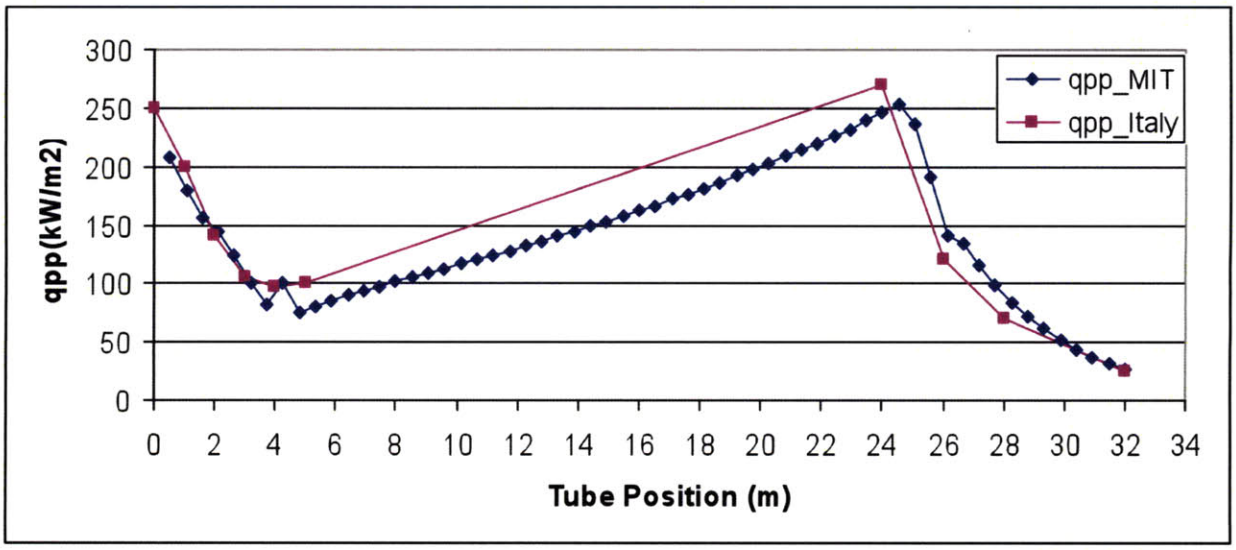

(b)

Figure 2-3: The SG (a) temperature profile and (b) heat flux (qpp) profile as predicted by the MIT and Italy models

As seen, the shape of the profiles in Figure 2-3 are very similar. However in case of the heat flux and the average wall temperature, there is about 25 kW/m^2 and 10 K difference between the Italian result from FLUENT and the MIT FORTRAN model. These differences don't affect the overall conditions significantly. Since the methodology used in the OTHSG

MIT code is very similar to the one used for the PCHE model, as described later, it was important to validate the model against other experimental and numerical models.

The code was tested for other cases to show the validity of the assumptions that was made for the hydraulic diameter of the OTHSG. There is only one other case shown with different tube lengths, number and SG height displayed in Table 2-3. The Fortran/Tk-Solver predicted the length to be 30.6 m compared to the reported value of 32 m. This is reassuring since the average distance between the helical coils was not reported, and was just guessed by scaling the nominal values by the number of tubes contained in the modified design. The only other parameter that differed was the hot side pressure drop, which was 106 kPa compared to the reported 136 kPa. This is also not troublesome, since there was no mention of what values of loss coefficient and height were used for headers and the same values as the nominal design were assumed.

Table 2-3 Comparison of OTHSG parameters for benchmarking MIT code

Parameters	Italy	MIT	
Power	125	125	MW
Primary side:			
Mass Flow rate	589	589	kg/s
Inlet Temperature	328.4	328.4	C
Outlet Temperature	292	291.9	C
Inlet Pressure	15.5	15.5	MPa
Pressure drop	136	144	kPa
Secondary side:			
Mass Flow rate	62.5	62.5	kg/s
Inlet Temperature	212	213.1	C
Outlet Temperature	317	316.34	C
Outlet Pressure	5.8	5.8	MPa
Pressure drop	101	91.3	kPa
Tube Length	32	30.6	m

2.3 Conclusion

The OTHSG of IRIS was accurately and successfully modeled with a 1-D thermal hydraulic model using an iterative scheme and published correlations that are applicable to the IRIS specific geometry. The code was able to show acceptable numerical stability and extrapolation for the purpose of this project. In general, helical steam generators have very helical tubes arrangement with a variety of wavelengths and helix diameters. It is noted that the MIT developed code was tested for specific conditions and the CHF occurred at very high qualities (greater than 95%). Therefore, the applicability of the Groeneveld correlation and the performance of the code under other conditions in which CHF way occur earlier have not been tested. However, for the purpose of steady state IRIS analyses, the above methods are sufficient.

Furthermore, fluids other than water can be used, such as sodium, for which the correlations will not be applicable.

Chapter 3 PCHE Analysis

3.1 Previous work on PCHE

PCHE is made up of diffusion bonded plates with chemically etched flow paths. The plates are bonded together in sequence of hot/cold plate. There is counter-current flow between the hot and cold plates. For the purpose of modeling the PCHE, the following assumptions were made:

- The total mass flow rate is uniformly distributed among the channels.
- There is a boundary condition of zero heat flux periodically between each pair of hot/cold plates
- The wall channel temperature is uniform at every axial node, along with zero axial conduction
- Cold and hot plates have the same number of flow channels

The nodalization scheme is shown in Figure 3-1.

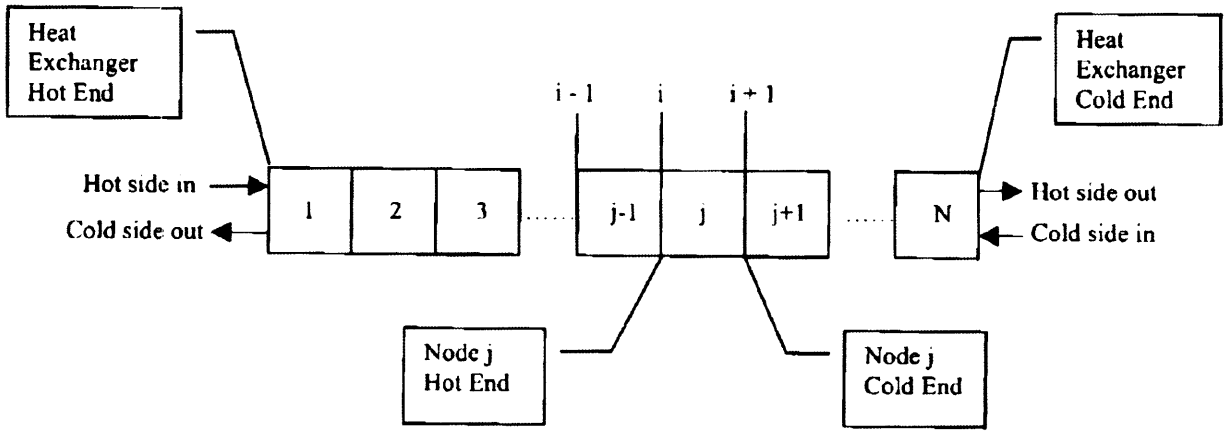

Figure 3-1 Heat exchanger nodalization (from Dostal, 2004)

Therefore a single channel has been modeled for each hot and cold side and the heat transfer is calculated between them and scaled to the total number of channels in the PCHE. Basically every node will obey an energy balance equation:

$$\dot{m}_{hot}(H_{in}-H_{out})_{hot}=\dot{m}_{cold}(H_{in}-H_{out})_{cold}=P_h\,\Delta z\,h_{tot}(\overline{T}_{hot}-\overline{T}_{cold}) \tag{3.1}$$

Where $\dot{m}$ is the mass flow rate, H is the enthalpy, P_h is the heated parameter, Δz is the axial length, $\overline{T}$ is the node-average temperature. The h_{tot} is total heat transfer coefficient, and is derived by using heat flux balance:

$$h_{tot}=\left(\frac{1}{h_h}+\frac{c_l P_h}{k\,2P}+\frac{P_h}{h_c P_c}\right)^{-1} \tag{3.2}$$

where h is the heat transfer coefficient, P is pitch of the channels, c_l conduction length which is 60% of the hot/cold channel distance calculated by the CFD code Fluent, k is the thermal conductivity of the plates.

The PCHE thermal parameters were calculated using a FORTRAN nodal code that estimates the necessary volume, given inlet conditions for both the primary (single phase) and secondary sides (two phase). This code is an expanded version of one that originally included single phase gas to gas calculations [Hejzlar et al, 2006]. Figure 3-2 shows a cut in the PCHE layout that was considered. PCHE is composed of multiple plates of the same geometry packed on top of each other, with 2mm diameter semicircular channels in a zigzag arrangement. The effects of the geometry were accounted for in the heat transfer coefficient and pressure drop, by using correction factors based on PCHE experimental results.

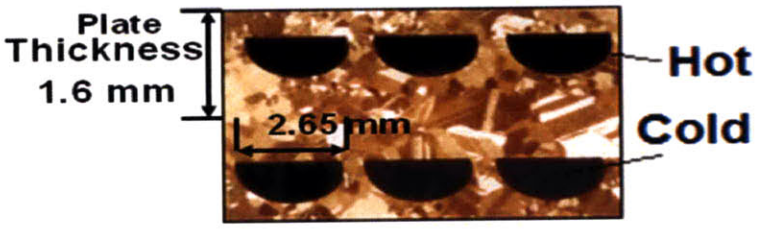

Figure 3-2 A crosssection of two layers of the PCHE showing the semicircular coolant paths (from Heatric, 2008)

The primary and secondary liquid heat transfer coefficient was calculated by the Gnielinski correlation for laminar flow, which has been experimentally validated for small diameter and velocity conditions of PCHE [Hesselgreaves, 2001],

$$Nu = \frac{\frac{f_c}{8}(\mathrm{Re}-1000)\,\mathrm{Pr}}{1+12.7(\mathrm{Pr}^{\frac{2}{3}}-1)\sqrt{\frac{f_c}{8}}} \qquad \mathrm{Re}>5000, \tag{3.3}$$

where Nu is the Nusselt number, Re is the Reynolds number, Pr is the Prandtl number and f_c is the Moody friction factor expressed by

$$f_c = \left(\frac{1}{1.8\log \mathrm{Re}-1.5}\right)^2, \tag{3.4}$$

where the Re is defined as

$$\mathrm{Re} = \frac{\rho v D_{eq}}{\mu}. \tag{3.5}$$

In Eq. (3-5), ρ, v and μ are density, velocity and viscosity of the fluid respectively. D_{eq} is the equivalent hydraulic diameter which in case of PCHE is

$$D_{eq} = \frac{4\pi d^2}{8\left(d + \pi\frac{d}{2}\right)}, \tag{3.6}$$

where d is the diameter of the semicircular flow channel.

For the laminar regime (Re < 2300), a constant Nu of 4.089 was used, which is good for semicircular channels. In the transition region between 2300 < Re < 5000, linear interpolation between the laminar and turbulent regimes was used [Dostal, 2004]:

$$h_{tran} = h_{lam} + \left(\frac{h_{turb}}{h_{lam}}\right)\left(\frac{\mathrm{Re} - 2300}{5000 - \mathrm{Re}}\right). \tag{3.7}$$

In Eq. (3-5), h_{lam} is heat transfer coefficient at laminar region and h_{turb} is the turbulent heat transfer coefficient at Re of 5000.

For the two-phase heat transfer coefficient, the Chen superposition correlation, Eq. (2.7) was used for qualities between 0 and 0.95. After reaching a quality of 0.95, due to the low velocity of the flow, the main mechanism of heat transfer is that of pure superheated vapor and the Gnielinski correlation is used again. For the zigzag channels, the above heat transfer coefficient is multiplied by 2.3, as derived by Ishizuka [Ishizukat .et al., 2005] based on experiments with PCHE. It is noted that in OTHSG experiments, it was found that the centrifugal force of helical tubes did not enhance heat transfer coefficient in the two phase regime. The same could be true for the zigzag channels in PCHE. However, as will be seen later, the cold side heat transfer coefficient in the boiling region affects the PCHE overall performance insignificantly.

The pressure drops for the single phase portions of the PCHE were modeled by using experimental results from Tokyo Institute of Technology [Ishizuka .et al., 2005]. The two-phase pressure drop was modeled by using the Taylor correlation [Hesselgreaves, 2001]. Headers and orifices pressure drops were modeled based on the geometric specifications. Refer to the appendix D for more details on header design and stress calculations.

The PCHE code requires the inlet mass flow rate, pressure and temperature for both hot and cold sides in order to produce results. The code first guesses the total length of the PCHE, and then it divides the length into 60 nodes. Starting with the node at the inlet of the primary side (or outlet of the secondary side), the code calculates the heat transfer coefficient and pressure drop in each node and estimates a new length for the individual nodes. The lengths of the nodes are summed up and are used to calculate the total transferred power of the PCHE. This value is compared to the target power value, if it is not within 0.1%, then the new total length is estimated by scaling the previous guess by the ratio of the estimated power to desired power. In case of the wall temperature iteration scheme and the subcooled boiling calculations, the same method as described in Section 2-1 was used.

3.2 Validation of PCHE model

Due to atypical thermal hydraulic conditions in the PCHE (e.g. low mass flux and small channel diameter) compared to most present experimental data and empirical formulation for two-phase flow, and lack of any experimental results with two-phase flow with water as the working fluid for the PCHE, it is very important to examine a range of correlations. For the base case (the first case in Figure 3-3) for subcooled nucleate boiling region, the Froster-Zuber, for two-phase heat transfer, the Chen and for the pressure drop, the Chisholm correlations were

originally used. The Jens and Lottes and Thom nucleate boiling correlations were also considered [Todreas .et al., 1990]. A new two-phase heat transfer correlation developed by Tokyo University for low Reynolds numbers in small diameter tubes was implemented [Zhang .et al., 2005]. In addition, another new two-phase heat transfer correlation developed by Argonne National Laboratory (ANL) for horizontal small diameter flows with comparable mass fluxes was used [Yu .et al., 2002]. Also, for compact surfaces, the Cooper correlation, recommended by Cornwell and Kew [Cornwell, 1999] was applied.

For pressure drop, the C coefficient in the Chisholm correlation was assumed to be zero due to the small diameter of the tube. Holt developed a correlation that correlates the C coefficient as an exponential function of the hydraulic diameter; Holt's experiments include a diameter size similar to the PCHE [Holt .et al., 1997]. A new pressure drop model was used as an alternative to Chisholm from the ANL experiment. The Taylor correlation was also recommended to be used for compact heat exchangers. Taylor treats the liquid phase and vapor phase separately as opposed to the Chisholm correlation, which assumes both phases are either turbulent or laminar [Hesselgreaves, 2001].

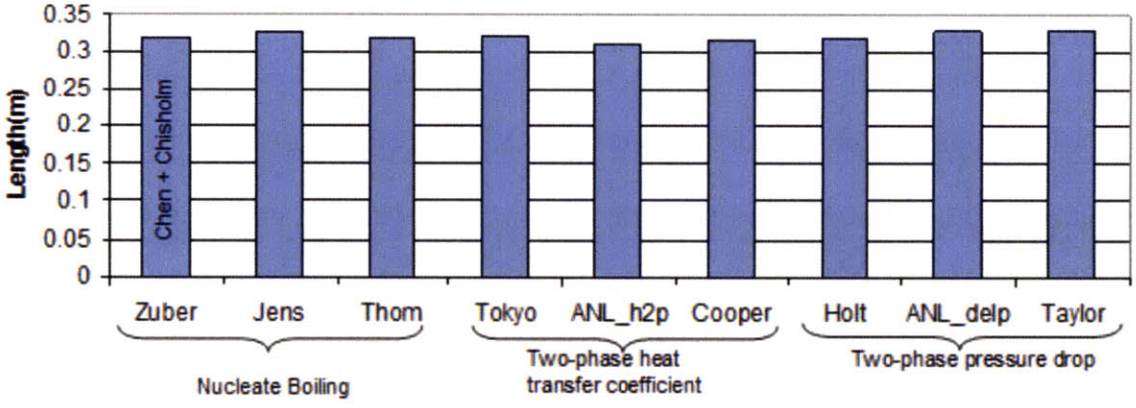

(a)

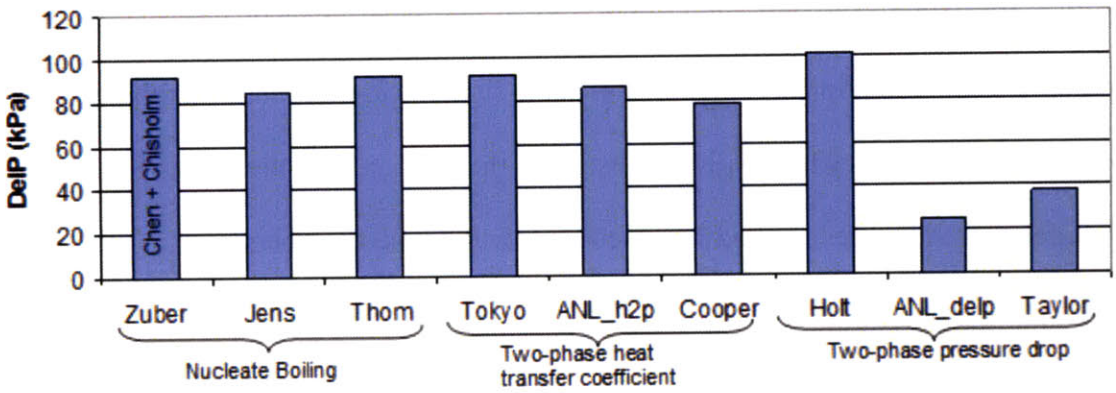

(b)

Figure 3-3 Effect of different correlations on (a) total length and (b) pressure drop of the PCHE

As seen in Figure 3-3, the overall effect of the new heat transfer correlation compared to Chen's is not very significant in terms of the PCHE overall length and pressure drop. However, some of the boiling correlations resulted in a heat transfer coefficient significantly greater than Chen's correlation. Yet, due to the laminar liquid phase and turbulent vapor phases present for the current PCHE case, which is based on the IRIS conditions, the Chisholm correlation over-predicts the pressure drop. In fact, this has been experimentally proven for small mass fluxes [Yu .et al., 2002]. Therefore, the Taylor correlation will be used for the rest of the analysis to compare the PCHE performance to that of the OTHSG.

The validity of the single phase friction factor developed by TITECH for water and CO_2 as the working fluids was also examined. As seen in Figure 3-4, the "Regular" uses the fanning friction factor for laminar and the Blasius friction factor for Turbulent [Todreas et al. 1990]. The "Advance" uses the "Regular" friction factors but also takes into account the laminar and turbulent entry regions [Idelchick, 1986]. The TITECH correlation calculates a straight channel friction factor and uses it to calculate the zigzag friction factor. However, as seen in Figure 3-4, this straight channel correlation differs from the "Regular" and "Advance" values for Reynolds

numbers less than 1000. Normally, this will not cause any problems, however, when calculating the two phase friction multiplier at high qualities the single phase Reynolds number will be very low, so, the TITECH correlation will underestimate the friction pressure drop. So for the final PCHE model, the "Advance" method was used for low Reynolds numbers.

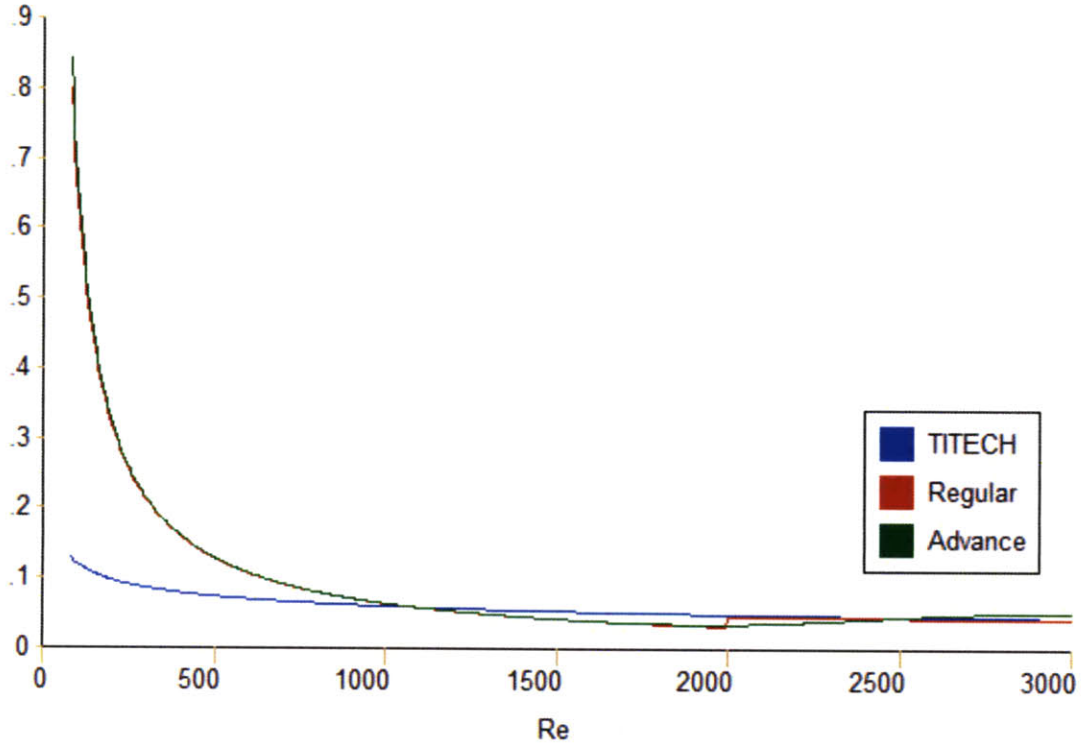

Figure 3-4 A comparison of different methods to calculate the straight channel single phase friction factor

3.3 Stability analysis of PCHE

This section discusses the stability issues that are relevant to PCHE and its operating conditions within the IRIS design. In general compact units are susceptible to have blocked passages due to particulates in the fluid stream. It is recommended to use two parallel compact units in place of each unit of the current OTHSGs or place filters at the inlet with relatively small

holes. Also, the reduced cost of maintenance and cleaning due to much less required space by PCHE usually offsets the added capital cost for the new unit. PCHEs are particularly sensitive to operation outside their design margins. Small changes to velocity could affect the temperature significantly, especially in the current case with high heat flux. The startup of the PCHE is also of concern especially under two phase conditions.

The PCHE is believed to be not susceptible to vibration instability, because of strong bonds between the plates. However, excursive instability, which is characterized by small perturbations in operating parameters that could result in a large departure from the steady state condition, has been observed in subcooled nucleate boiling regions of small diameter tubes caused by blocked channels. Since the flow is subcooled at the inlet and super heated at the outlet, the internal pressure gradient with mass flux change must be positive at all times in addition to being less than the pump applied gradient. Density wave instability is not expected to be observed for PCHE due to high operating pressure and higher pressure drop at the inlet than the exit [Kakac, 1991].

The Critical Heat Flux (CHF) will also need to be addressed to understand its safety implications, and also to see the effects on the total length required by the PCHE. In general, for a horizontal flow in tube, if the flow is stratified then the CHF is zero at the vapor side. To check the stratification of the flow regime Taitel and Dukler Flow regime map was used [Hewitt .et al., 1987]. Figure 3-5 shows that the nominal PCHE mass flux is well below the stratification limit.

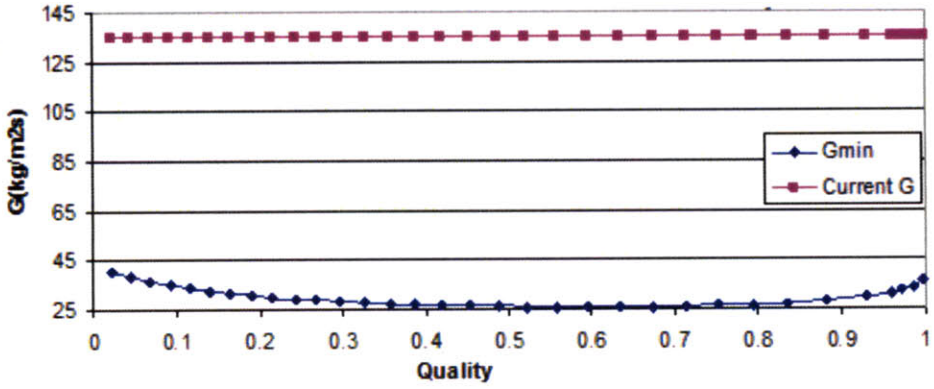

Figure 3-5 Minimum Mass Flux for Stratification vs. Quality

To calculate the CHF for the PCHE, two correction factors are used. The first correction factor changes the vertical CHF to its equivalent horizontal CHF with 8mm diameter tube [Yu, 2002]. Three options for the correction factors were used, the Duckler correction factor [Groeneveld et al., 1986], the Wong correction factor [Wong et al., 1990] with CISE [Triplett et al., 1999] and Drift flux [Todreas et al., 1990] models for the void coefficient correlation. It is noted that Yu recommended the Wong correlation to be used with CISE void correlation [Yu et al., 2002]. For the full equations of the above correlations Appendix D can be consulted. As seen in Figure 3-7, the small difference in void coefficients makes an enormous impact on the k_{hor}, the horizontal critical heat flux correction factor due to the presence of the exponential function in the Wong correlation. The values of K_{hor} can be obtained as a function of flow rate and void coefficients from equation:

$$k_{hor}=1-\exp[-(T_1/3)^{.5}] \qquad (3.8)$$

Where T_1 is given by a complex function in terms of flow rate and void coefficient shown in Appendix D [Wong et al., 1990].

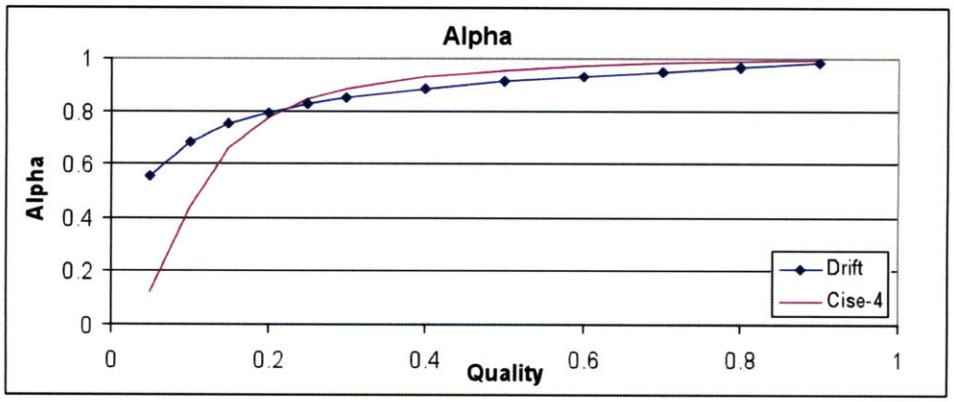

(a)

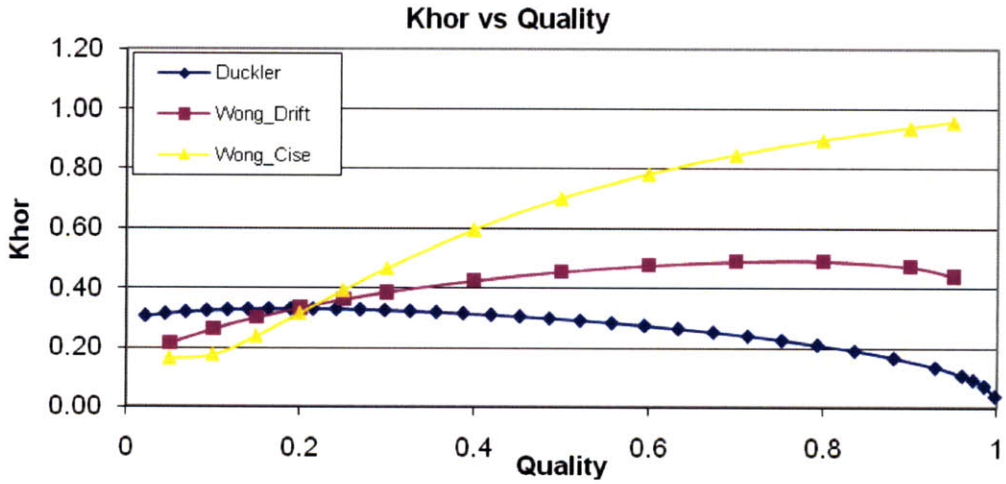

(b)

Figure 3-6 The void coefficient (a) that was used to calculate the khor (b)

The second correction changes the CHF representation at small diameters, in particular the 8 mm CHF to 1.22 mm (PCHE hydraulic diameter) CHF [Tanasea .et al., 2008]. There are a lot of variations at the PCHE conditions. Table 3-1 was provided by Tanasea et al. to represent the conservative values found in literature:

Table 3-1 The diameter correction factors at different mass flux, quality and pressure (from Tanasea .et al., 2008)

Pressure (kPa)	Mass flux (kg m^{-2} s^{-1})	Quality (X)			
		−0.5 to −0.25	−0.25 to 0	0 to 0.5	0.5 to 1
100–14000	0–250	−0.2	−0.2	−0.2	−0.3
	250–3000	0.4	0.4	0.5	0.6
	3000–8000	0.3	0.3	0.4	0.4
14000–21000	0–250	−0.2	−0.2	−0.2	−0.3
	250–3000	0.4	0.2	0.4	0.4
	3000–8000	0.3	0.2	0.2	0.2

Therefore, by Table 3-1 conservative assumption would result in a value of -0.2 for qualities up to 0.5 and -0.3 to for quality between 0.51 and unity.

The DNB at qualities below 30% in the nucleate boiling or subcooled boiling regions is of great importance. If the DNB is reached at these conditions the performance of PCHE will suffer significantly. The DNB margin using the Biasi correlation [Todreas .et al., 1990] and 1995 Groeneveld .et al. lookup table proved to be very sufficient, with MDNBR of 32 and 2 respectively for each correlation. Three correlations were used to calculate the CHF: Biasi, Bowring [Todreas .et al., 1990], in which it's lowest data point for mass flux corresponds to PCHE mass flux, and the CHF lookup table devised by Groeneveld .et al. in 1986 and 1995.

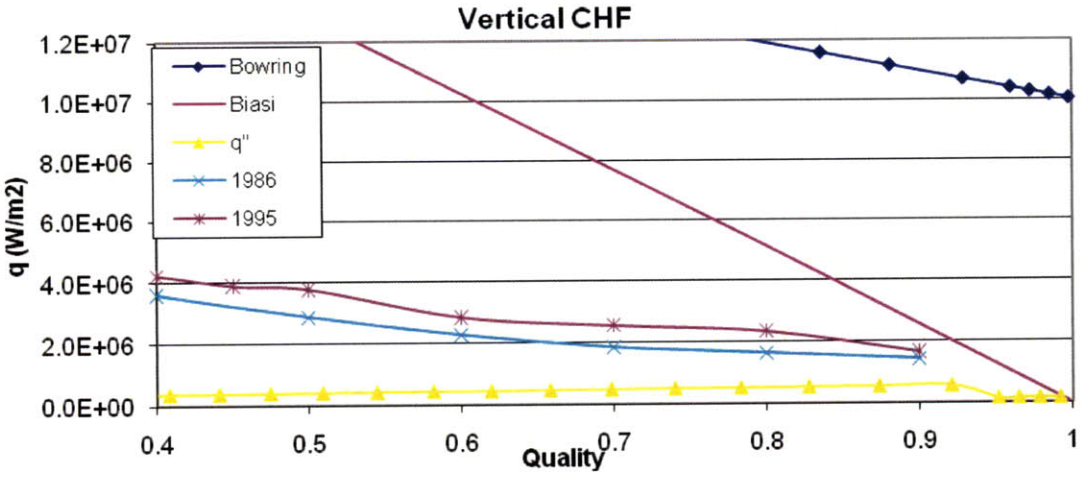

Figure 3-7 The PCHE CHF values assuming vertical flow

As seen in the Figure 3-7, the CHF does not reach the PCHE heat flux until the very high qualities, without taking into account the horizontal factors in Figure 3-6. Using the Wong/Cise correlation with correction factors from Figure 3-6 gives the results in Figure 3-8:

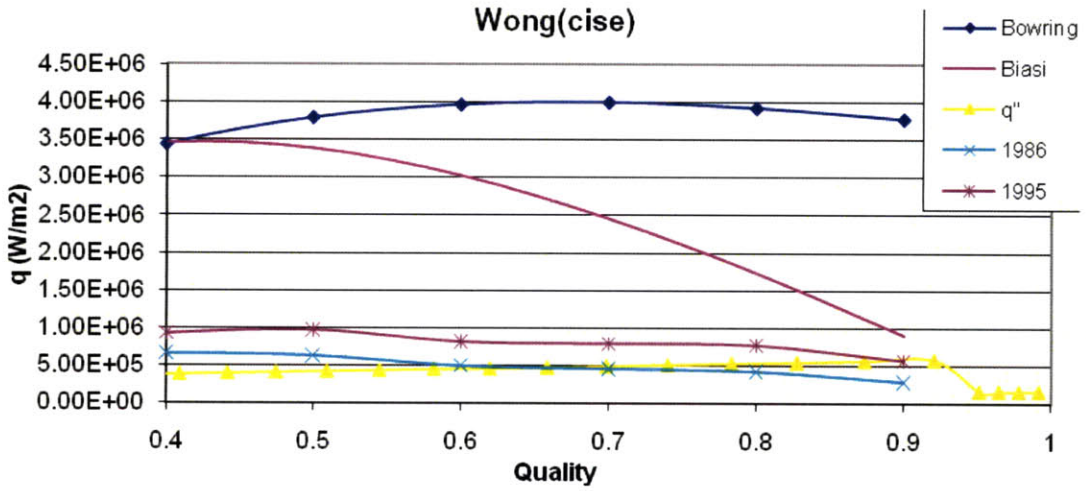

Figure 3-8 The PCHE CHF comparison of different correlation by using the same khor

Using the more recent 1995 heat flux tables instead of the 1985 tables, and applying the different horizontal correction factors from Figure 3-6 yields the results plotted in Figure 3-9.

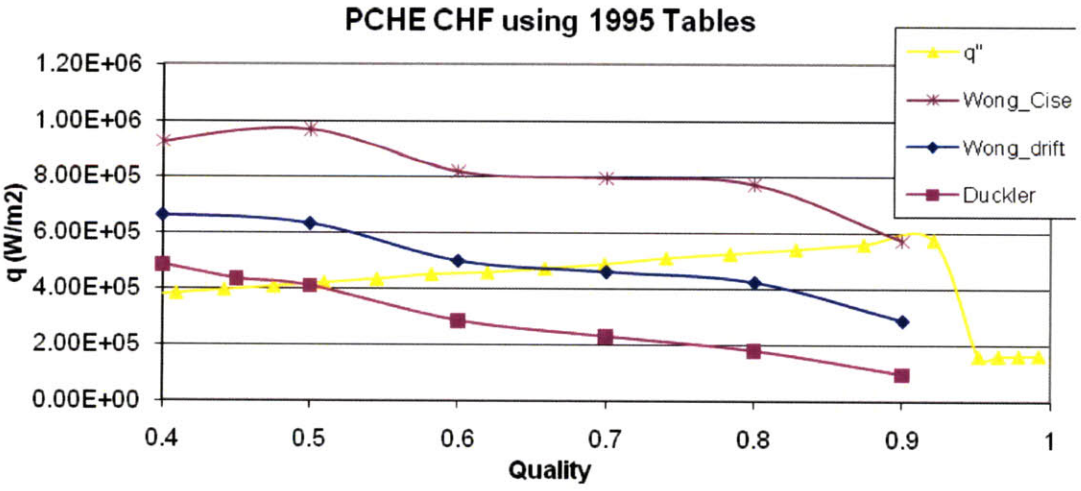

Figure 3-9 Comparison of CHF correlation for the PCHE

If the most conservative assumption is used, then the CHF is reached at about 50% quality. Since there are no correlations for post-CHF heat transfer for the current design mass flux, pressure and diameter, single phase vapor convection is assumed. For the case of 50% quality, the length of the PCHE should be increased from 0.27 m to 0.37 m. These CHF results are conservative, since as seen in Figure 3-2, the top of the channels is flat, which allows for more even wetting of the wall compared to a complete circle. Also, if the Wong-CISE CHF factor were to be used, CHF would occur at qualities greater than 0.9 as recommended. In terms of temperature increase beyond CHF, the PCHE is designed to withstand temperatures up to 1073 K, much greater than the upper limit temperature for the secondary side, which is the primary inlet temperature (602 K). Even if a constant heat flux condition is assumed, the temperature will never exceed 800 K, using Varone's method for post-CHF assuming dry-out at 50% quality [Varone et. al., 1988]. Another concern about the CHF for PCHE geometry is that while CHF occurs at higher qualities, as the mass flux decreases, CHF decreases at high qualities, the reverse of what one would expect for normal diameter tubes [Yu .et. al., 2002].

The current PCHE specification are compared to what is listed on the Heatric website in Figure 3-10. As seen, the only unusual parameter is the hot side Re number which might cause corrosion issues, especially considering the use of zigzag channels.

HEATRIC (WEBSITE)	PRINTED CIRCUIT HEAT EXCHANGERS	MIT DESIGN
	1 kg to 60 tonnes as a single unit	4383 kg
Unit weight range	However larger modular assemblies are possible	
Maximum design pressure	Current maximum design pressure 650 bar (9500 psi)	155 bar
Design temperature range	Currently from 2°K to 1160°K (-450°F to 1650°F)	224-328° K
Maximum nozzle size	900 mm NB (36 in NB)	178 mm
Maximum surface area	10,000 m^2 (108,000 ft^2) per PCHE	967 m2
	1300 m^2/m^3 at 100 bar (400 ft^2/ft^3 at 1450 psi)	1420 m2/m3
Typical area/unit volume	650 m^2/m^3 at 500 bar (200 ft^2/ft^3 at 7250 psi)	NA
Minimum temperature approach	1°C (typically 3 - 5°C) 2°F (typically 5 - 10°F)	NA
Heat exchanger effectiveness	up to 98%	95.50%
	LP gas cooler 500 - 1,000 W/m^2K (90 - 180 Btu/hrft^2°F)	NA
	HP gas cooler 1,000 - 4,000 W/m^2K (180 - 700 Btu/hrft^2°F)	NA
Typical overall heat transfer coefficients	Water/water 7,000 - 10,000 W/m^2K (1230 - 1750 Btu/hrft^2°F)	7289
Plate thickness	0.5 mm(1) to 5.0 mm	1.6 mm
Passage width	0.5 mm to 5.0 mm(2)	2 mm
Typical Reynolds number range	Gases: 1,000 - 100,000	NA
	Liquids: 10 - 5,000	1380-20300

Figure 3-10 The PCHE comparison to typical PCHE values from Heatric™ website (2008)

In order to enhance the margin for CHF, the PCHE geometry can be changed. The width is already to the maximum manufacturing size, the height is also already high. The flow channel diameter can be increased from 2 mm to 5 mm, which will result in the peak operating heat flux decreasing from 575 to 340 kW/m^2. However, the mass flux will be dangerously close to the stratification limit shown in Figure 3-5. Changing the thickness of the plate will change the heat flux but it will have adverse effects on efficiency. The most effective approach to fix this problem is to use 2 hot plates for every cold plate. Not only will this strategy bring down the heat flux considerably, but it will reduce the Reynolds number on the hot side significantly,

which was a concern for corrosion at the much higher than typical values. It will also increase the mass flux of the secondary side to 200 kg/m^2-s, which will increase the critical heat flux and goes further away from stratification point.

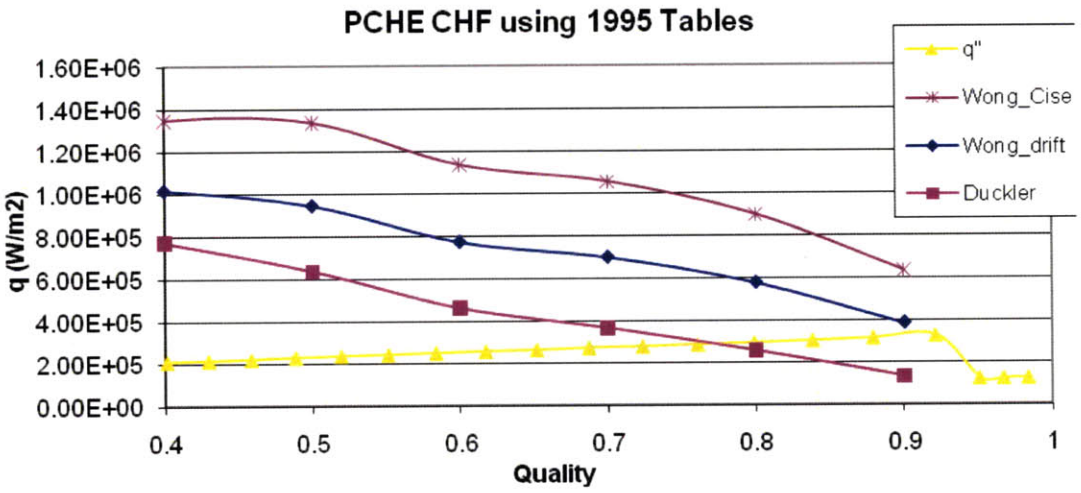

Figure 3-11 The PCHE CHF for two hot plate for every one cold plate case

As seen on Figure 3-11, all the possible problems that could arise from the PCHE geometry can be addressed by only adding 10 cm to the length. The cold side pressure drop also increases from 38.6 to 157 kPa, still less than the 300 kPa of the OTHSGs. On the bright side, the hot side pressure drop decreases by 20 kPa from the PCHE normal design and the Re number is reduced from 20,000 to 14,000.

Due to the small overall volume of the PCHE, the conduction resistance worth could be changed via the heat transfer surface. For single-phase flow or subcooled boiling, conjugate effects will be related to both the entry region effects, where locally high heat transfer coefficient (h) may lead to heat conduction away from the low h regions, and also geometrical effects, by which conduction resistance will reduce heat flow to the parts of the channel perimeter that are

more distant from the heat source. As the passage size is reduced, the heat transfer coefficients rise, but conjugate effects are a stronger function of the design geometry. Conjugate heat transfer effects will occur when too little material separates adjacent passages, if the flow is stratified, or if the passages have finlike separators. Under these conditions, heating will increasingly show a one-sided character, and both heat transfer coefficients and pressure drop will be affected considerably. These geometric effects can be designed out, if desired, and are not intrinsic to the use of small diameter passages, pressure drop or mass flux [Bergles .et al. 2003]. Experiments have shown that CHF of subcooled flow boiling through uniformly heated tubes is mainly affected by five variables: mass flux, inlet subcooling, exit pressure, tube diameter, and length-to-diameter ratio. It was found that an upstream compressible volume can cause flow oscillations, which may result in premature failure [Tong et al, 1997]. However, the secondary side is pressurized to about 6 MPa, which is at higher pressures that the pressures for which this type of failures has been observed. However, such failure might be experienced at lower pressure during transients.

In terms of fouling and corrosion, since PCHEs have better well-defined wall temperature distribution than the regular heat exchangers, less conservative approaches can be taken. However, the compact surfaces provide higher heat transfer coefficient-to-surface area ratio, hence fouling effects could be more significant. Although, to increase the fouling margin, an increase in surface area may be included in the design, which will be less costly for PCHEs [Hesselgreaves, 2001]. Effects of fouling on thermal performance are not comparable among various types of heat exchangers. The fouling thermal effects are strong function of temperature gradient, geometry and velocity of the fluid. In general, 20-25% increase in size of PCHE is recommended to account for fouling [Helalizadeh et. al, 2003]. Deposition of solid particles on a

surface could be a problem especially at low liquid velocity of the PCHE. The old Babcock and Wilcox PWR used full flow demineralizers and multiple filters for their once-through steam generators, which is a possibility here. Some experiments found that the zigzag flow path similar to the PCHE will help with detachment of particles on the surface due to tangential hydrodynamic forces caused by the zigzags. Changing the pumping characteristics can reduce fouling, specifically by increasing the pumps specific speed [Hesselgreaves, 2001].

The crystallization or precipitation fouling is caused by deposition of calcium or magnesium salts from water. A good solution is chemical treatments. Mechanical cleaning methods will not be a likely choice due to the small flow area of the individual channels in the PCHE. A new electromagnetic descaling technology was used for plate compact heat exchangers and was very successful. It agitated the calcium and bicarbonate ions and resulted in their precipitation. This will create an increase in the level of super-saturation of water which results in elimination of degradation of heat transfer coefficient [Cho, 1997]. Surface treatments such as an ion implantation and magnetron sputtering, before the plates are bonded, can also considerably reduce fouling and corrosion [Hesselgreaves, 2001].

3.4 Comparison of PCHE to OTHSG

The most compact version of the PCHE main thermal hydraulic parameters are compared to the OTHSG parameters that is being planned for IRIS [Cinotti et. al, 2002], in Table 3-2.

Table 3-2 Comparison of thermal hydraulic parameters of the PCHE with OTHSG

Parameters	Helical	PCHE	
Power	125	125	MW
Primary side:			
Mass Flow rate	589	589	kg/s
Mass Flux	897	1276	kg/m2s
Inlet Temperature	328.4	328.4	C
Outlet Temperature	292	291.9	C
Inlet Pressure	15.5	15.5	MPa
Pressure drop	72	64	kPa
H Transfer Coefficient	6,843	56,057	W/m2K
Secondary side:			
Mass Flow rate	62.5	62.5	kg/s
Mass Flux	693	135	kg/m2s
Inlet Temperature	223.9	223.88	C
Outlet Temperature	317	319.95	C
Outlet Pressure	5.8	5.8	MPa
Pressure drop	296	77	MPa
H Transfer Coefficient	130,160	466,755	W/m2K
Geometry			
Diameter	variable	0.002	m
Width	-	0.6	m
Height	7.9	4.2	m
Length(core)	-	0.277	m
Volume (no headers)	65	0.7	m3
Volume w/headers	70	1.45	m3
Volume Ratio	48.28	0.02	-
Surface Area Density	44.5	1420	m2/m3
Power Density	1.92	178.57	MW/m3

As seen from Table 3-2, the use of PCHE instead of OTHSG will yield a volume reduction of 48 times per steam generator. Also, the pressure drop for the secondary side is smaller by 200 kPa, which results into 3 degrees more superheat than the OTHSG. The height of the heat exchanger is reduced by 4 meters by using PCHE. This will result in the PCHE being at higher effective elevation than OTHSG and, therefore, an increase of natural circulation power. The main concern arising from using PCHE instead of OTHSG is the large reduction in the

volume of water present in the heat exchanger, which will be discussed in upcoming chapters. The heat flux and the temperature profiles are plotted against results obtained from FLUENT calculation for OTHSG, modeled in Italy [Cioncolini et. al., 2003] in Figure 3-12.

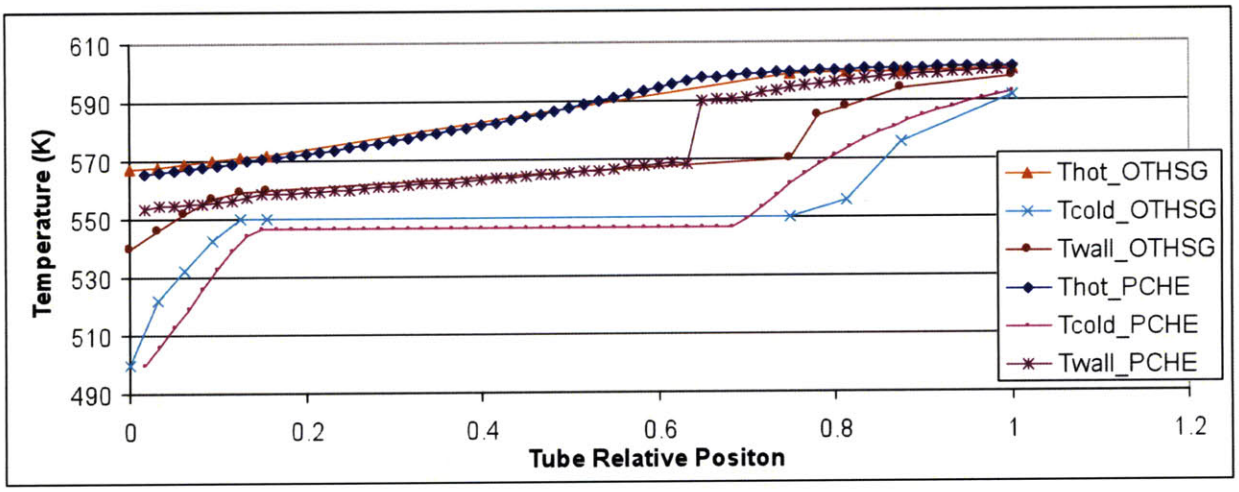

(a)

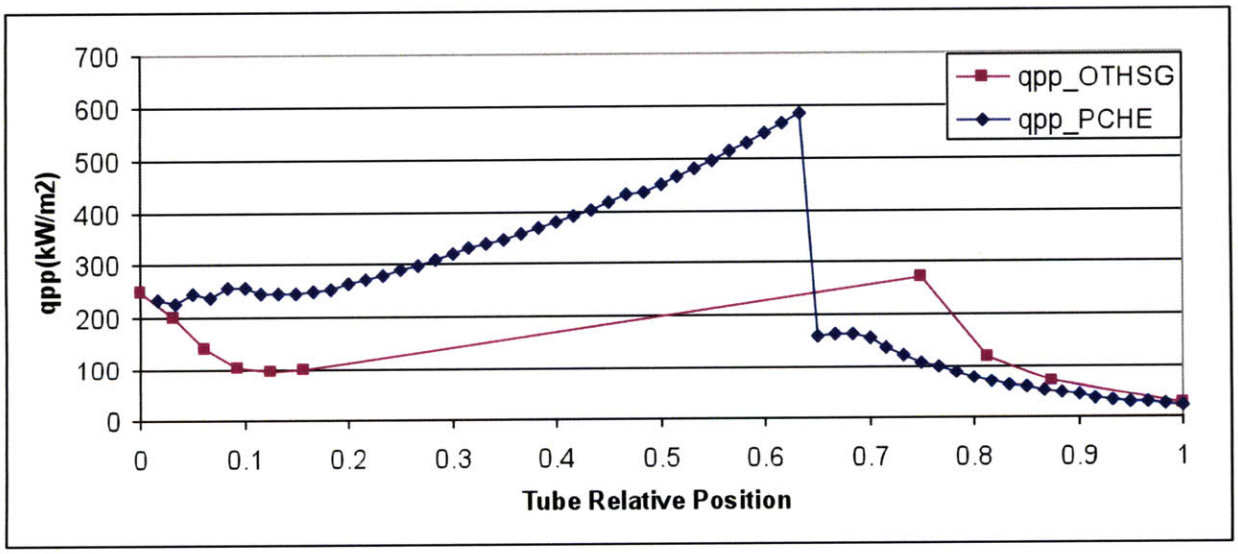

(b)

Figure 3-12 A comparison of (a) temperature profile and (b) heat flux profile of PCHE and OTHSG

From Figure 3-12, it can be seen that the PCHE will have subcooled nucleate boiling at the inlet. Hence the heat flux and wall temperature gradient at the inlet are flatter than those of

the OTHSG. Also, the heat flux increases more rapidly in the PCHE than OTHSG; due to the small diameter of the channels and low mass flux, the convective term in the Chen correlation dominates more than the nucleate boiling. The increase in vapor fraction increases the heat transfer coefficient. Furthermore, the two phase flow reaches dry out relatively sooner than the OTHG, due to a lower pressure drop (36 kPa compare to 260 kPa). Using the above results, the new IRIS layout can be seen in Figure 3-13 configurations. As seen, with PCHE, the reactor vessel diameter can be reduced from 6.1 to 4.5 m. The much smaller heat exchange volume would enable increasing the total SG capacity thus allowing an increase of the total power output without enlarging the vessel volume. Alternatively, it could allow more redundancy in the heat exchanger capacity, so that units can be switched off and on as needed without reducing the total reactor output. Obviously, some reduction in vessel volume while still enabling heat exchanger redundancy for the original power level is also possible.

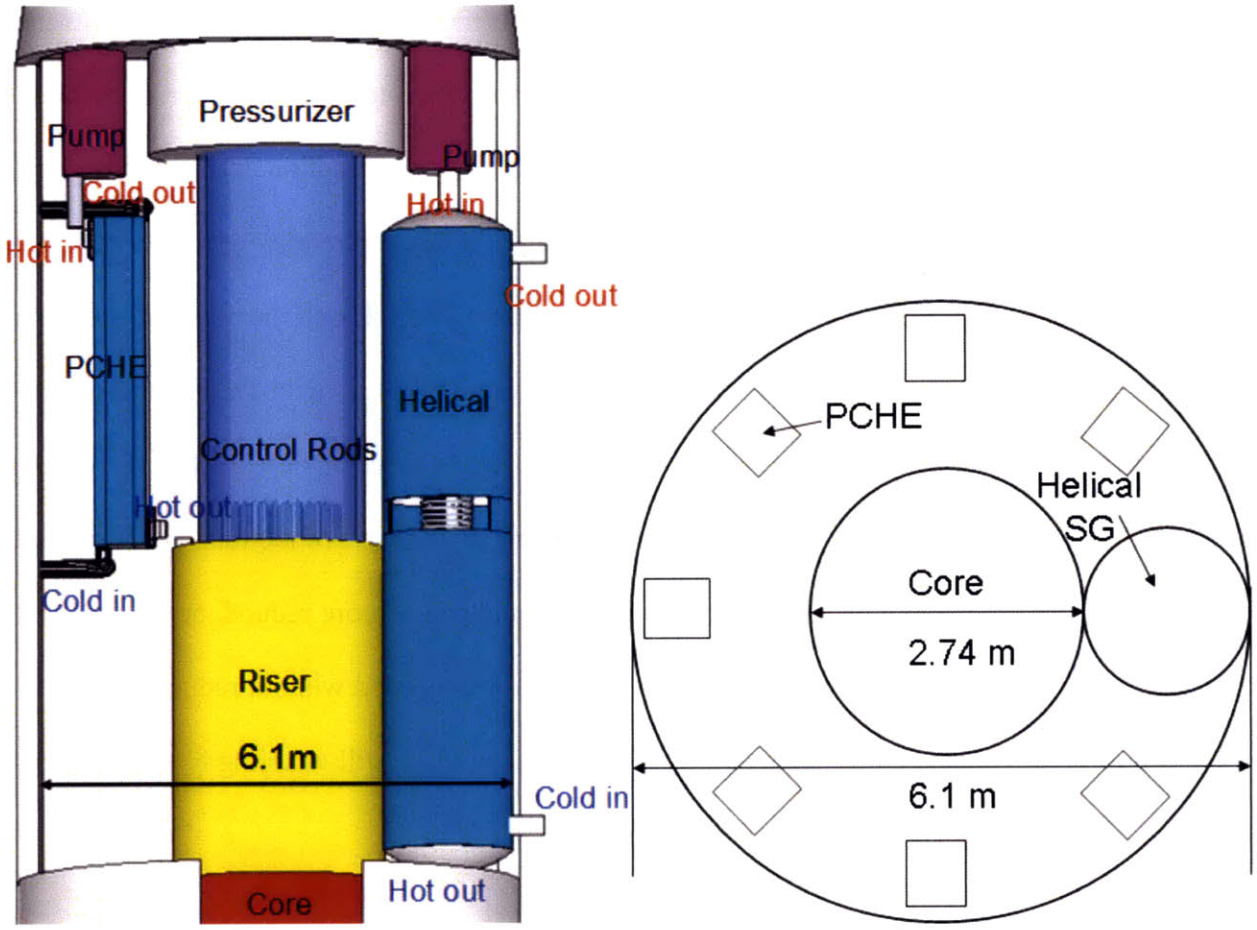

Figure 3-13 Side view and cross sectional view of the PCHE in the IRIS layout

Chapter 4 IRIS Plant Model

4.1 Previous work

An IRIS RELAP model has been developed over several years by investigators from 4 different countries and its results have been published [Bajs et al, 2002]. However, the model input is proprietary, and not available to us. A best estimate RELAP model of the IRIS reactor vessel with the important safety features is needed in order to successfully draw conclusions on the PCHE's safety implications under IRIS's nominal operating and transient conditions. Considering that the goal of the project is not to model every detail of the reactor, and given the fact that the layout of the reactor is very different from a typical PWR, modifying existing inputs would be a harder task than creating a completely new one. While this is a challenging task, a model was developed gradually and different components were added, such as safety systems, to eventually evolve into a complete reactor model.

4.2 Model of IRIS SGs

4.2.1 Model of IRIS OTHSG

The RELAP model of OTHSG developed by the international project [Cioncolini et al, 2003] that had acceptable output was produced by using 15 nodes, with the majority of the nodes concentrated at the inlet. Our RELAP model has been created by using individual pipe control volumes for the primary and secondary sides. The primary side pipe is oriented vertically with the same flow and hydraulic diameter as described in Chapter 2. The secondary side pipe is oriented in a slant making 14.5 degrees angle with the horizontal. Its flow area is the flow area of a single tube multiplied by the number of tubes, and the diameter of the tube is used as the

tube hydraulic diameter. A heat structure has to be used in order to establish heat transfer between the two pipes. The two pipes were modeled as circular tubes with the conduction length set to the single tube thickness. The convective boundary condition was used for both pipes with built in critical heat flux calculations. The default values for surface roughness and pressure drop correlations were used. The pipes were divided into 20 nodes and the total power output of each pipe was calculated by adding the RELAP-calculated power transferred in each node using control variables. The SG heat structure was also divided into 20 nodes with 5 radial meshes. The material used was TT-690 defined by a constant thermal conductivity and heat capacity at operating temperatures. ``The preliminary result did not yield stable numerical solution. The same configuration as above was transformed to rectangular coordinates and a much more stable solution was reached. After 150 sec of simulation the following results were achieved:

Table 4-1 The MIT Fortran vs. initial RELAP results for one OTHSG

	Fortran	RELAP	Units
Tcold Out	320.27	280.22	C
Thot Out	291.96	298.979	C
Delp cold	296	170	kPa
Delp hot	72	49	kPa
Cold Htc	23473	2.34E+04	W/m2k
Hot Htc	6843	6.44E+03	W/m2k
Power	125	103.045	MW

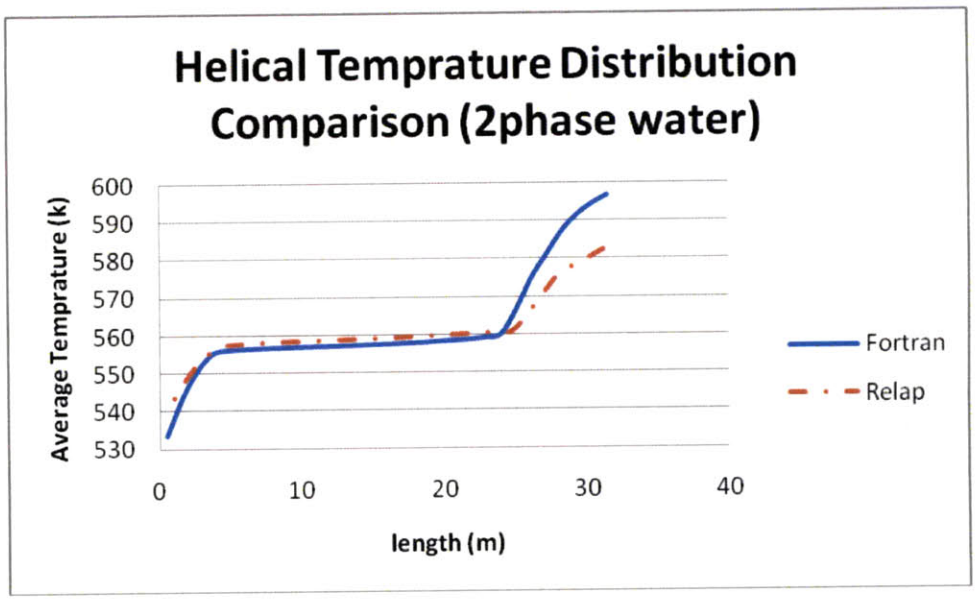

(a)

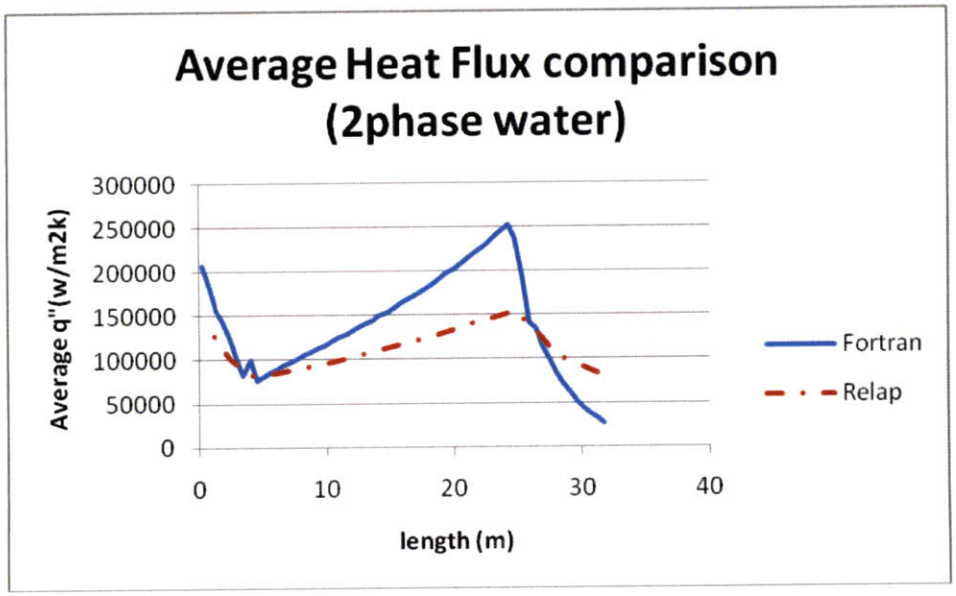

(b)

Figure 4-1 The MIT Fortran vs RELAP (a) temperature distribution and (b) heat flux for one OTHSG

As seen the true physicall OTHSG model could not match the characteristics of the current IRIS OTHSG thermal conditions. While the heat transfer coefficients are very close to the design conditions, the heat flux and total power are significantly lower in RELAP. This is

typically a problem that is encountered when modeling steam generators with complex geometry. There are many measures that can be taken to correct the system model and improve the results:

- Changing the flow area: this will result in unphysical results during transients
- Multiplying heat transfer coefficient by factors to match the correlation results for different regimes: This strategy was taken by the Westinghouse study, however, this will run into issues during transients. During the transients the node in which different heat transfer regimes take place, such as nucleate boiling or convective boiling, will change their position and one cannot change the correcting factors accordingly.
- Changing the conduction length: this is the most ideal solution, since it will not change the thermal parameters and time constant of the system and impacts the heat flux.
- Changing the heated surface area: while this will fix the power to its nominal value, it will impact the total thermal capacity of the system and will not greatly affect the heat flux, which is very different under nominal conditions
- Boiling factor: RELAP provides the user with this option in case the user wishes to adjust the CHF package in RELAP which uses the 1986 Groeneveld data with their suggestions in scaling the CHF based on mass flux, diameter and other factors described in Appendix B.
- Thermal conductivity of the material: while this is an option, the magnitude of change of the thermal conductivity will be very large to attempt to force the above results to their nominal values.
- Changing the loss coefficient: this will enable us to match the pressure distribution, whether through orificing the first channels or adding a distribution of loss coefficients

with Re dependence that would resemble the nominal OTHSG design. However, as seen in Appendix B, this strategy does not provide consistent behavior and all conditions, therefore the channel is orificed at the inlet.

The conduction length was changed from 2.11 mm to 1.0 mm and the boiling factors were adjusted to eliminate having critical heat flux toward the end of the channel. The boiling factor was set to a value to force earlier occurrence of the CHF. Therefore in case of transients, the CHF package is still being used. The final results of the OTHSG RELAP model are shown in Table 4-2 and Figure 4-2.

Table 4-2 The MIT Fortran vs. final RELAP results for one OTHSG

	Fortran	RELAP	Units
Tcold Out	320.27	317.7	C
Thot Out	291.96	291.6	C
Delp cold	296	256	kPa
Delp hot	72	63	kPa
Cold Htc	23473	2.11E+04	W/m2k
Hot Htc	6843	1.12E+04	W/m2k
Power	125	125	MW

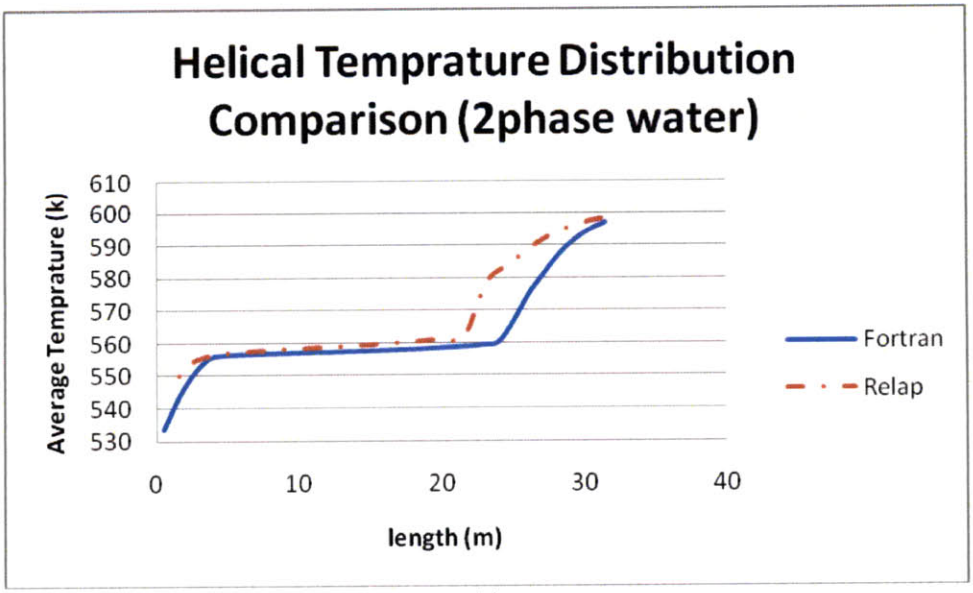

(a)

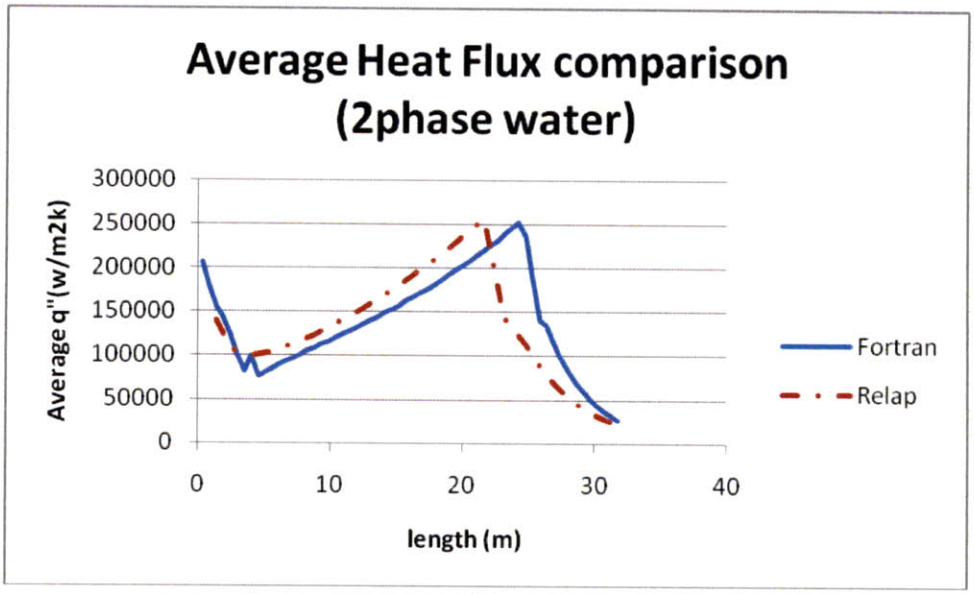

(b)

Figure 4-2 The MIT Fortran vs RELAP (a) temperature distribution and (b) heat flux for one OTHSG

4.2.2 Model of IRIS PCHE

The same methodology as followed in modeling the OTHSG was used to model the PCHE, two single channels of each cold and hot plate were considered and both were scaled according to their total PCHE surface and flow areas. The detailed validation of the model is given in Appendix B. The same parameters as the OTHSG were changed (the conduction length and the boiling factor), to match the existing PCHE code. Both the straight and the equivalent zigzag PCHE were modeled. The only difference between the straight and zigzag models is that the heat transfer coefficient is multiplied by 2.3 through changing the fouling factors for the zigzag geometry, which results into a shorter length. Once the straight PCHE model was successfully benchmarked, changing the fouling factors for each pipe to 2.3 gave the same results as the MIT PCHE code. For all the models 20 nodes and 5 radial meshes were used. The

material used is Stainless-Steel, which is defined by constant thermal conductivity and heat capacity at IRIS average operating temperature.

Table 4-3 The MIT Fortran vs. RELAP results for one PCHE with straight or zigzag channels

Straight	Fortran	RELAP	Units
Tcold Out	320.3	317.8	C
Thot Out	292.0	292.6	C
Delp cold	6.45	5.33	kPa
Delp hot	16.67	14.4	kPa
Cold Htc	24505	23035	W/m2k
Hot Htc	20501	24380	W/m2k
Power	125	124.2	MW

Zigzag	Fortran	RELAP	Units
Tcold Out	319.9	314.7	C
Thot Out	291.9	292.5	C
Delp cold	44.5	3.6	kPa
Delp hot	66	8.5	kPa
Cold Htc	44774	52755	W/m2k
Hot Htc	55988	53955	W/m2k
Power	125	123.6	MW

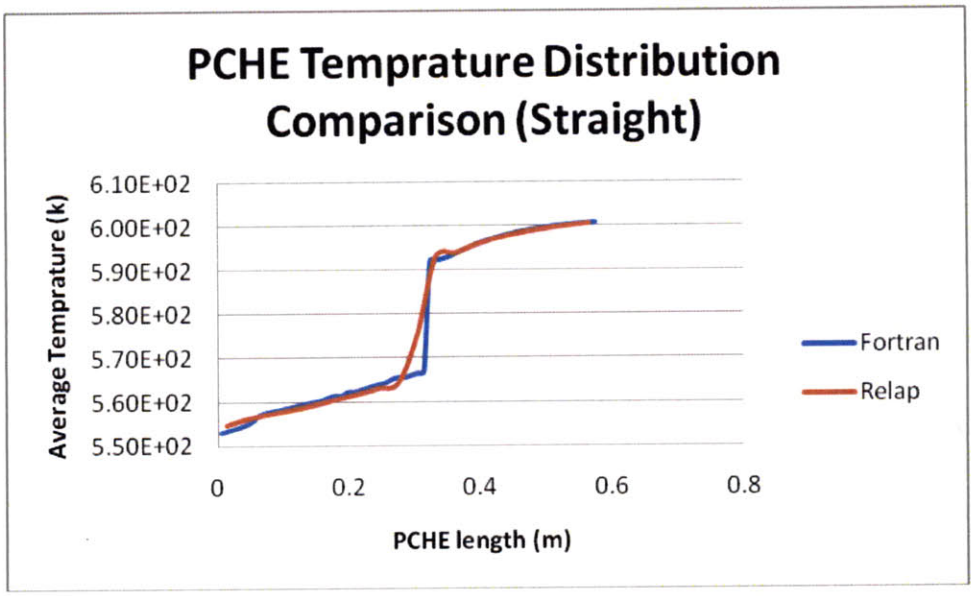

(a)

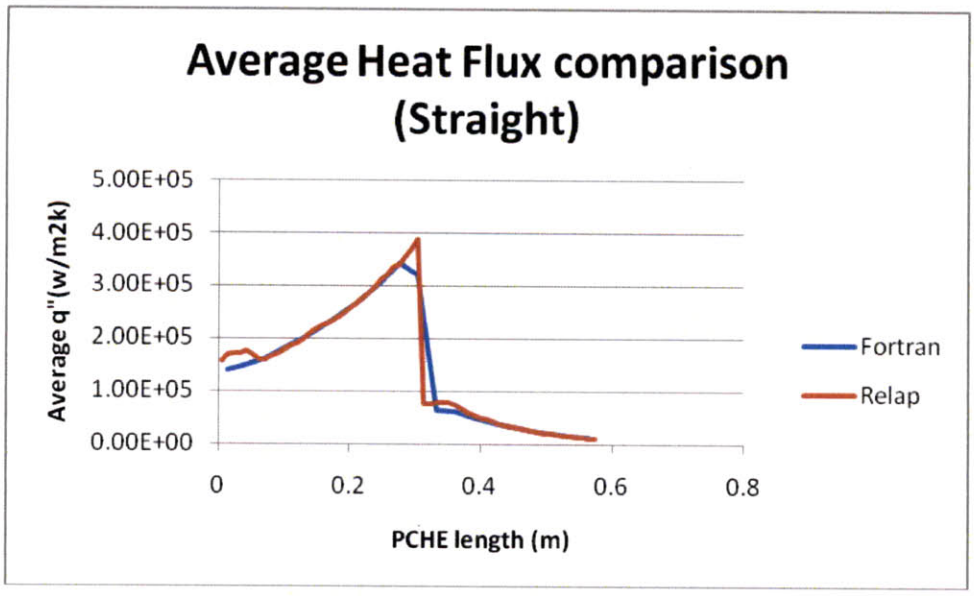
Average Heat Flux comparison (Straight)
Average q"(w/m2k)
5.00E+05
4.00E+05
3.00E+05
2.00E+05
1.00E+05
0.00E+00
0
0.2
0.4
0.6
0.8
PCHE length (m)
Fortran
Relap

(b)

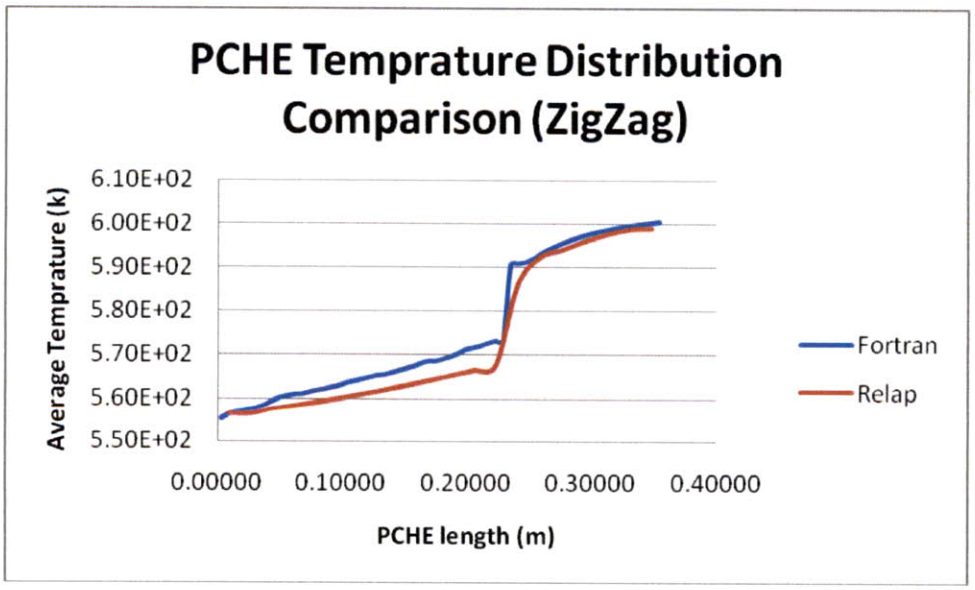
PCHE Temprature Distribution Comparison (ZigZag)
Average Temprature (k)
6.10E+02
6.00E+02
5.90E+02
5.80E+02
5.70E+02
5.60E+02
5.50E+02
0.00000
0.10000
0.20000
0.30000
0.40000
PCHE length (m)
Fortran
Relap

(c)

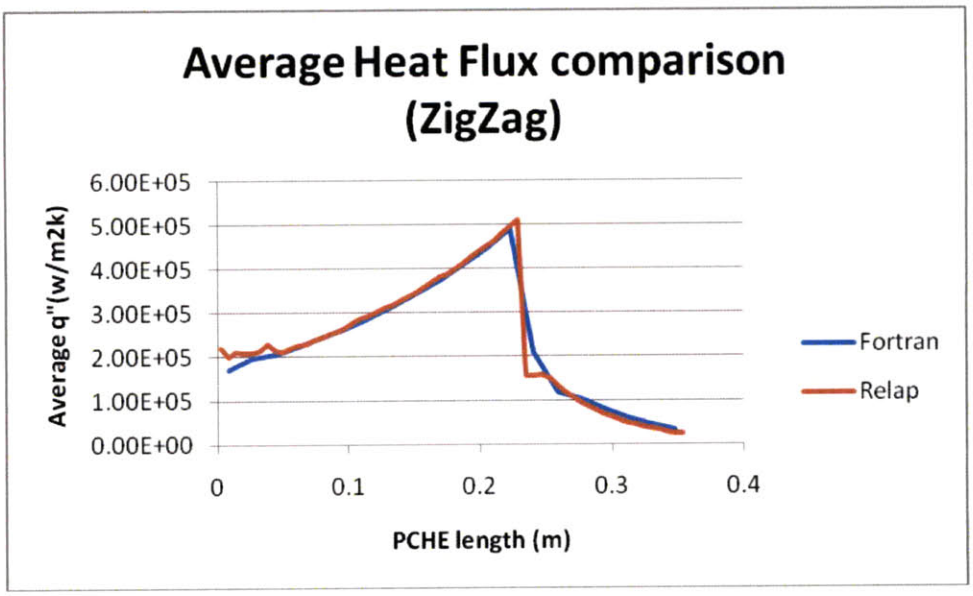

(d)

Figure 4-3 The MIT Fortran vs RELAP (a) temperature distribution for straight and (c) zigzag channels and (b) heat flux for straight and (d) zigzag for one PCHE

As seen in Table 4-3, while the straight PCHE pressure drop is close to the MIT model, the zigzag pressure drop is not very close. Using a distribution of loss coefficients as shown in Appendix B, the RELAP model can match the right values. However, for other conditions such as transients these pressure drops will not be the same as the MIT Code, due to inconsistency in the RELAP code. Therefore, only the inlet channel is orificed to give the desired pressure drop values for the reactor model. The inlet channel loss coefficient of the straight channel was 8.0 and for a zigzag channel a loss coefficient of 15.0 was used. Figure 4-3 (a) through (d) shows that the heat flux and temperature distributions of the Fortran and RELAP models are very similar.

4.3 Model of IRIS Core

4.3.1 Model of IRIS Solid Fuel Core

The IRIS Core is made up of the 17x17 XL standard Westinghouse fuel with 24 positions available for guide tubes/rods, similar to the AP1000 fuel. The XL means that the fuel is 14 feet tall instead of 12 feet, the exact specification of the rods are listed in Table 4-4:

Table 4-4 The IRIS nominal fuel geometric specifications

Pitch	**Clad OD**	**Clad ID**	**Pellet OD**	**Fuel Length**	Units
0.496	0.374	0.0225	0.3225	168	Inches

The longer rods, along with 89 total assemblies rated at 1000 MWth, operate at about 62.5 percent of the power density of AP600. The core is encapsulated in a steel lining for reflector and radiation shielding reasons. The bypass region is taken into account in the final model of the core, but for PCHE and OTHSG comparisons it was neglected for the preliminary study; especially when the MDNBR analysis was done by VIPRE, not RELAP. Also, the heat losses from the steel structure and the vessel bottom were ignored for simplification and lack of accurate data. These structures provide little heat sink and affect the core conditions insignificantly for the first few minutes of a transient, which, as will be seen later is the only time period that will be of concern, when replacing the OTHSG with PCHE.

For the fuel, uranium oxide was used. Its thermal conductivity and heat capacity variance with temperature was supplied in the form of tables. For cladding, Zirconium cladding data was supplied and for the gap, helium data was supplied in addition to using the RELAP gap conductance model. The entire core was lumped into one channel representing the entire core by inputting proper flow area and heat surface areas. The heat structure was divided into 6 axial

nodes with 10 radial meshes: 5 for the fuel region, 1 for the gap and 4 radial meshes for the cladding. The convective boundary condition is used on one side and zero heat flux boundary condition is used at the fuel centerline. The Figure 4-4 power profile was used based on a typical PWR [Todreas et al., 1990].

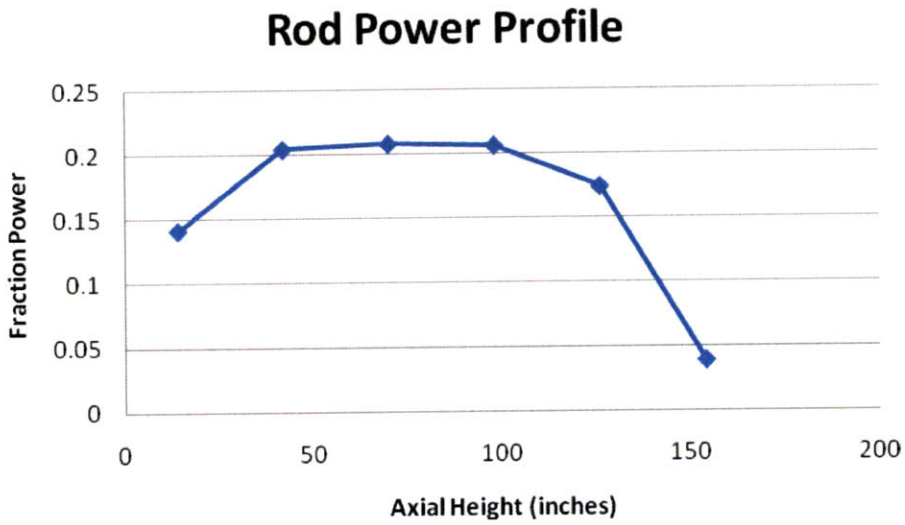

Figure 4-4 The rod Axial power fraction resembling chopped cosine

Westinghouse has reported the number of assemblies in IRIS, which was 89 [Carelli, 2003]. However, the arrangment of these assemblies is not known. Based on previous Westinghouse cores, which are represented by $1/8^{th}$ core symmetric columns with dimensions given in various papers, the core is assumed to look like Figure 4-5.

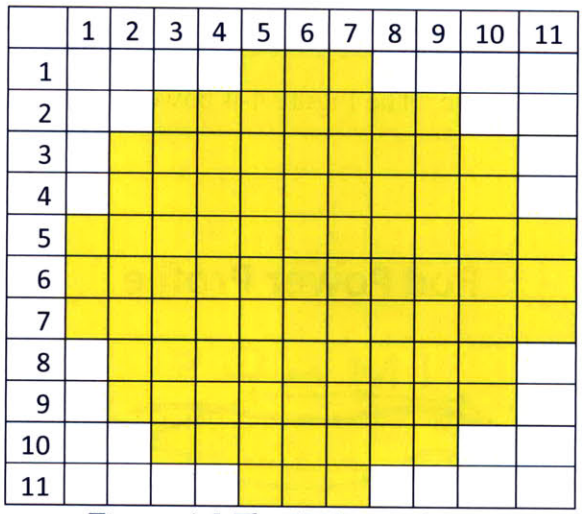

Figure 4-5 The IRIS core layout

In order to accurately assess the behavior of the core during transients, there is a need to add neutronic feedback to the core since it plays a significant part in all transients. To perform the neutronic calculation a point kinetics model is chosen instead of a nodal 1D or 3D model. The decay heat due to fission products and actinides is part of the calculation. The conservative Westinghouse 193 assembly coolant temperature/density and fuel doppler feedback coefficients were used for the core, similar to the coefficients used in the IRIS final technical report [2003] as seen in Figure 4-6.

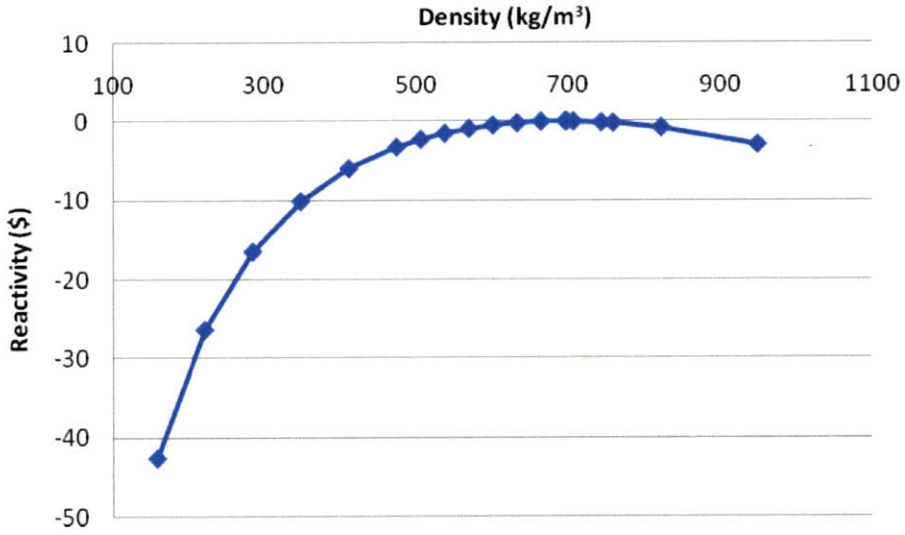

(a)

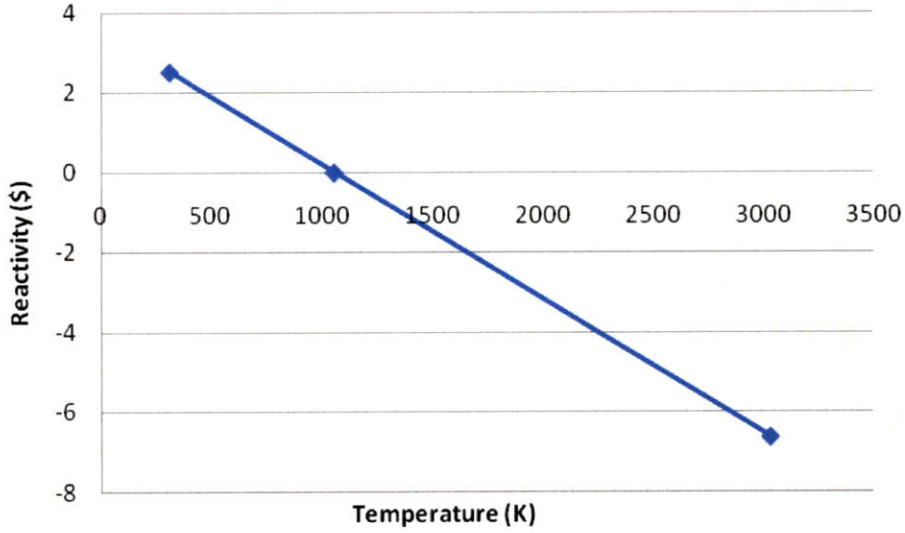

(b)

Figure 4-6 The reactivity feedback values used for (a) moderator density and (b) fuel temperature in the core

The separable model for point kinetics with feedback was chosen, which asssumes nonlinear feedback from moderator density and fuel temperature changes and linear feedback from moderator and fuel temperature changes [RELAP, 2001]. The same reactivity feedback values as in Westinghouse four loop plant for SCRAM were assumed as shown in Table 4-5.

Since the IRIS core is smaller and the boron concentration is at a lower level than the nominal Westinghouse design, these values should be conservative.

Table 4-5 SCRAM reactivity values for IRIS RELAP model

Time (sec)	Reactivity ($)
0	0
1.8	0
2.5	0
3	-0.217
3.5	-0.318
4	-1.012
4.5	-2.891
4.6	-4.336
4.7	-7.227
4.8	-10.11
5	-12.29
5.25	-13.3
5.5	-13.95
6	-14.45
¥	-14.45

4.3.2 Model of IRIS Annular Fuel Core

MIT has published several journal papers and extensive work has been done on annular fuel resulting in multiple PhD and MS theses. It was found that the 13 x 13 annular fuel assembly, with the dimensions in Table 4-6 which corresponds to Figure 1-3, results into uprating the 3411 MWth Westinghouse PWR core to 150% that power while keeping or improving the same safety margins and thermal parameters [Dandong et al., 2007].

Table 4-6 The IXAF fuel geometric specifications for 13 x 13 assembly

Parameters	Values(cm)
Dcii	0.8633
Dcio	0.9776
Dfi	0.99
Dfo	1.41
Dcoi	1.4224
Dcoo	1.5367
Pitch	1.651
Height	366

Annular fuel benefits from much lower peak fuel temperature, so that even the uprated core has a peak pellet temperature that is1300^{o}C lower compared to solid fuel, as shown on Figure 4-7.

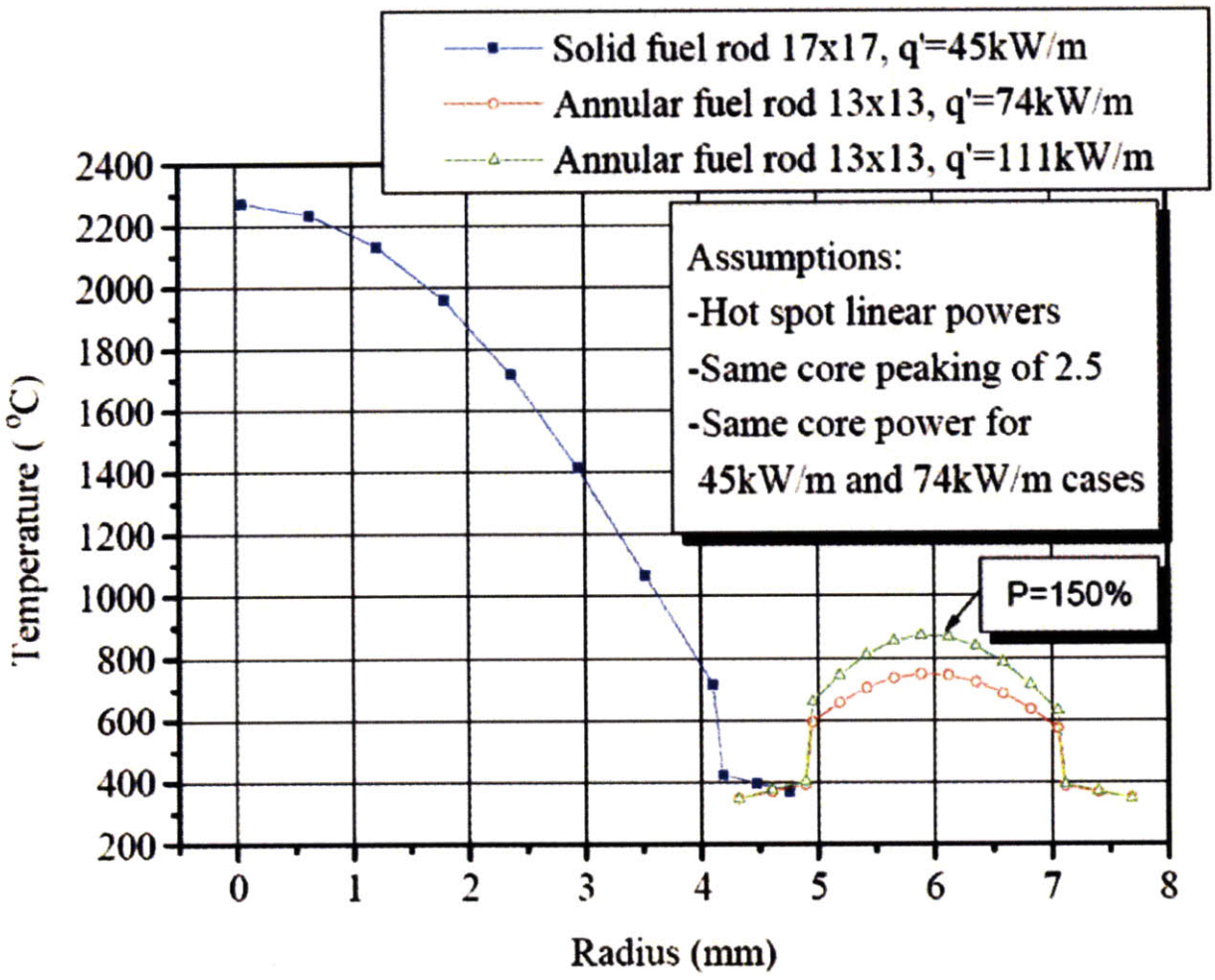

Figure 4-7 The compraison of peak fuel temperature at peak conditions for solid fuel and annular fuel (from Kazimi et al., 2006)

A complete neutronic performance of the core was made and the results show that the 18 month nominal cycle can be achieved with key parameters comparable to those of solid fuel. The rod worth, delay neutron fraction and peaking factors were almost the same value. Therefore, the Wesitinghouse 17 x 17 XL nominal fuel assemblies can be replaced with above 13 x 13 IXAF fuel assembly.

In RELAP, the core was modeled as three PIPE components, two representing the core, which are coupled together in a HEAT STRUCTURE component, and the other is the bypass

region in the core, which was neglected in the preliminary analysis, both the annular and the solid fuel core. One of the PIPE components represents the internal flow in the IXAF fuel and the other the external flow, therefore both have different flow areas, heat transfer areas and hydraulic diameters. Both PIPEs are coupled to each other by a convective boundary condition in a cylindrical geometery that is represented in Table 4-6. The number of radial meshes is increased from 10 to 14 due to the higher complexity of the IXAF geometry compared to its solid fuel counterpart. Each cladding has 3 radial meshesm with 1 for each gap and the rest are in the fuel region. It was found that RELAP only allows one gap conductance model to be used in a heat structure, therefore the gap conductance model was not used for IXAF.

The same axial power profile as for the solid fuel case (from Figure 4-4) was used, and the same temperature dependent composition data for the cladding, the gap and the fuel material. It was previously shown that the rod worth in annular fuel in case of 150% uprate is 65% of the PWR core, therefore the SCRAM reactivity data worth in Table 4-5 were adjusted for annular fuel. The same reactivity feedback coefficient use for the solid core were used for the annular core. Other components remained the same as recommended in the previous section.

4.4 Model of IRIS Pressurizer

The Brazilian Comissao Nacional de Energia Nuclear (CNEN) and the equipment manufacturer Nuclebras Equipa-mentos Pesados (NUCLEP) were responsible for the design and analysis of the IRIS pressurizer. The pressurizer of IRIS is located at the highest point in the pressure vessel. The pressurizer takes the shape of a hat attached to the primary side flow, similar to a regular PWR pressurizer. The IRIS pressurizer is insulated, which minimizes the heat transfer between the saturated fluid inside its boundary and the adjacent subcooled primary

water. The inflow and outflow of the water through the surge line is located at the bottom of the vessel. The advantage of positioning the pressurizer at the top is to avoid a separate component, which is possible since the IRIS PV has large room, which allows for large water and steam volume per unit power campared to a nominal Westinghouse PWR design [Carelli et al., 2003].

Luckily, the IRIS design team released the values of the volume of the pressurizer and the volume of steam that is present in it, which allows for an accurate RELAP model. The IRIS pressurizer volume is about 1.6 times greater than AP1000. At the same time, IRIS rated power is less than one-third of the AP1000 [Carelli et al., 2003]. This huge difference in the ratio of pressurizer volume to power allows one for elimination of the pressurizer spray function to prevent the pressurizer safety valves from lifting for any design basis heatup transients.

In RELAP, the pressurizer is designed by attaching a BRANCH to the primary fluid flow path and connecting it to a pressurizer surge line modeled as a PIPE. This PIPE is divided into 4 volumes, the first volume has an area of 0.0145 m^2, which is scaled based on IRIS pressurizer volume compared to a typical PWR and represents the surge line. The remaining volumes represent the liquid portion of the pressurizer based on the given data. The surge line is about 8 meters long while the water portion is about 1 m long with a volume of 20 m^3. The PIPE is set initially at 15.5 MPa and zero quality conditions. The water portion of the PIPE is connected to the steam portion, which is also reperesented by a PIPE connected through a SINGLE JUNCTION. The steam portion PIPE is divided into two volumes of equal size, 2.4 meters total in height, with a volume of 49 m^3. This section is initially set at 15.5 MPa and 100 percent quality, representing saturated steam.

There is a pressurizer relief valve, also modeled in RELAP, in order to maintain the core pressure while a steady state value is being reached. The relief valve is modeled as a VALVE,

and it connets the steam portion of the pressurizer to a TIME DEPENDENT VOLUME which reperesents the containment boundary. The boundary is assumed to be at 2 atmospheres of pressure and 375 K which is conservative. The valve is coupled by control variables to maintain the IRIS pressure. If the pressure of the the pressurizer rises above 16.0 MPa, the valve opens and reduces the pressure of the system by allowing primary fluid to flow out through the surgeline. Consequently, once the pressurizer pressure reaches 15.48 MPa pressure, the relief valve will be closed. A tighter band on the pressure range for IRIS with the PCHE as the SG resulted in none-steady state results. Hence the above values were the tightest ones possible for both the PHCE and the OTHSG.

4.5 Model of IRIS Pump

The IRIS pump differs from the typical Centrifugal pumps for traditional PWRs. IRIS uses "spool type" pumps, which have been used in chemical plants and marine applications. They are characterized by low head with high flow rates, operating without seals. The pump and motor are made up of two concentric cylinders, with the outer ring being the stationary stator and the inner ring being the rotor that carries high specific speed pump impellers. The advantages, compared to typical "canned pumps", are the smaller space required and that with electrical power cables becomes the only penetration to the IRIS RV. Currently, using high temperature materials is being evaluated to eliminate the cooling of the pumps. The IRIS design team claims that the spool pump geometry results in maximum rotating inertia and run-out flow that will achieve better performance under Loss-OF-Flow Accidents (LOFAs) [Kujawski et al., 2002]. However, the performance is not better compared to typical PWR as will be shown later. Table 4-7 lists some of the specification of the IRIS pumps.

Table 4-7 The spool type pump calculated specifications

Specification	Value	Units
Flow Area	0.07	m^2
Speed	1800	rpm
Moment of Inertia	1.43	kg-m^2
Flow Rating	8.1	m^3/s
Torque	500	N-m

A vertical cross-section of a pump and a horizontal view of the pumps are shown below in Figure 4-8. The dimensions given in the patent description of the pump agree with the dimensions of the IRIS reactor [Kitch et al., 2004]. Therefore, it is assumed that the same dimensions apply to a realistic view of the pumps. The side view of the pump in right side of Figure 4-8, has the impeller more upstream in relation to the cylindrical hub compared to an ordinary spool type pump. Due to the rating (flow and head) of the pump, there is a need for providing some mixed flow, which the configuration in Figure 4-8 provides. This configuration provides specific speed of about 5,000 to 9,000 units at a rotation of 1800 rpm. Furthermore, if more motor cooling is needed, additional cooling tubes can be provided to establish heat transfer from the stator to the reactor coolant.

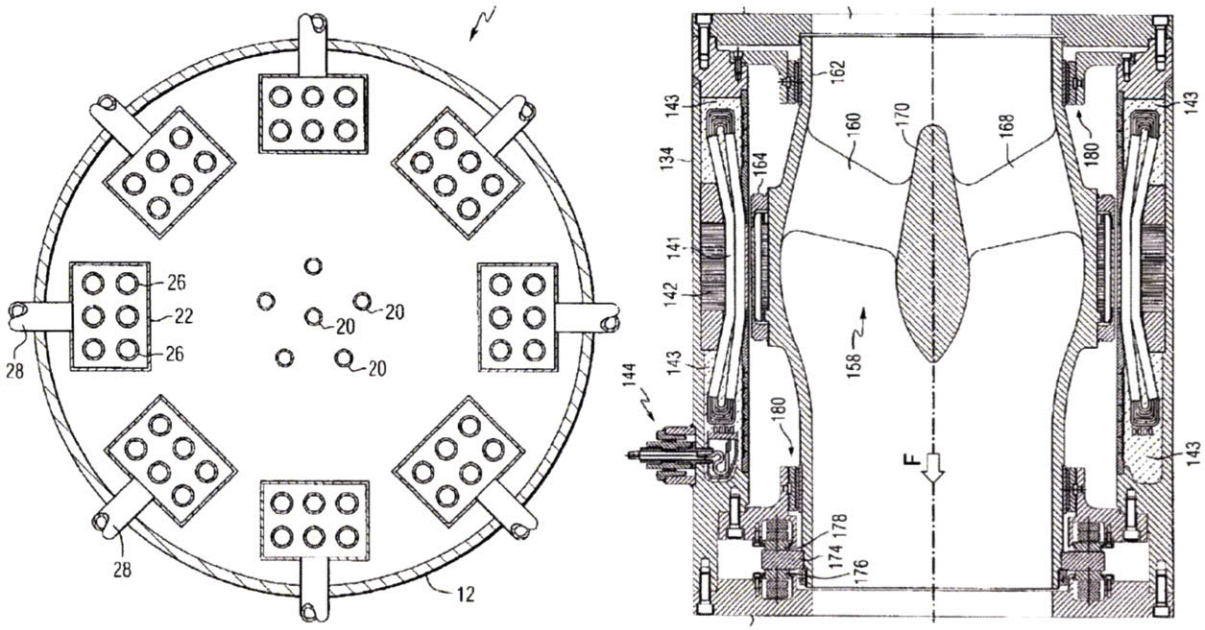

Figure 4-8 The view of pumps in the IRIS reactor from the top and side (from Kitch et al., 2004)

The RELAP model of all the 8 pumps in IRIS is designed as one PUMP component, located in a region just above the steam generator. The pumps have vertical rotation and are 2 m in length, which is estimated based on IRIS drawings. Most of the pump specifications were estimated based on the required flow rate and IRIS head. Other specifications are based on typical centrifugal pumps such as tables for void and torque friction coefficients. The flow rate through the pump is monitored through control variables after 100 sec of simulation to achieve the desired mass flow rate. The flow rate in the section before and after the pump is recorded and the error between the flow rates is signaled through the pump rotational velocity. This added control logic resulted in an exact mass flow rate value to 6 significant figures, agreeing across the IRIS RELAP model.

4.6 Model of IRIS Pipes/secondary side

The lack of complex piping makes the RELAP modeling of the IRIS reactor convenient. The down comer is modeled as an annulus of water with 1.6 m width. This down comer is

orders of magnitude larger than typical PWR which provides the IRIS vessel with significant shielding against neutron dose. The large downcomer also slows down fluid flow accounting for about 50% of the total time needed for the primary fluid to circulate through the reactor. The entire IRIS piping was modeled as PIPE components, and no time dependent volumes were used to control the operating pressure and the temperature. The model was actuated as a transient and allowed to reach steady state conditions by reaching equilibrium after 500 sec of simulation. The total vertical height in RELAP excluding the pressurizer was modeled to be 17.3 m, which is a key parameter for natural circulation during an accident scenario.

The secondary side of the RELAP model does not include any turbines or pumps. The inlet water flow rate, temperature and pressure is fixed by TIMEDEPENDENT JUNCTION and TIMEDEPENDENT VOLUME components in RELAP and set to IRIS nominal conditions. Under the Loss of Feed Water Accident (LOFWA) conditions, these time dependent sections are bypassed to produce physical conditions during the accident.

4.7 Model of IRIS Safety Systems

4.7.1 Model of IRIS EHRS

To analyze the long term decay heat removal using PCHE, a passive Emergency Heat Removal System (EHRS) has to be designed in the RELAP model. The EHRS as designed in IRIS is composed of horizontal, U-tube heat exchanger connected to a separate SG feed/steam line. The separate lines enable the IRIS reactor to be separated from any possible "radioactive" water leaking through the secondary side to the turbine, and keep the consequences from such accident inside the containment, disallowing containment bypass. The U-tube heat exchangers

are located inside the Refueling Water Storage Tank (RWST) located outside the containment. Once an accident occurs, the secondary pipe valves are closed and the EHRS valve to the secondary side of the SG is opened. The water flows through the pipes depending on the gravity head provided by the height of the SG relative to RWST. The water is heated up and then returned to RWST, where it condenses/cools down and the sub cooled water is returned to the pressure vessel to remove decay heat of the reactor. The current EHRS also has the ability to provide make up water to the primary side in case of a LOCA, and the primary mode of system depressurization. Therefore, it is responsible for core cooling and containment depressurization. There are also two emergency borated tanks (EBTs) to provide another way of shutting down the reactor and can be both directly injected in the vessel [Carelli et al., 2003].

In RELAP, the RWST is represented as a VOLUME component. The U-tube heat exchangers are not explicitly modeled due to the ambiguity in their exact design and features. However, the RWST water and the EHRS temperature and pressure behave accordingly compared to the published results by the IRIS design team. The SG secondary inlet and outlet are connected to two valves from which one set connects the SG to the time dependent volumes described above and the other set connects it to the EHRS. The RWST is located about 1.8 meters below the SG inlet, approximated from the drawings provided by the IRIS design team. It is noted that there is same ambiguity even within the IRIS team about the exact specifications of the EHRS and the design can be changing with time. However, as it will be seen later, this uncertainty will not affect the safety performance of IRIS if the OTHSG is replaced by the PCHE.

4.7.2 Model of IRIS ADS

The IRIS reactor also contains a small Automatic Depressurization System (ADS) that helps the EHRS by depressurizing the primary side inside the reactor vessel. In some cases the pressurizer water level could drop below a specific value and the abrupt pressure change could affect the core significantly and may cause fuel melting. The ADS is composed of two 4 inch lines where they are connected to the suppression system pool tanks through a sparger. The ADS is not used under the nominal operating conditions and its job is to ensure that the vessel and containment pressure are decreased safely and prevent the core from being uncovered [Carelli et al., 2003].

The inclusion of an ADS model in the RELAP model is necessary, especially in case of using the PCHEs instead of the OTHSGs. The smaller size of PCHE will make the transient occur faster and the system pressure needs to be controlled. This is achieved by creating a VALVE component connected to the steam side of the pressurizer. The valve is connected to two PIPE components, one going horizontally outward and the other going downward about 1 m below the pressurizer. Again, the length is an approximation based on IRIS design layouts, however the flow pipe is 8 inch in diameter and consistent with reported IRIS specifications. The pipes are connected to a SINGLE VOLUME component, representing the suppression pool. The suppuration pool is initially at the containment pressure of 5 bars. Using control logic variables, the ADS is shut off until the accident sequence begins. The ADS function is used in the RELAP5 model, when the pressurizer safety valve logic signal is open and the pressure exceeds 2600 psi. In the case of reducing the vessel diameter size will consequently reduce the pressurizer volume, making the ADS function more important in controlling peak pressure.

4.8 IRIS Plant Calculated Results

4.8.1 IRIS Plant preliminary steady state

The above description provides the logic and explanation behind the IRIS RELAP model developed for this project. There is room to improve the complexity of the design, especially accounting for vessel walls thermal inertia and adding remaining safety systems. Figure 4-9 illustrates most of the components modeled in the simplified RELAP input. Also, Table 4-8 describes the various steady state models that were created.

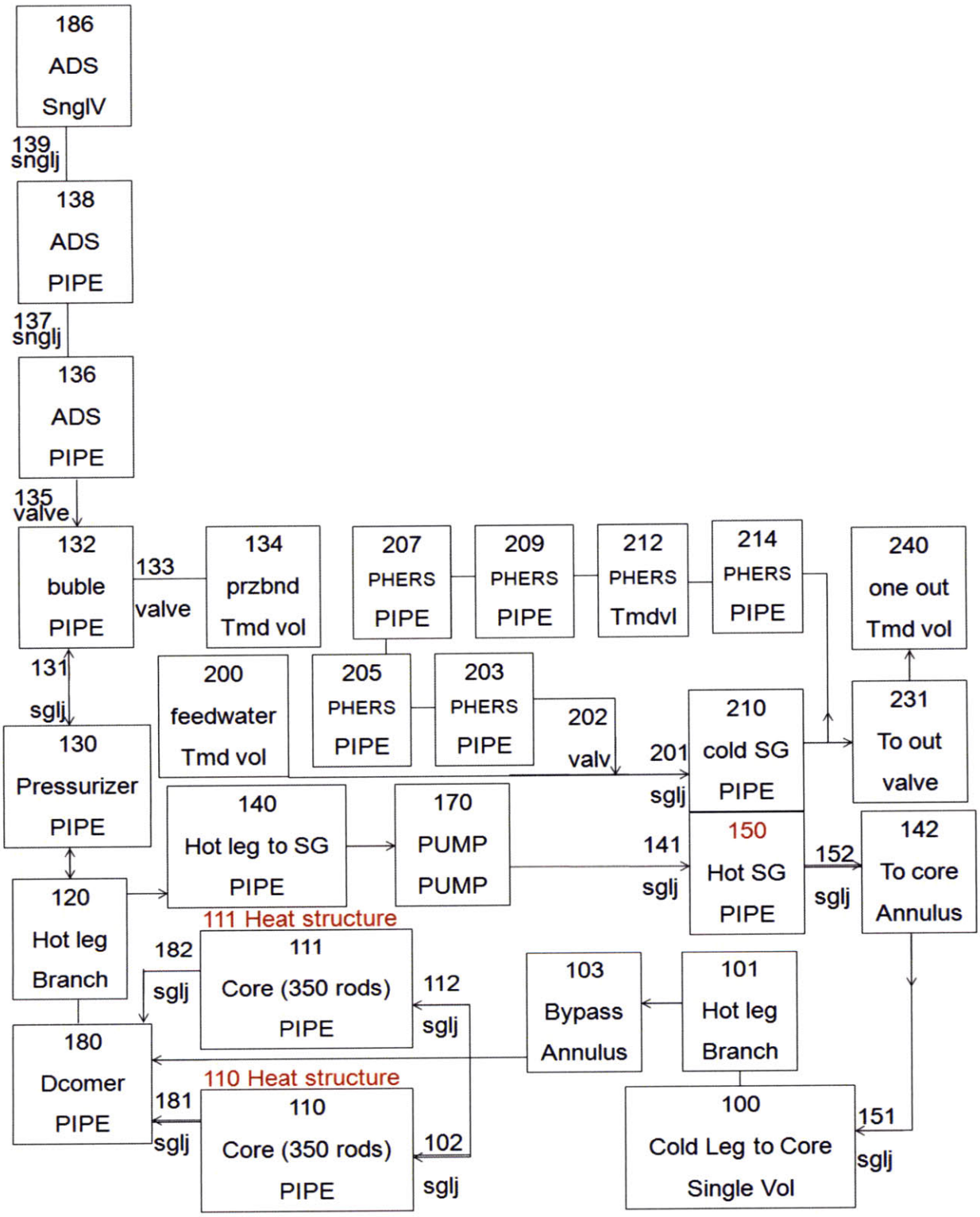

Figure 4-9 IRIS simplified RELAP model

Table 4-8 The Steady-State results for the simplified RELAP model

Parameter	Unit	Reference	RELAP5 Creators	RELAP5 MIT HSG	RELAP5 MIT SPCHE	RELAP5 MIT ZPCHE
Pressurizer pressure	MPa	15.5	15.56	15.51	15.46	15.48
BE vessel flow	kg/s	4707	4702	4706.9	4707	4707.3
BE core flow	kg/s	4504	4503.6	NA	NA	NA
Core inlet temperature	K	565.2	564.7	564.9	564.841	564.84
Core outlet temperature	K	601.5	601.4	601.354	601.348	601.35
SG pressure	MPa	5.8	5.79-5.82	5.8-6.06	5.8-5.81	5.8-5.82
Steam exit temperature	K	590.2	589.6-590.2	590.588	591.594	591.143
Total steam flow	kg/s	502.8	502.8	502.8	502.8	502.8
Dp core	kPa	52.0	53.8	48	47	47
Dp SG1 prim/sec	kPa	72.0/296	70.7/294.4	50/256	22/14	50/50
Core power	MW	1000.0	1000.0	9999	1000.4	1000.1
Total SG power	MW	1001.47	1000.3	1000.6	1000.7	996
RCP head	m	19.1	19.8	11.33	11.33	11.35

The MIT RELAP cases in Table 4-8 do not exactly correspond to the final IRIS design model since these are more simplified models as described in the above section. They provide fast and easy way to compare the performance of the PCHE vs. OTHSG for conditions and geometry close to those of the IRIS reactor. Once confidence is built about the PCHE safety performance, more accurate design considerations will be taken into consideration, such as accounting for system bypass flow rate. Overall, the performance of the MIT developed RELAP model is very close to the reference model, with the key difference being in the pump head, which is due to use of default roughness and pressure loss coefficient in RELAP and simplification of the overall design.

To examine the PCHE safety performance, two PCHE geometries were considered, straight and zigzag channels. The reason the straight channels case was considered is because of uncertainty about the zigzag PCHE performance under high Re number and boiling conditions. The equivalent straight PCHE specifications were listed in Chapter 3, which showed the straight channels to be almost twice as long as the zigzag channels.

Table 4-9 lists a summary of accidents consequences in the IRIS reactor compared to a typical PWR. The safety of the nominal design with the OTHSG and the two PCHE geometries were examined by simulation of the two main accidents in which short term and long term behavior of the IRIS system was monitored: the LOFA and the LOFWA. In fact, these are the only two accidents mentioned in Westinghouse WCAP on IRIS preliminary safety analysis [2003], which were affected by the OTHSG being a once through SG. The LOCA was not analyzed since the IRIS integral vessel eliminates large break LOCAs. In order to model a small break LOCA, the detailed model of the vessel and EHRS is needed. It was decided, as it will be seen shortly, that the impact of using PCHE instead of OTHSG would not be of any concern due to comparable heat transfer areas. More discussion of why the small break LOCA will not be affected by the steam generator option in final IRIS design will be given later. Also, the transients such as steam tube rupture, or the sudden increase in inlet temperature that are considered in traditional PWRs will not be considered here, since both OTHSG and PCHE are once-through type steam generators.

Table 4-9 The list of design basis accidents and IRIS's general response (from Carelli et al., 2003)

Condition IV Design Basis Events		IRIS Design Characteristic	Results of IRIS Safety-by-Design
1	Large Break LOCA	Integral RV Layout – No loop piping	Eliminated by design
2	Steam Generator Tube Rupture	High design pressure once-through SGs, EHRS, piping, and isolation valves	Reduced consequences, simplified mitigation
3	Steam System Piping Failure	High design pressure SGs, piping, and isolation valves. SGs have small water inventory.	Reduced probability, reduced (limited containment effect, limited cooldown) or eliminated (no potential for return to power) consequences
4	Feedwater System Pipe Break	High design pressure SGs, piping, and isolation valves. Integral RV has large primary water heat capacity.	Reduced probability, reduced consequences
5	Reactor Coolant Pump Shaft Break	Spool pumps have no shaft	Eliminated by design
6	Reactor Coolant Pump Seizure	No DNB for failure of 1 out of 8 RCPs, even without Reactor Trip.	Reduced consequences
7	Spectrum of RCCA ejection accidents	With internal CRDMs there is no ejection driving force	Eliminated by design
8	Design Basis Fuel Handling Accidents	No IRIS specific design feature	No impact

4.8.2 IRIS Plant Transient Analysis

In this section, the impact of PCHE and IXAF fuel on the IRIS reactor response during two main transients: LOFA and LOFWA are analyzed for the short term and long term. The analysis is done using the simplified models described earlier to obtain reasonable runtime before the final optimization is done. Furthermore, the circulation loop time was cut in half, for conservative estimates by reducing the loop length. This allows the analysis to be extrapolated to all designs and does not require the final optimized IRIS results to be rerun in detail, since the preliminary results will be more conservative.

4.8.3 IRIS Plant LOFA transient Analysis

The following sequence was used for the LOFA accident as proposed by one of the published works of IRIS design team [Ricotti et al., 2002].

Table 4-10 The Accident sequence for a complete LOFA for the IRIS reactor

Accidents Sequence:	**Initiation**
Pump loss of power	t = 0
Scram	delta T across core reaches 118% of nominal value
The Feed water isolation Valve closure	Scram time + 5.0 sec
Main steam isolation Valve closure	Scram time + 10.0 sec
Emergency Heat Removal Valve Opening	Scram time + 15.0 sec

In general, what initiates LOFA is loss of electrical power to the pump, in this case loss of electrical power to all 8 pumps. Then, the pumps start to coastdown, where their coastdown rate depends on their rotational characteristics. RELAP provides many options to trip the PUMP components by supplying rotational and torque tables or using predefined equations during loss of power to pumps until the natural circulation is established. However, there is little known about the spool type pumps and for this analysis it was assumed that the pumps do not provide any coast down.

The event was initiated by replacing the PUMP component by its effective length PIPE. Once this occurs, the immediate effect is a rapid increase in the primary coolant temperature. In RELAP, control variables are defined to monitor the temperature across the core inlet and the outlet, and once this difference reaches 118% of the steady state variable, the SCRAM signal is initiated. It is noted that the core reaches the steady state after 80 seconds, however, the simulation was ran to 200 sec to obtain the optimum results. The feed water isolation valves are

closed 5 sec after the SCRAM time, and it was assumed that it takes another 5 seconds to close the steam isolation valve. Fifteen seconds after SCRAM time the EHRS valves are open.

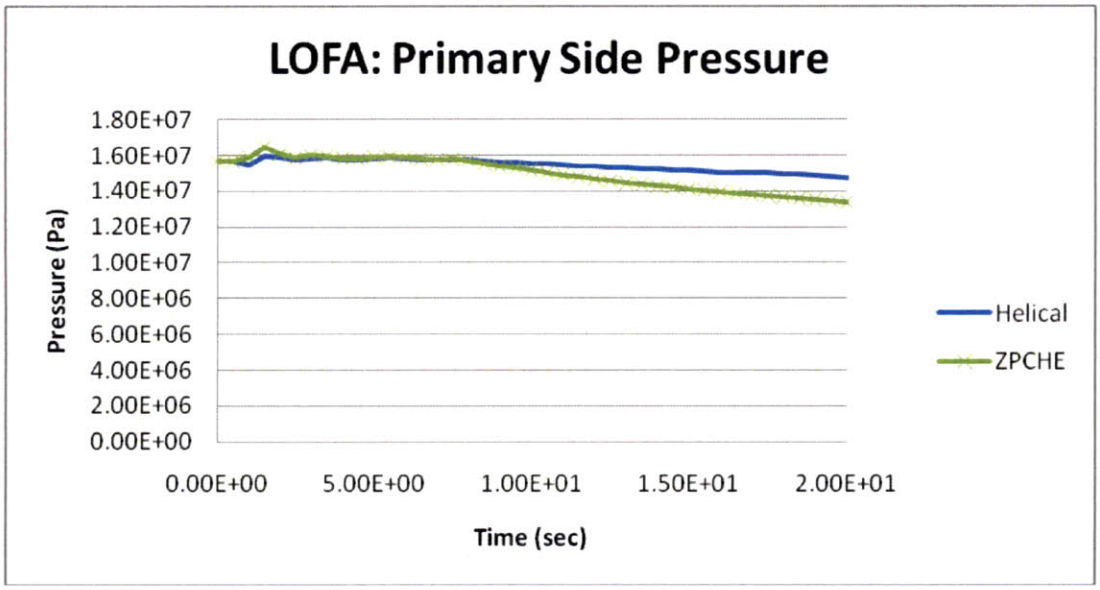

(a)

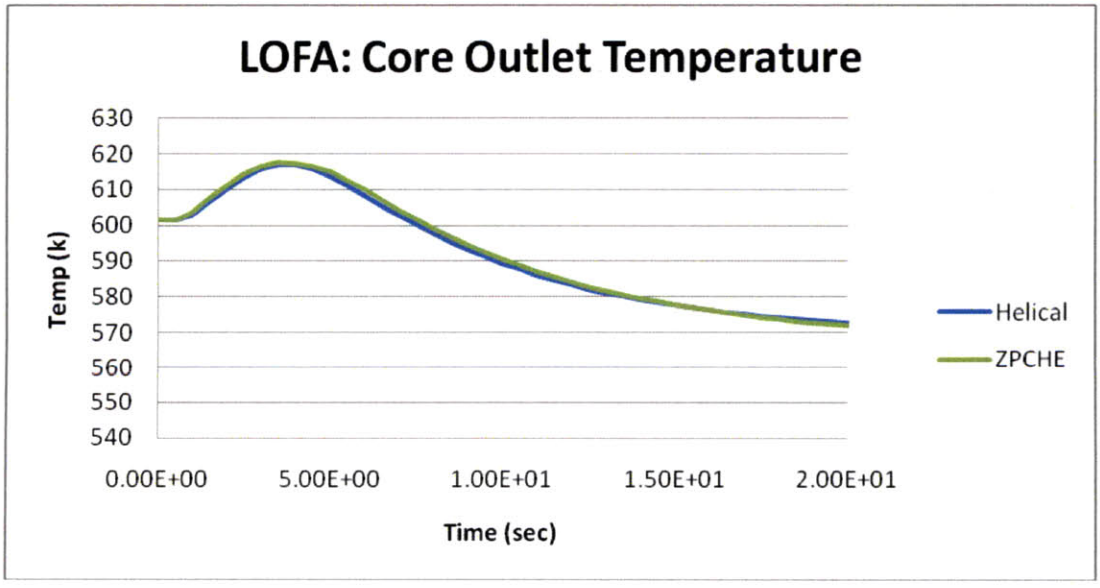

(b)

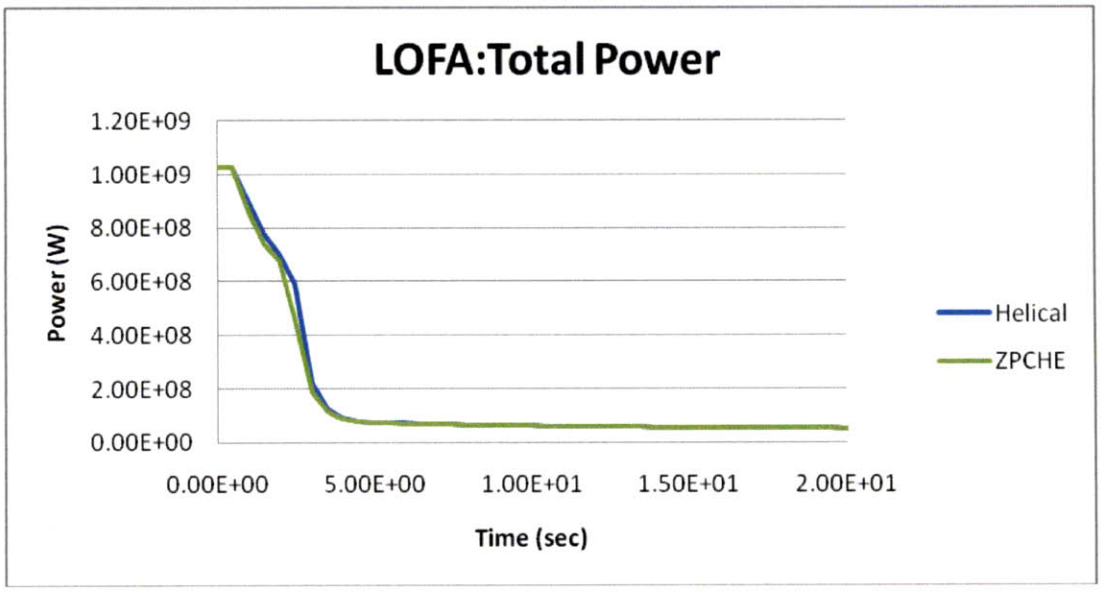
LOFA:Total Power
1.20E+09
1.00E+09
8.00E+08
6.00E+08
4.00E+08
2.00E+08
0.00E+00
Power (W)
0.00E+00
5.00E+00
1.00E+01
1.50E+01
2.00E+01
Time (sec)
Helical
ZPCHE

(c)

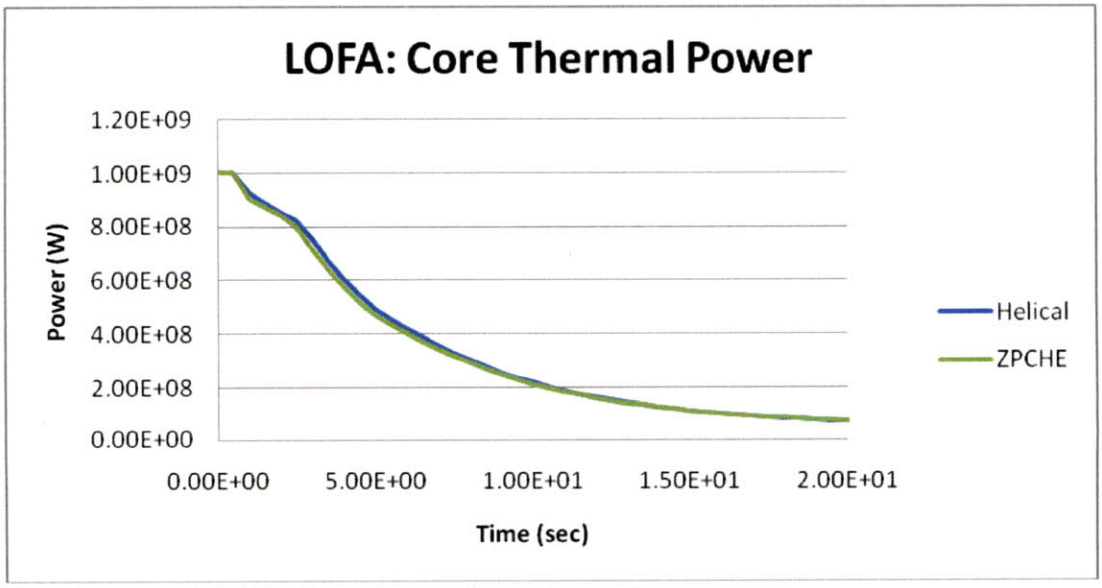
LOFA: Core Thermal Power
1.20E+09
1.00E+09
8.00E+08
6.00E+08
4.00E+08
2.00E+08
0.00E+00
Power (W)
0.00E+00
5.00E+00
1.00E+01
1.50E+01
2.00E+01
Time (sec)
Helical
ZPCHE

(d)

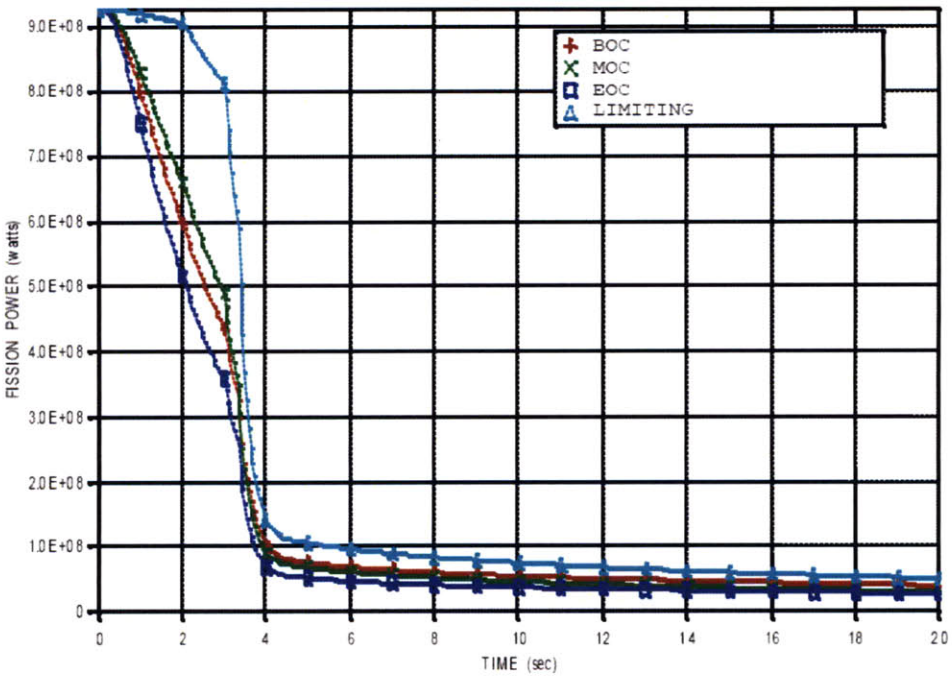

(e)

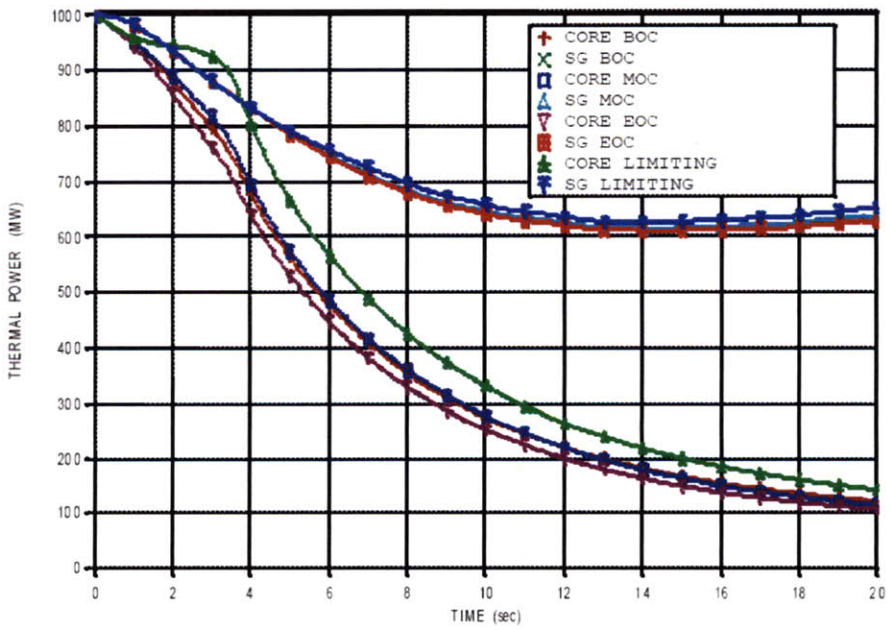

(f)

Figure 4-10 The MIT RELAP model calculated response following LOFA (a) the core pressure, (b) the Temperature, (c) the Fission power, (d) the Thermal power and the Westinghouse results for (e) the fission power and (f) the thermal power (from Bajs et al., 2002)

Figure 4-10 presents the predictions of the MIT and Design Team RELAP models for core pressure, inlet core temperature and the fission thermal power. It shows that the predicted behavior is very similar for both models. It also shows that the MIT simplified model is on the conservative side, since the total fission power behavior is closer to the limiting case in Figure 4-10e. The liquid fraction in the core was tracked and it remained above 95%, which means the core was not uncovered.

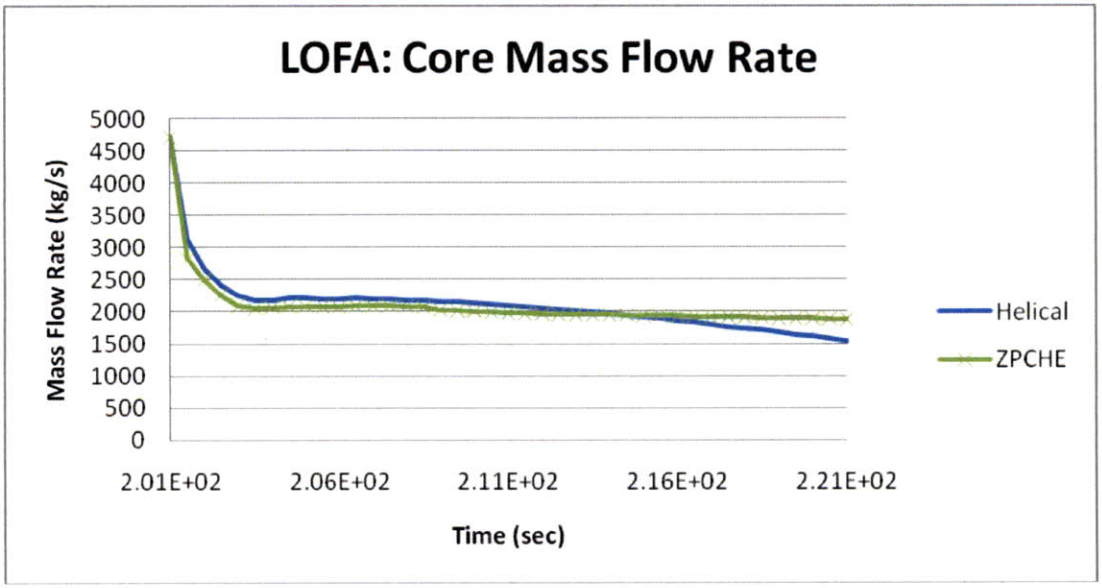

(a)

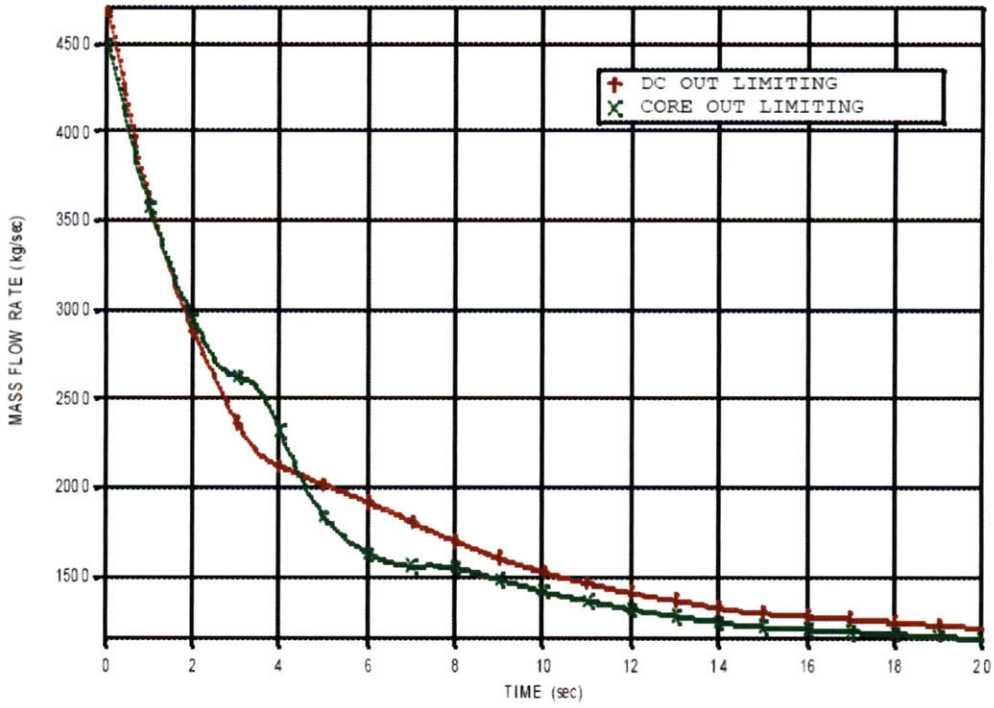

(b)

Figure 4-11 The MIT RELAP model during the LOFA of the core mass flow rate (a) and the Westinghouse results (b) (from Bajs et al., 2002)

The Figure 4-11 presents the results of the MIT and Design Team RELAP models for the total mass flow rate. Both figures are very similar to each other, however, the MIT predicted flow decreases far quicker than the published result. This is due to not accounting for the pump coastdown rate. However, after 20 seconds of accident time the amount of flow rate for natural circulation is about the same for both models. It is noted (as can be seen in Figure 4-11a) that the core with PCHE reaches natural circulation limit faster due to its much smaller thermal inertia. Also, the steady state natural circulation flow is higher due to the smaller pressure drop of the PCHEs and larger height difference between the core and the SG centers.

The longer term behavior of the core was also analyzed to make sure that the PCHE can provide long term cooling to remove the decay heat. For this section the ADS plays an important role as can be seen in Appendix C.

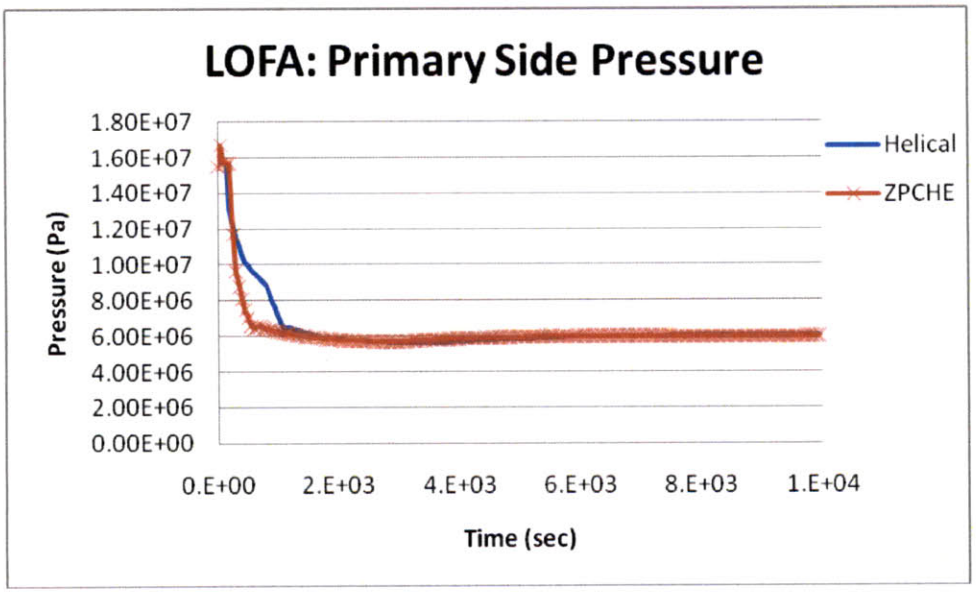

(a)

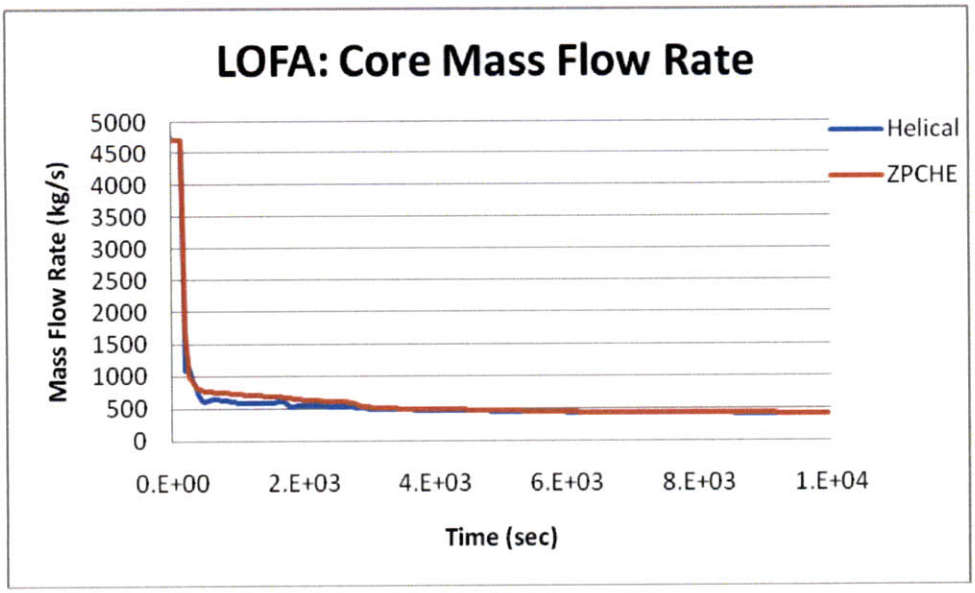

(b)

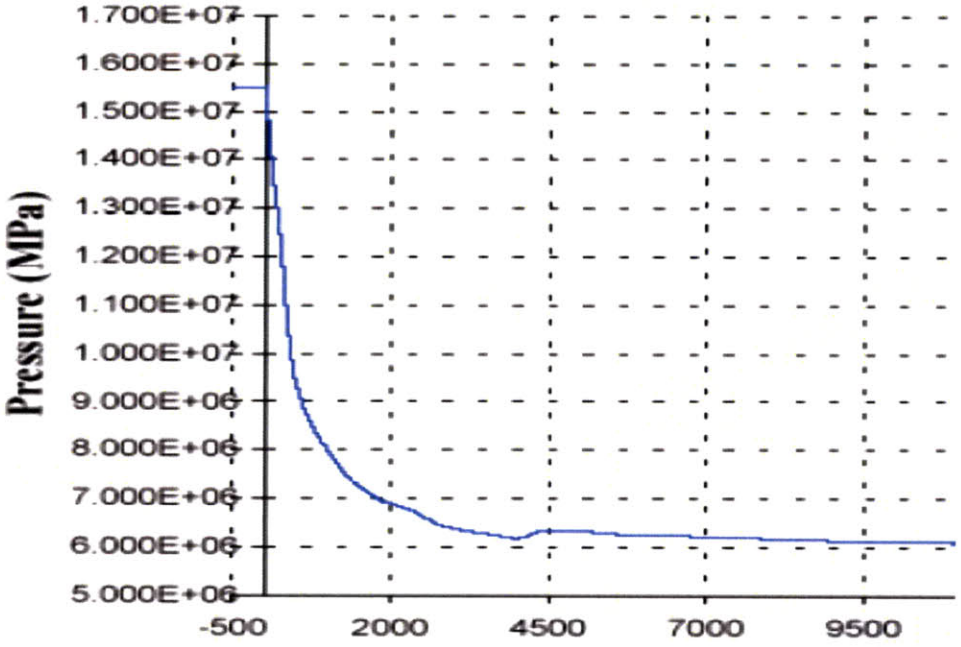

(c)

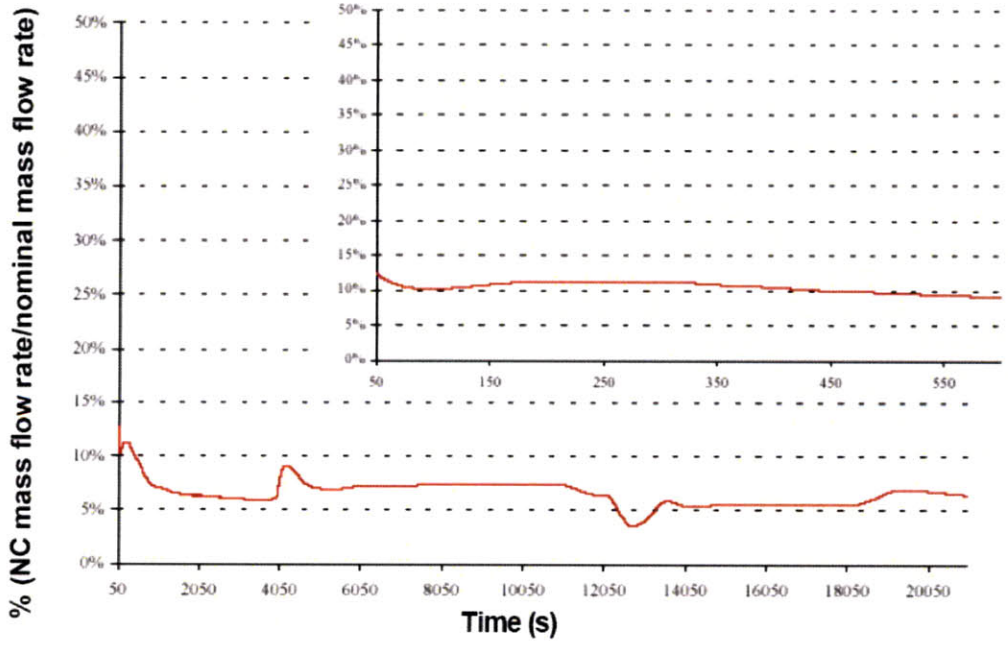

(d)

Figure 4-12 The long term behavior prediction of MIT RELAP model following a LOFA of (a) the core pressure and (b) the mass flow rate and the Westinghouse results for (c) the core pressure and (d) the mass flow rate (from Ricotti et al., 2002)

Even if longer times are considered, it is shown in Figure 4-12 that the RELAP results for system pressure are almost identical to the published results by IRIS team. Similar to the system pressure, the long term behavior of the core mass flow rate was found to be very close to the Westinghouse results in terms of the amount of natural circulation in the core. It is noted that Figure 4-12d shows some oscillations, which according to the authors are likely to be unphysical and due to errors in their RELAP model.

The above overall results indicate that replacing the OTHSG with the PCHE has very little effect on both the short term and long term behavior of the system.

4.8.4 IRIS Plant LOFWA transient Analysis

The following sequence was used for the Loss Of FeedWater Accident (LOFWA) as proposed by one of the published works of IRIS design team [Ricotti et al., 2002].

Table 4-11 The Accident sequence for a LOFWA for the IRIS reactor

Accidents Sequence:	**Initiation**
Break in Feedline	t = 0
Scram	10 sec
The Feed water isolation Valve closure	Scram time + 5.0 sec
Main steam isolation Valve closure	Scram time + 5.0 sec
Emergency Heat Removal Valve Opening	Scram time + 10.0 sec

In general, what initiates the LOFWA is a break in the secondary pipe, due to reasons which were previously discussed. Also, the break will have to be outside of the IRIS reactor

vessel due to the integral nature of the IRIS reactor. In RELAP, the break is modeled as the inlet main feed water valve closing, once steady state has been reached. The reactor is SCRAMed after 10 seconds of accident initiation, and 10 after that the EHRS valves are opened. Since the turbine and other NSSS components were not modeled and the break is at the inlet of SG, it is expected that the PCHE very small size will have a significant effect on the accident, unlike the LOFA accident as discussed in more detail in Appendix C.

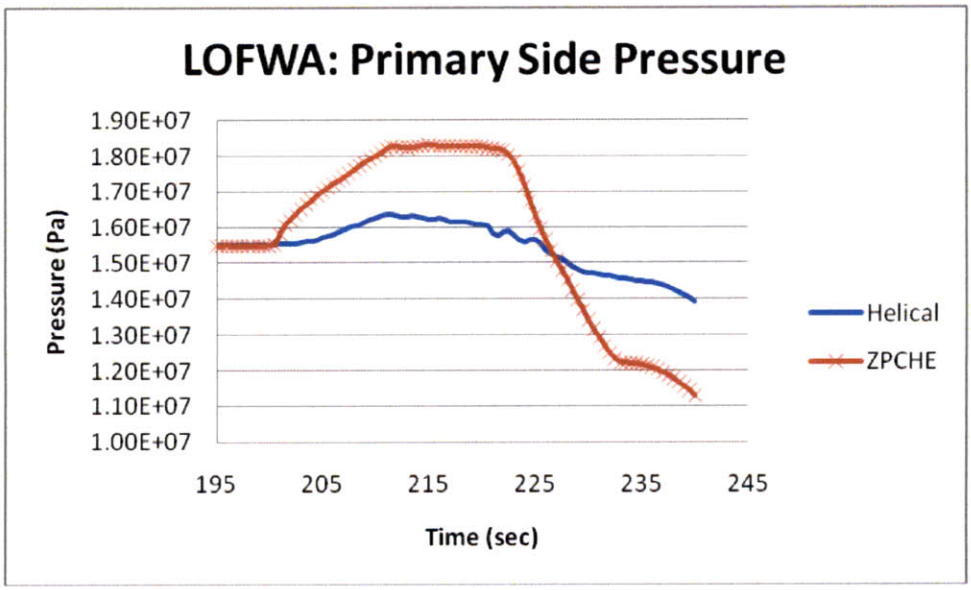

(a)

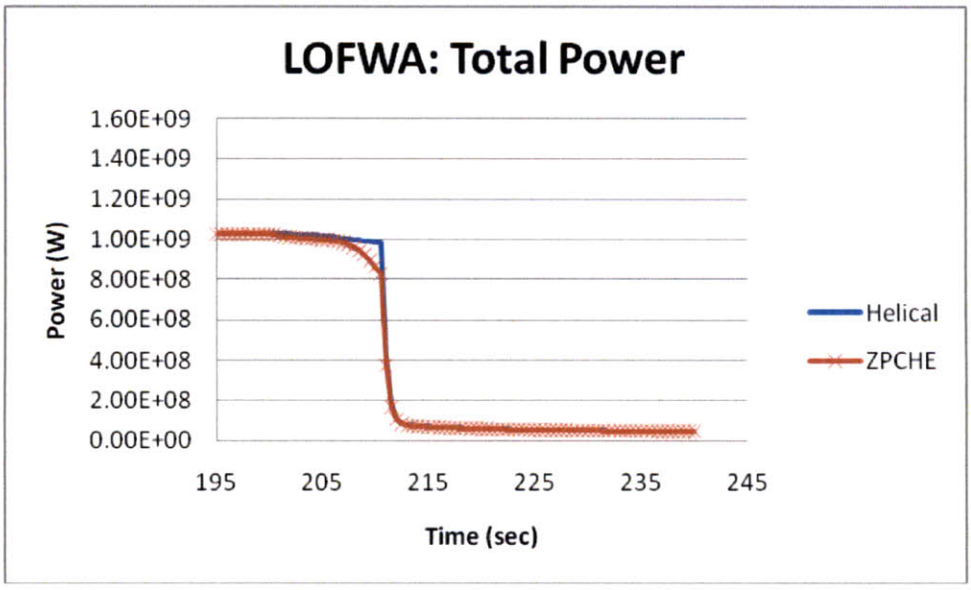

(b)

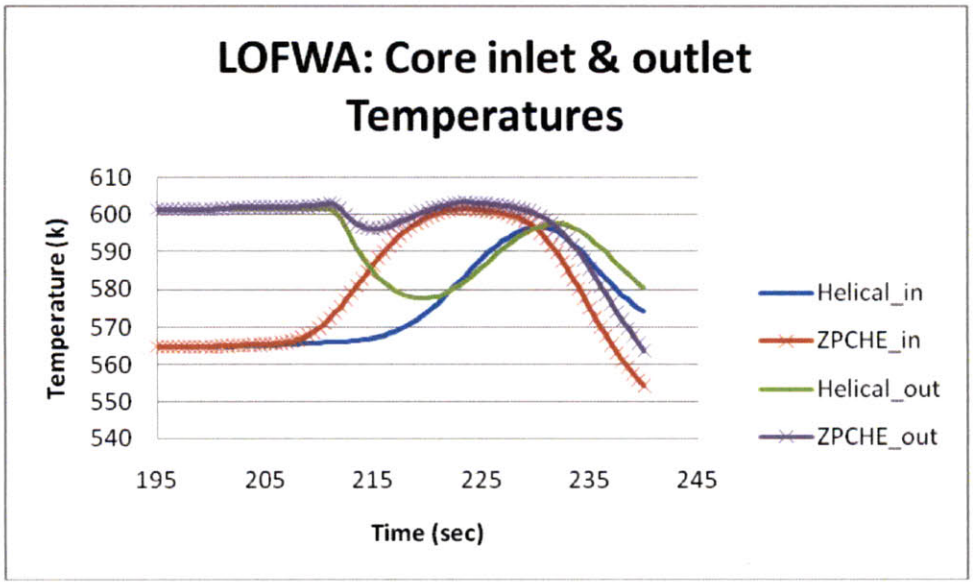

(c)

Figure 4-13 The short term behavior of MIT RELAP model during the LOFWA of (a) the core pressure, (b) the total power and (c) the inlet and outlet temperature

Figure 4-13 shows the system power, inlet/outlet temprature and pressure as the transient progresses 20 seconds after the EHRS valve opening. The replacement of the OTHSG with the PCHE has magnified the results for the LOFWA. The total power decreases significantly in the

10 seconds untill the SCRAM time and the core temperature reaches higher peak values than the OTHSG after the transient.

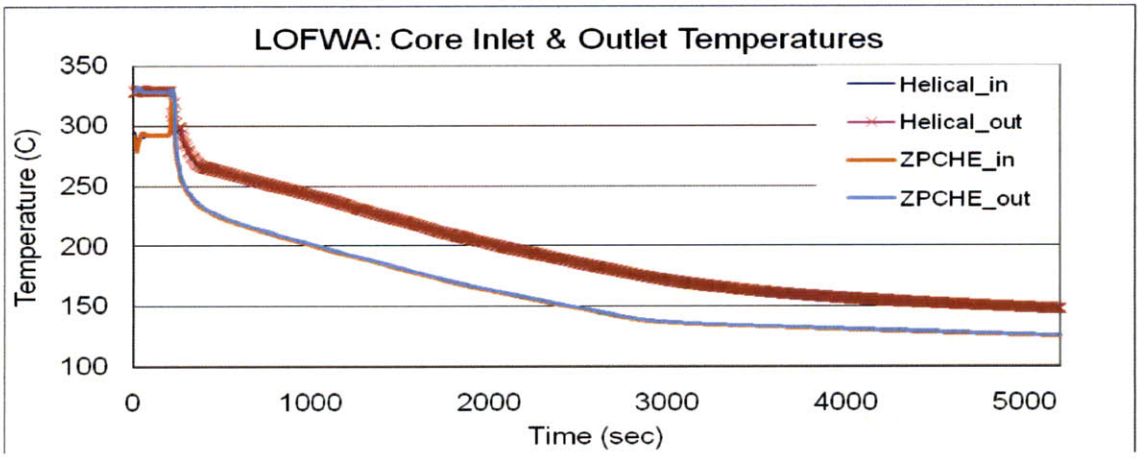

(a)

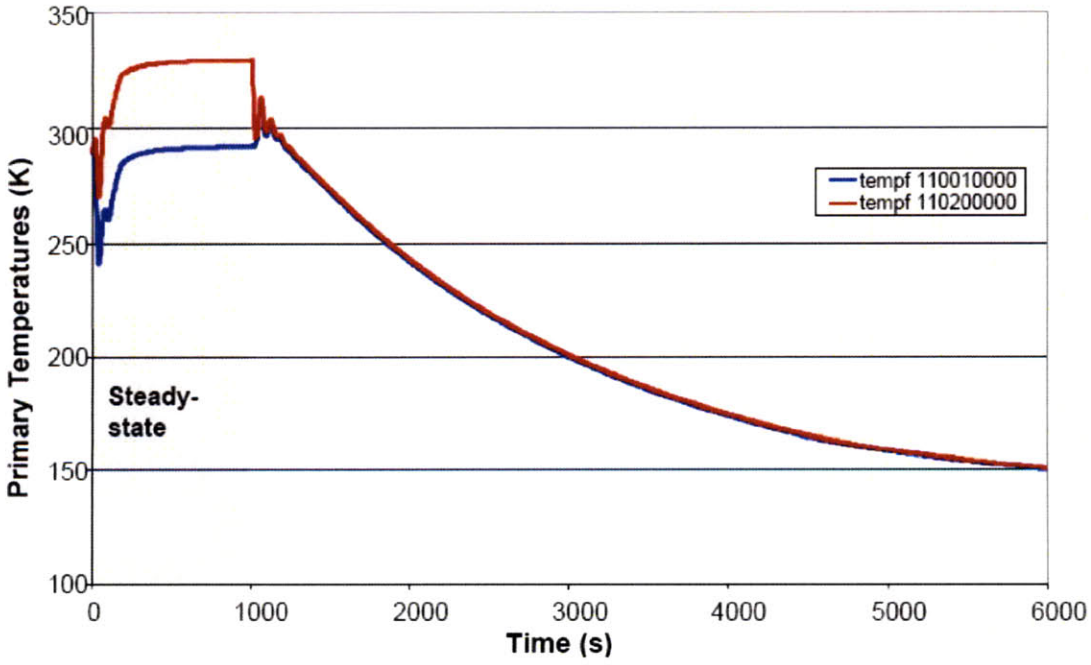

(b)

Figure 4-14 The long term behavior of MIT RELAP model during the LOFWA of (a) the core inlet and outlet temperatures and the (b) Westinghouse results (from Ricotti et al., 2002)

Figure 4-14 compares the MIT and the published results of the RELAP models for long term behavior during the LOFWA for the core inlet/outlet tempratures. As shown for the case with OTHSG the curves are almost identical, while for the PCHE the core temperature reaches lower value compared to the OTHSG, in part due to the higher natural circulation height and shorter channel length compared to the OTHSG.

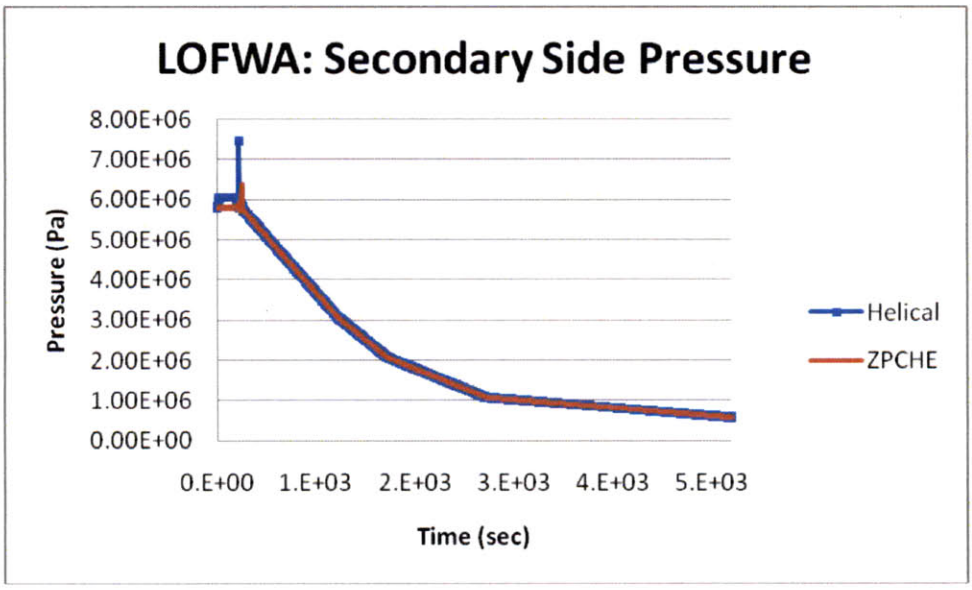

(a)

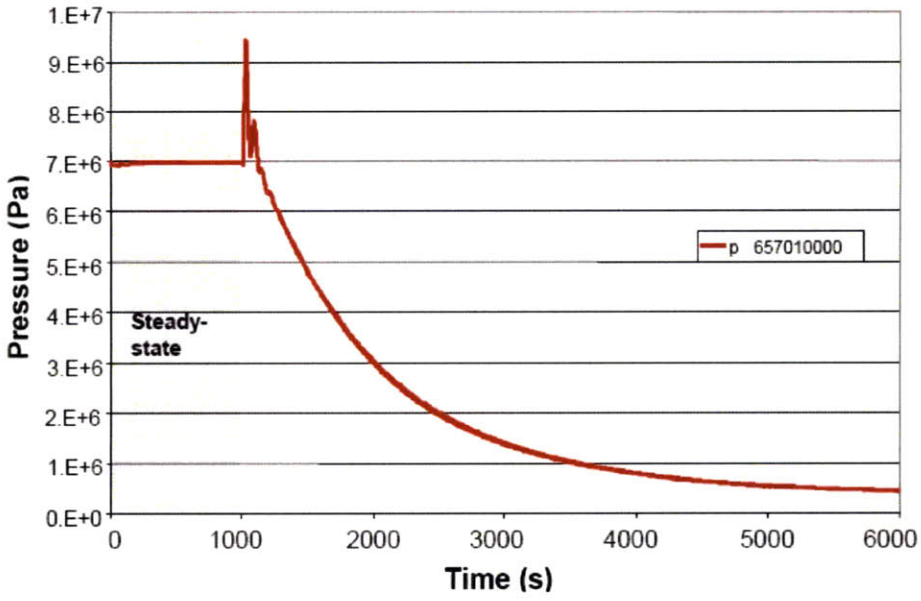

(b)

Figure 4-15 The long term behavior of MIT RELAP model during the LOFWA of (a) the core pressure and the Westinghouse results for (b) the core pressure (from Ricotti et al., 2002)

Figure 4-15 compares the MIT and the published results of the RELAP models for the long term behavior following a LOFWA for the secondary side pressures. This is further proof that the MIT RELAP model behaves the same as the Design Team RELAP model, and the PCHE experiences lower peak pressure in the secondary side due to much faster fluid flow through its channels compared to the OTHSG tubes. Just like in the LOFA, the core liquid fraction was monitored durign the entire accident and it never changed significantly.

4.8.5 IRIS Plant with Annular Fuel Model

The solid fuel RELAP model was modified to account for the IXAF geometry as described in the previous section. The core power and mass flow rates were raised to 150%. The total flow and heat transfer areas for the pumps, both type of SGs and the EHRS loops were

also raised by 150%. Some pipe sizes for the inlet and outlet of the SGs were changed but the total flow area above the core remained the same, including the ADS system size. The height of the vessel also remained the same for this analysis. As mentioned in section 4.3.2 the RELAP neutronic prameters stayed the same, excpet in case of 150% power uprate the rod worth were decreased by 35%. The preliminary steady state results are shown in Table 4-12:

Table 4-12 The Steady-State RELAP results for the simplified IRIS with IXAF model

Parameter	Unit	Reference	MIT+ Helical+IXAF	UPRATE+Helical+IXAF	UPRATE+ZPCHE+IXAF
Pressurizer pressure	MPa	15.5	15.46	15.49	15.49
BE vessel flow	kg/s	4707	4707	7060.5	7060.5
BE core flow	kg/s	4504	NA	NA	NA
Core inlet temperature	K	565.2	565.601	564.722	564.755
Core outlet temperature	K	601.5	602.075	601.323	601.341
SG pressure	MPa	5.8	5.8-6.1	5.8-6.1	5.8-6.1
Steam exit temperature	K	590.2	593.01	590.712	591.45
Total steam flow	kg/s	502.8	502.8	754.2	754.2
Dp core	kPa	52.0	55.6	92.4	91.5
Dp SG1 prim/sec	kPa	72.0/296	56/270	70/281	51/36
Core power	MW	1000.0	1004.4	1500.61	1499.1
Total SG power	MW	1001.47	1004.75	1501.46	1499.8
RCP head	m	19.1 (18.3-21.3)	11.37	21.4	21.3

The inlet and outlet temperatures are close to each other. The core pressure drop as expected was much higher (about 80%); also the pressure drop across the reactor vessel is about twice what it was for nominal mass flow rates. One consequence is that the pumps head rating needs to be larger. The LOFA and LOFWA cases were run for the conditions described in the previous section and the results are described in the following paragraphs and figures.

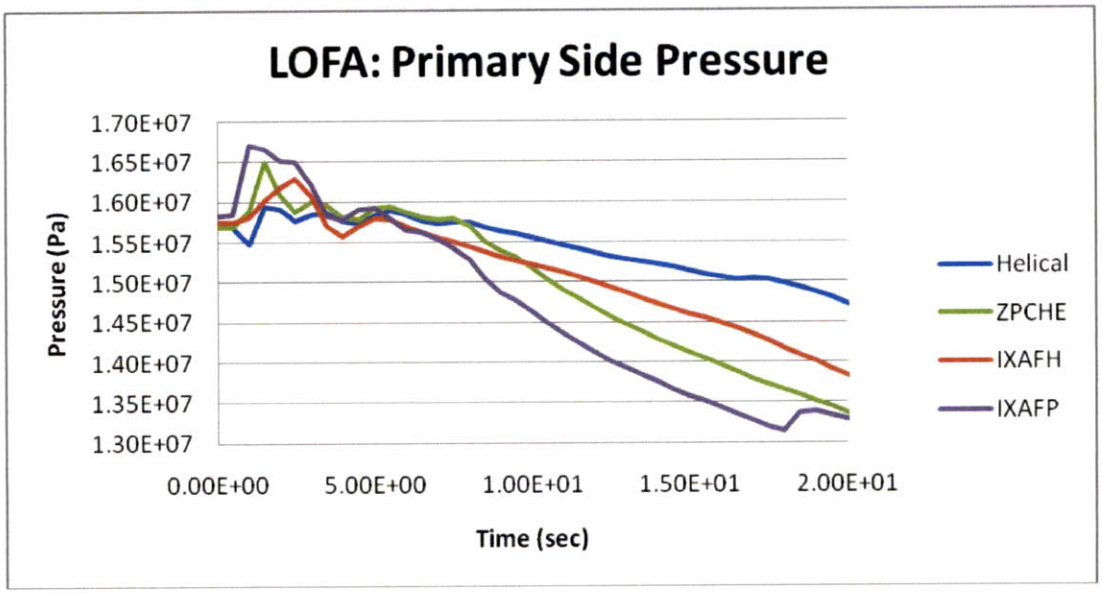
LOFA: Primary Side Pressure
1.70E+07
1.65E+07
1.60E+07
1.55E+07
1.50E+07
1.45E+07
1.40E+07
1.35E+07
1.30E+07
Pressure (Pa)
0.00E+00
5.00E+00
1.00E+01
1.50E+01
2.00E+01
Time (sec)
Helical
ZPCHE
IXAFH
IXAFP

(a)

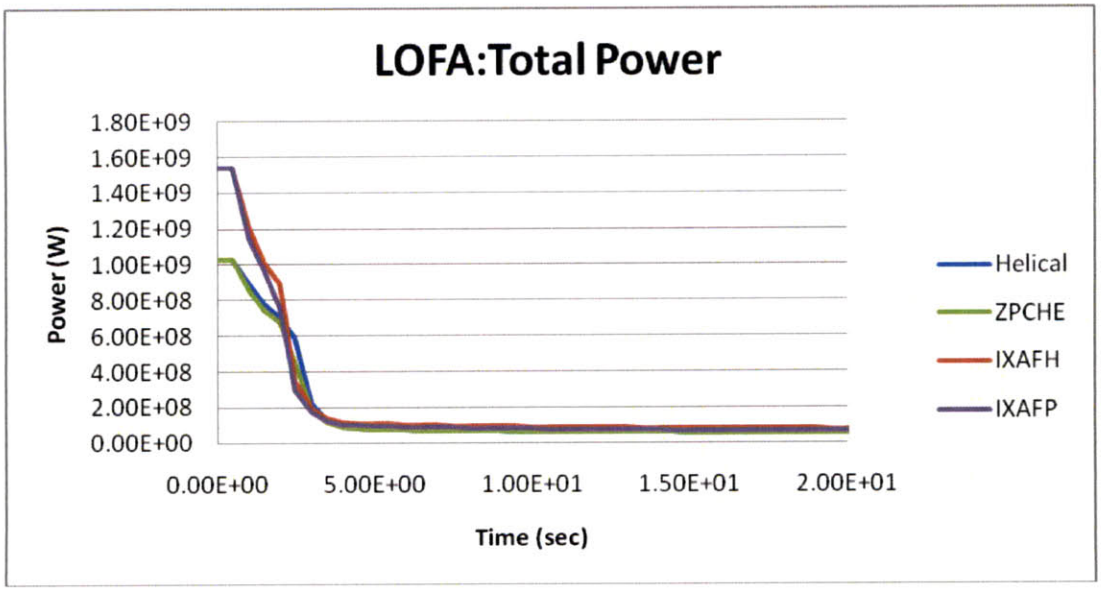
LOFA:Total Power
1.80E+09
1.60E+09
1.40E+09
1.20E+09
1.00E+09
8.00E+08
6.00E+08
4.00E+08
2.00E+08
0.00E+00
Power (W)
0.00E+00
5.00E+00
1.00E+01
1.50E+01
2.00E+01
Time (sec)
Helical
ZPCHE
IXAFH
IXAFP

(b)

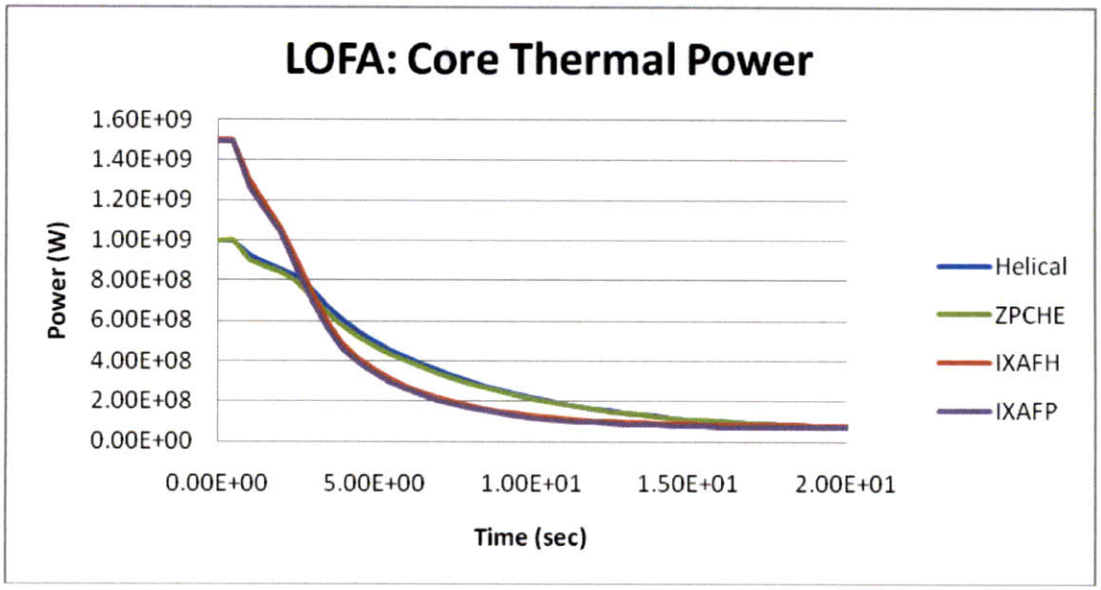
LOFA: Core Thermal Power
1.60E+09
1.40E+09
1.20E+09
1.00E+09
8.00E+08
6.00E+08
4.00E+08
2.00E+08
0.00E+00
Power (W)
0.00E+00
5.00E+00
1.00E+01
1.50E+01
2.00E+01
Time (sec)
Helical
ZPCHE
IXAFH
IXAFP

(c)

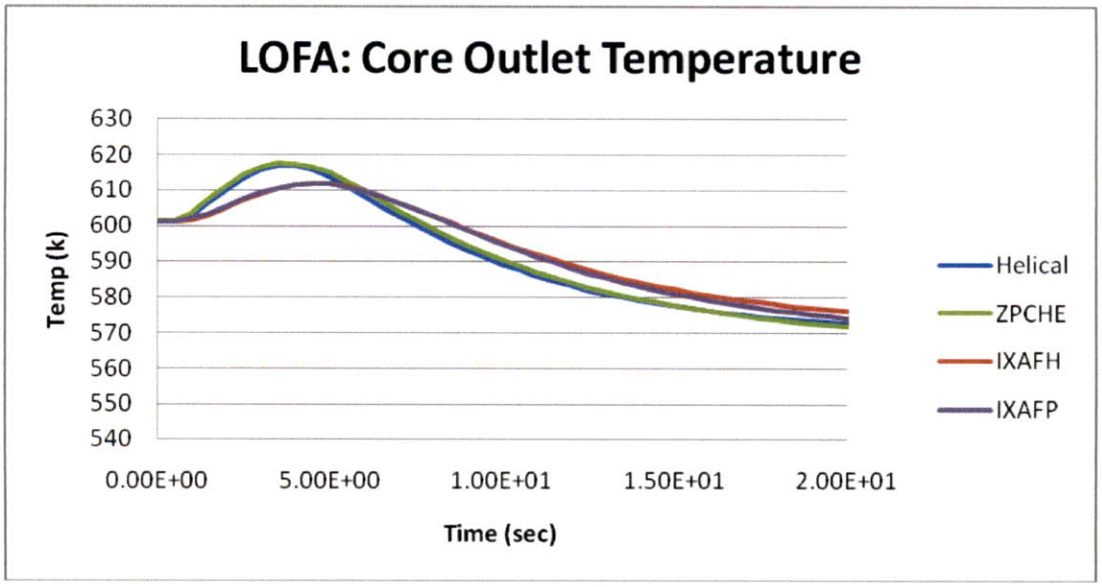
LOFA: Core Outlet Temperature
630
620
610
600
590
580
570
560
550
540
Temp (k)
0.00E+00
5.00E+00
1.00E+01
1.50E+01
2.00E+01
Time (sec)
Helical
ZPCHE
IXAFH
IXAFP

(d)

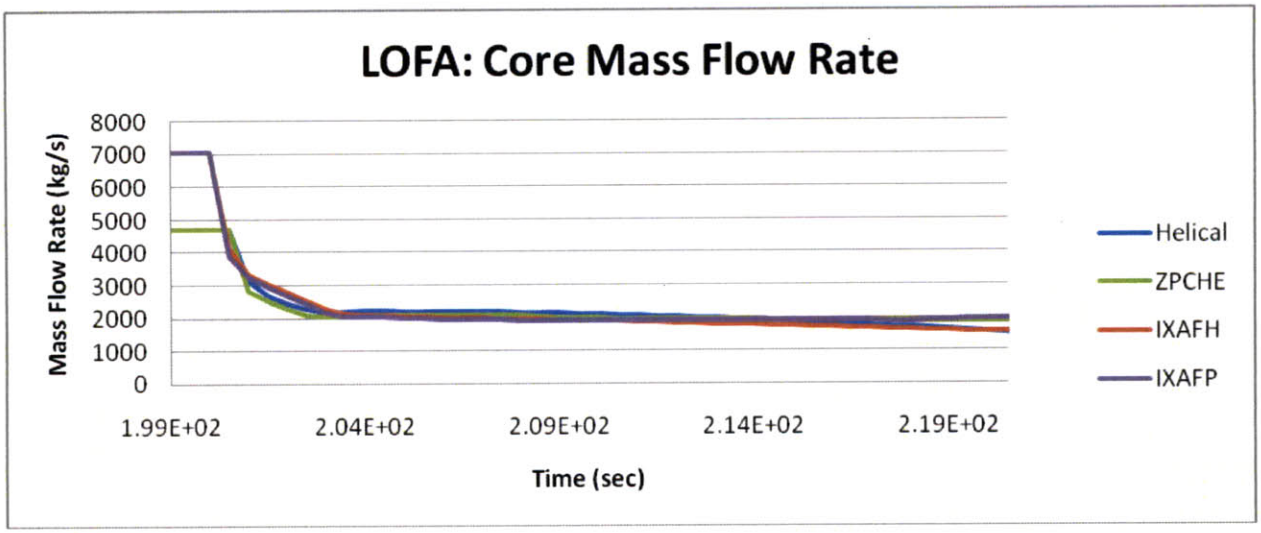

(e)

Figure 4-16 The behavior of main thermal hydraulic parameters for the IXAF fuel core with PCHE compared to the solid fuel core in the MIT RELAP model

Figure 4-16b and 4-16c show that the total power and thermal power the decreases occur more rapidly compared to the 1000 MWth IRIS nominal case. The core outlet temperature is lower for the case of IXAF fuel at 1500 MWth, while the pressure is also higher. This combination resulted in the saturation temperature being higher than the core outlet temperature at all times. The outlet tempreature does not rise as much as the 100% power case due to the higher rate of power decrease, because of the reactivity feedback coefficients described in Section 4.3.2. The mass flow rate decreases much more rapidly, but both designs reach their own steady state mass flow rate value since the reactor geometry is still the same. However, as the simulation time increases, the mass flow rate decreases faster for the IXAF fuel, because of the higher pressure drop due to the IXAF geometry. By that time the core is sufficiently below any uncovery limits and the long term behavior was not affected by this reduction in the natural circulation.

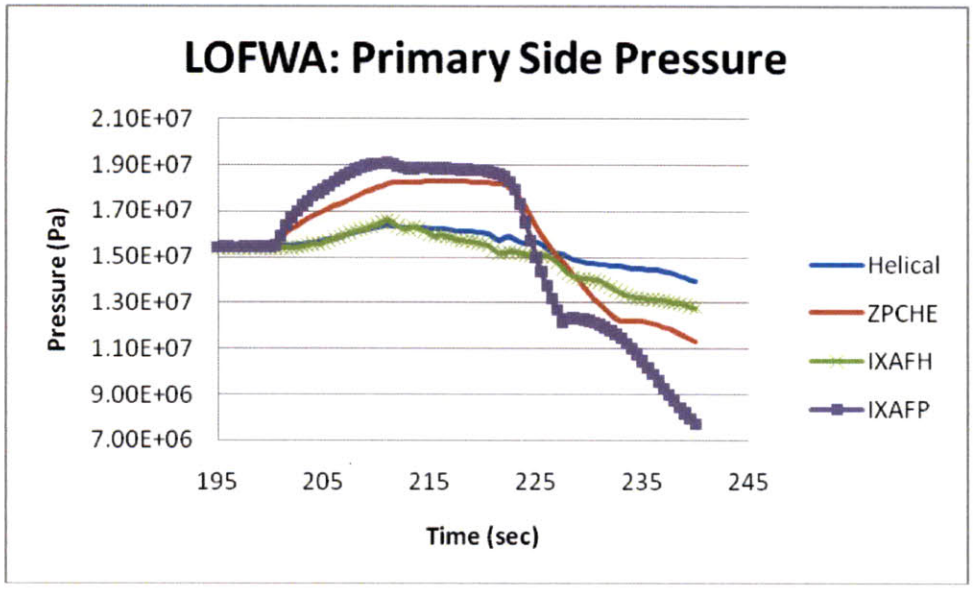

(a)

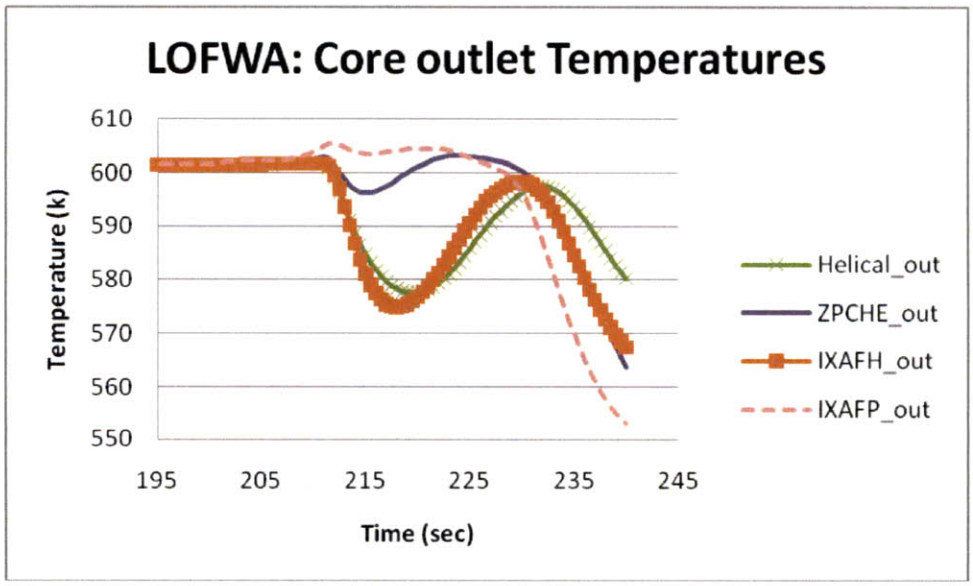

(b)

Figure 4-17 The behavior of MIT RELAP model during the LOFWA of (a) the core pressure and (b) the core outlet temperature for the IXAF and solid fuel cases

Figure 4-17 results show the core pressure and the core outlet temperatures, as seen for the combination of PCHE and IXAF fuel, the core outlet temperature increases significantly more than the other cases. However, the pressure also increases more than the other cases which

prevents the uncovering of the core. The reason for higher pressure is that even though in both models the depressuriization valve is set at 16 MPa, the transient occurs faster for the IXAF design and higher pressure is achieved. Due to the higher mass flow rate in the core during the LOFWA, this trasient takes place faster than the solid fuel case.

4.8.6 IRIS Response to SBLOCAs

As mentioned, the large break LOCA is not possible in the IRIS reactor due to small diameter of the pipe. The SBLOCA is limited to at least 2 m above the core. During the SBLOCA, IRIS's integral vessel limits the loss of coolant from the vessel without depending on injection systems. The IRIS design uses the initial large coolant inventory in the vessel, condensing steam in the vessel by using internal SGs and the small, compact containment that will allow for higher design pressure than typical containments, to safely react to SBLOCA.

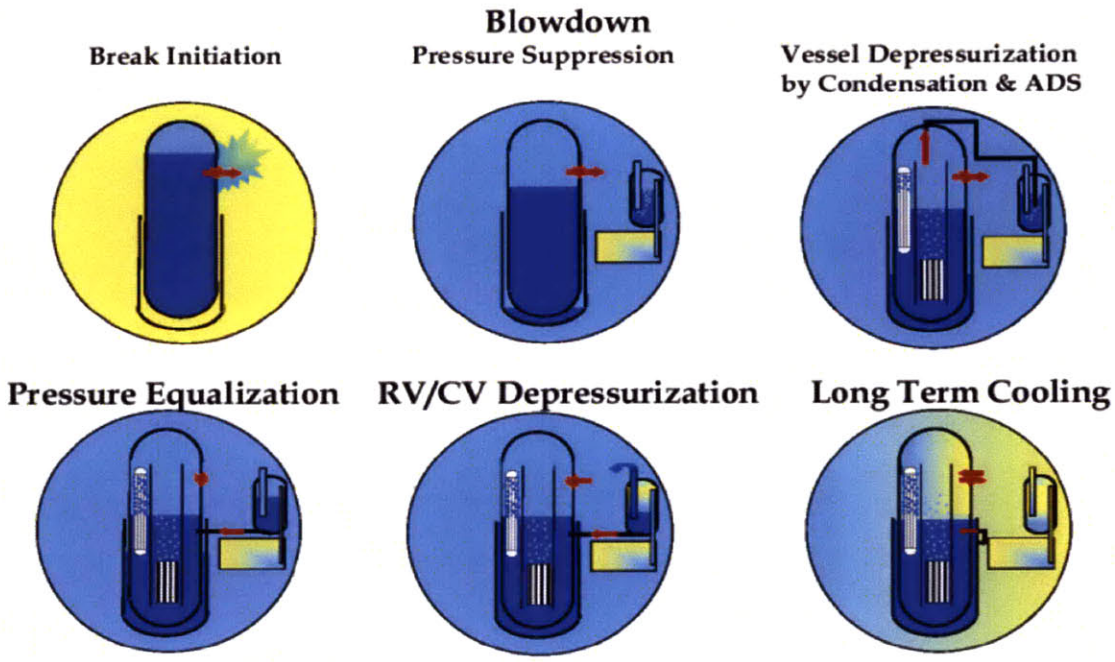

Figure 4-18 IRIS response to SBLOCA (from Oriani et al., 2003)

The SBLOCA does not need to be analyzed even though it was analyzed by the IRIS team and showed promising results [Oriani et al., 2003]. The reason for this is that the coolant flow rate to the containment will be the same for the uprated IRIS and the nominal IRIS. While the flow rate was increased by 50%, the flow rate through the pipes that will cause SBLOCA stayed the same. Since IRIS has the SGs inside the reactor vessel, the steam will condense inside the vessel and PCHE will perform that function faster than OTHSGs. The faster this process, the faster the vessel cavity fills and as seen in Figure 4-18, once the cavity fills, the reactor is impossible to uncover. Furthermore, the IRIS final technical report [2003] specifically mentions that in IRIS during SBLOCA, the long term cooling of the core has little to do with the decay heat.

Chapter 5 IRIS DNBR Analysis

5.1 Previous work

VIPRE is a state of art thermal-hydraulic code used for LWR cores by nuclear power utilities and is certified by NRC. The code has an ability to calulate fuel, clad, coolant temperatures, the MDNBR and critical power ratio (CPR) under nominal operating and transients conditions. The code has the ability to calculate the above parameters for four different rod geometries: solid cylindrical rods, annular fuel rods, hollow tubes and flat plates.

The previous chapter's RELAP analysis assumed that all the fuel rods in the core have the same core average conditions. However, in reality the core power is not equally distributed among rods and individual rods could be associated with higher power due to the peaking factors resulting from neutronic analysis. While in the above analysis, the core average conditions did not result in reaching the MDNBR limit, a more detailed analysis in VIPRE that accounts for the peaking factors of individual rods and the effects of lateral flow mixing is needed to analyze the MDNBR of the core more accurately. Analysis of PWR cores using VIPRE has been done for a variety of conditions and its input and results have been extensively published. The inputs for 3411 MWth Westinghouse fuel and the 5400 MWth IXAF fuel that were available from previous work [Dandong et al., 2007] were modified for the IRIS operating conditions. After steady state conditions have been reached for both fuel geometries, the LOFA and LOFWA can be simulated by VIPRE if the core pressure, mass flow rate, inlet temperature and power history obtained from RELAP results are used to dive the VIPRE calculations.

5.2 IRIS Reference Reactor DNBR Model

The VIPRE reference 17 x 17 standard Westinghous fuel 3411 MWth PWR model is taken from [Dandong et al., 2007]. The VIPRE model is $1/8^{th}$ of a total core divided into different subchannels. The model lumps some groups of fuel rods, channels and assemblies for simplification. The hot assembly is modeled in the center of the core and its individual rods are explicitly modeled in the input file. The following modifications were made to obtain the IRIS nominal VIPRE model:

- The number of assembly channels modeled were reduced from $1/8^{th}$ of 193 to $1/8^{th}$ of 89, this involved changing the channel flow areas, the heated perimeters, the wetted perimeters and the power generated by the rods of effected channels.
- The core operating conditions such as the power, the effective core mass flow rate (without bypass) and the inlet temperature were changed to the IRIS nominal conditions.
- The fuel height was changed from 12 feet to 14 feet, consequently changing the position of the grid spacers.

The peaking factor representation for the hot fuel assembly modeled in VIPRE is given in Figure 5-1a. Other peaking factors for other assemblies were used, as shown in Figure 5-1b.

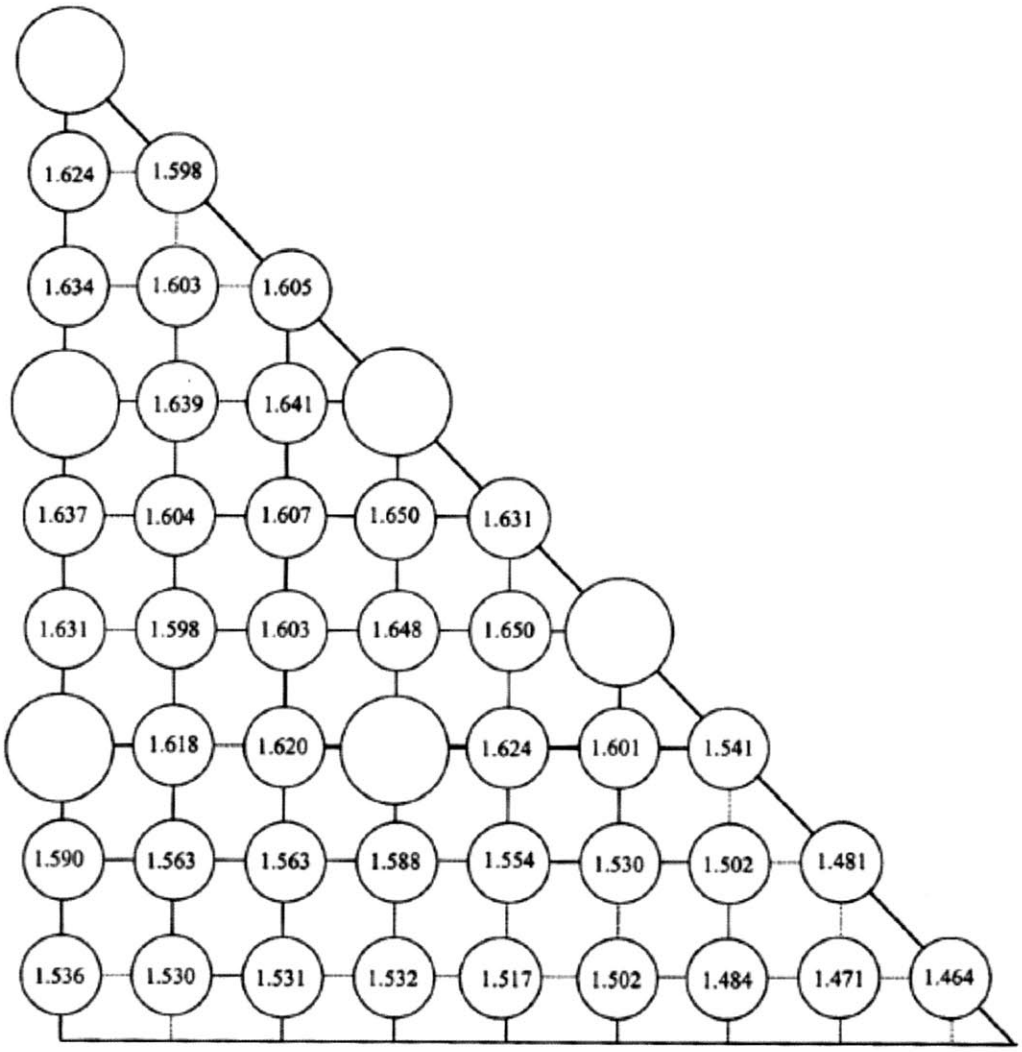
1.624
1.598
1.634
1.603
1.605
1.639
1.641
1.637
1.604
1.607
1.650
1.631
1.631
1.598
1.603
1.648
1.650
1.618
1.620
1.624
1.601
1.541
1.590
1.563
1.563
1.588
1.554
1.530
1.502
1.481
1.536
1.530
1.531
1.532
1.517
1.502
1.484
1.471
1.464

(a)

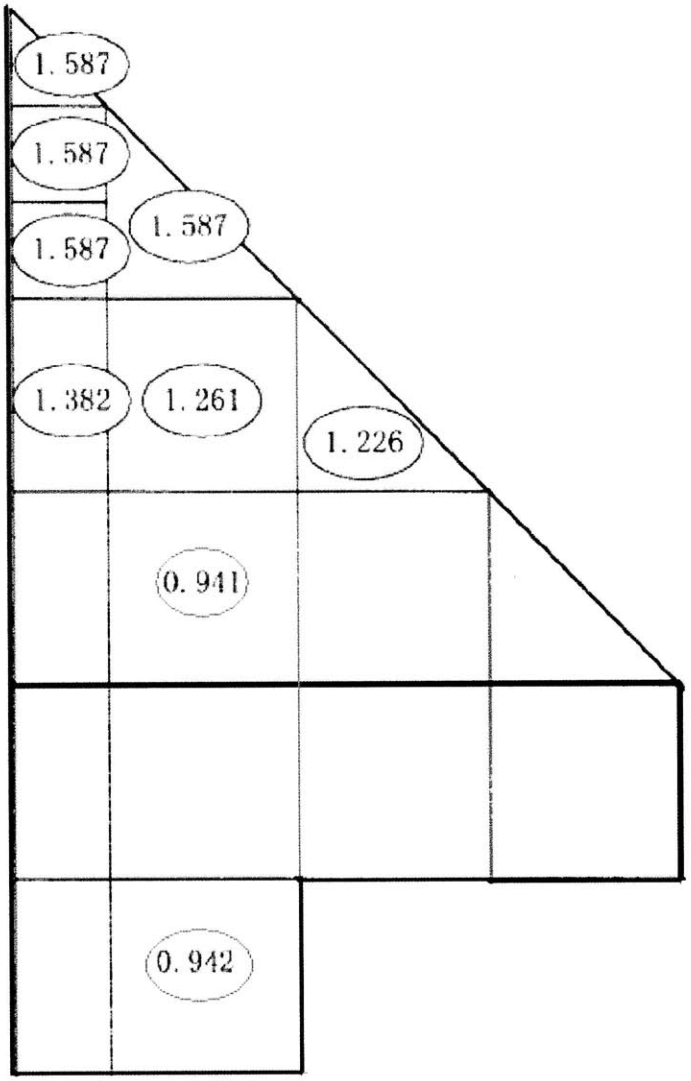

(b)

Figure 5-1 The pin power distribution used for (a) the hot fuel assembly and (b) other lumbed assemblies in VIPRE (from Dandong et l., 2007)

Since the VIPRE model is divided into channels and rods, modeling each subchannel will be very time consuming, therefore the subchannles were lumped in larger region when they are far from the core center, as shown in Figure 5-2.

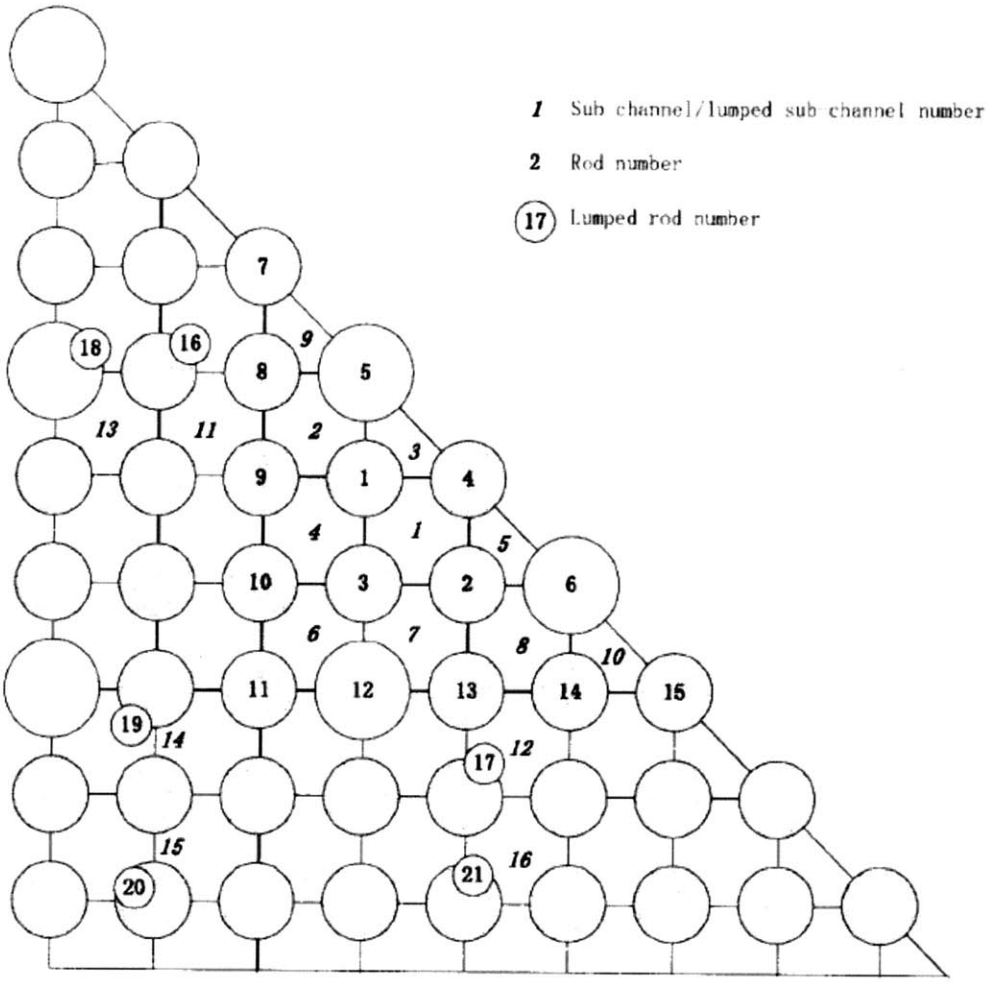
1 Sub channel/lumped sub channel number
2 Rod number
17 Lumped rod number
7
18
16
9
8
5
13
11
2
3
9
1
4
4
1
5
10
3
2
6
6
7
8
10
11
12
13
14
15
19
14
17
12
15
16
20
21

(a)

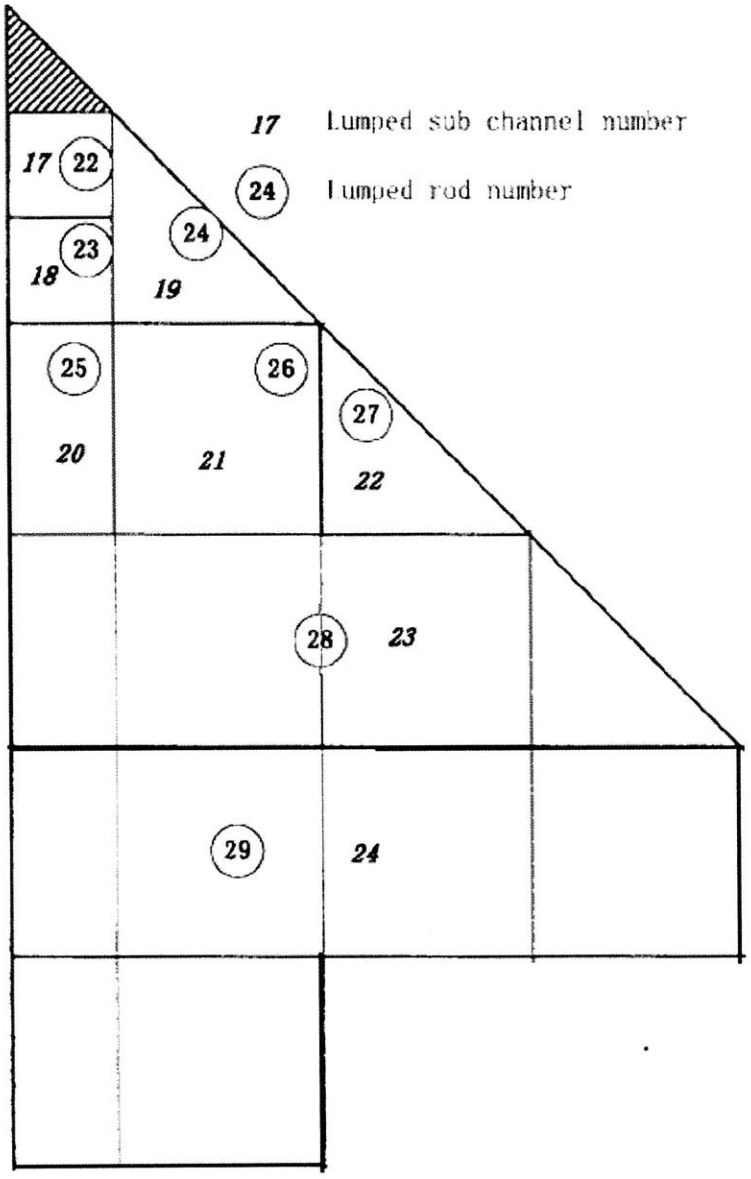

(b)

Figure 5-2 Channel and rod numbering scheme in the 1/8 core model for the IRIS reactor (from Dandong et l., 2007)

5.3 IRIS IXAF Reactor DNBR Model

As mentioned previously, the VIPRE model of the 3411 MWth 13 x 13 IXAF fuel was created at MIT. The subchannel representation is shown below and the following changes were made to the input file:

- The number of assembly channels modeled were reduced from $1/8^{th}$ of 193 to $1/8^{th}$ of 89, this involved changing the same parameters as the solid fuel case.

- The core operating conditions such as the power and the effective core mass flow rate (without bypass) were changed to 150% IRIS conditions, while the pressure and the inlet temperature were set to IRIS nominal condtions.

The represention of the IXAF fuel core VIPRE model is shown in Figure 5-3, which is similar to the solid fuel core model described in the previous section.

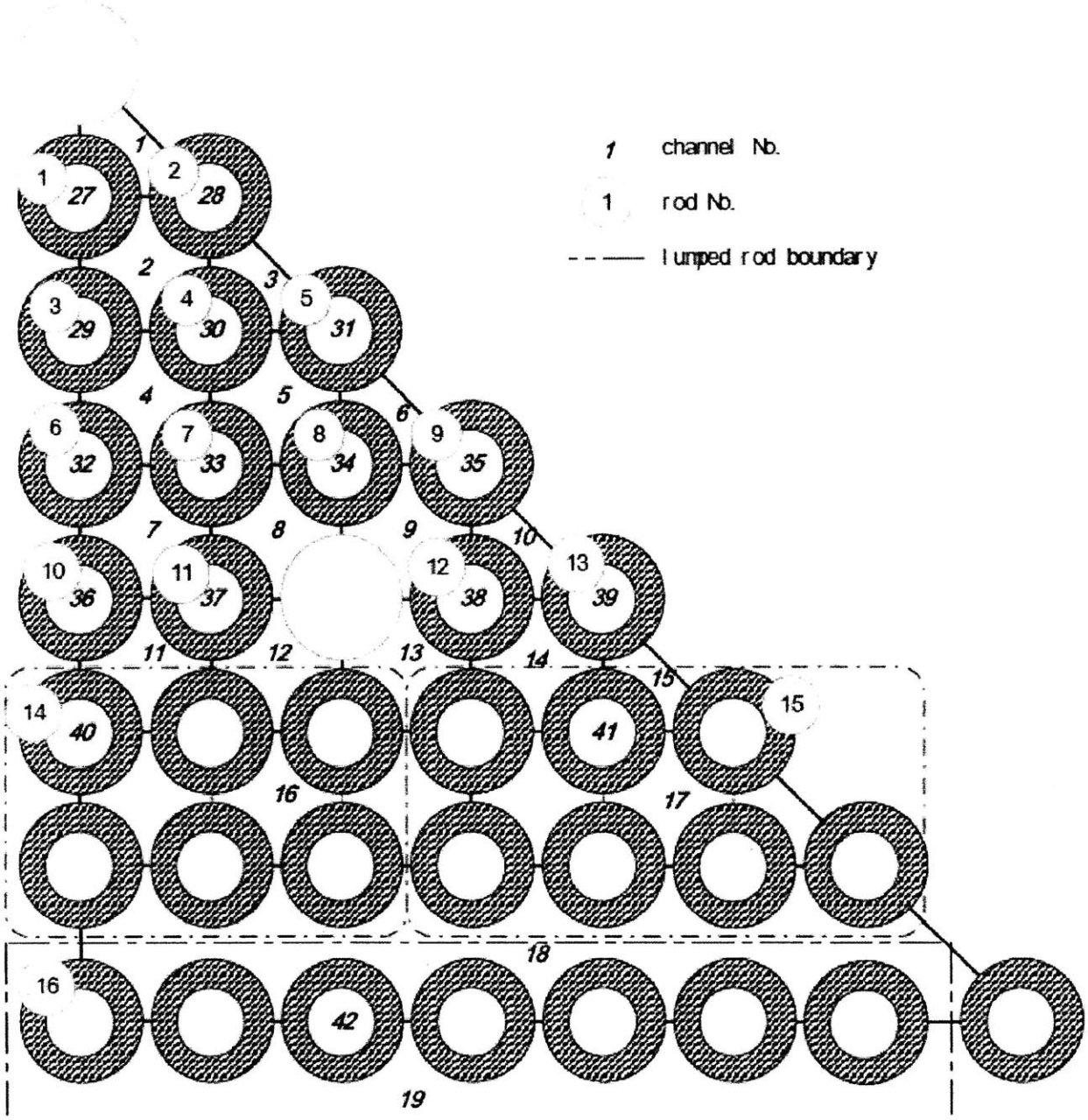

(a)

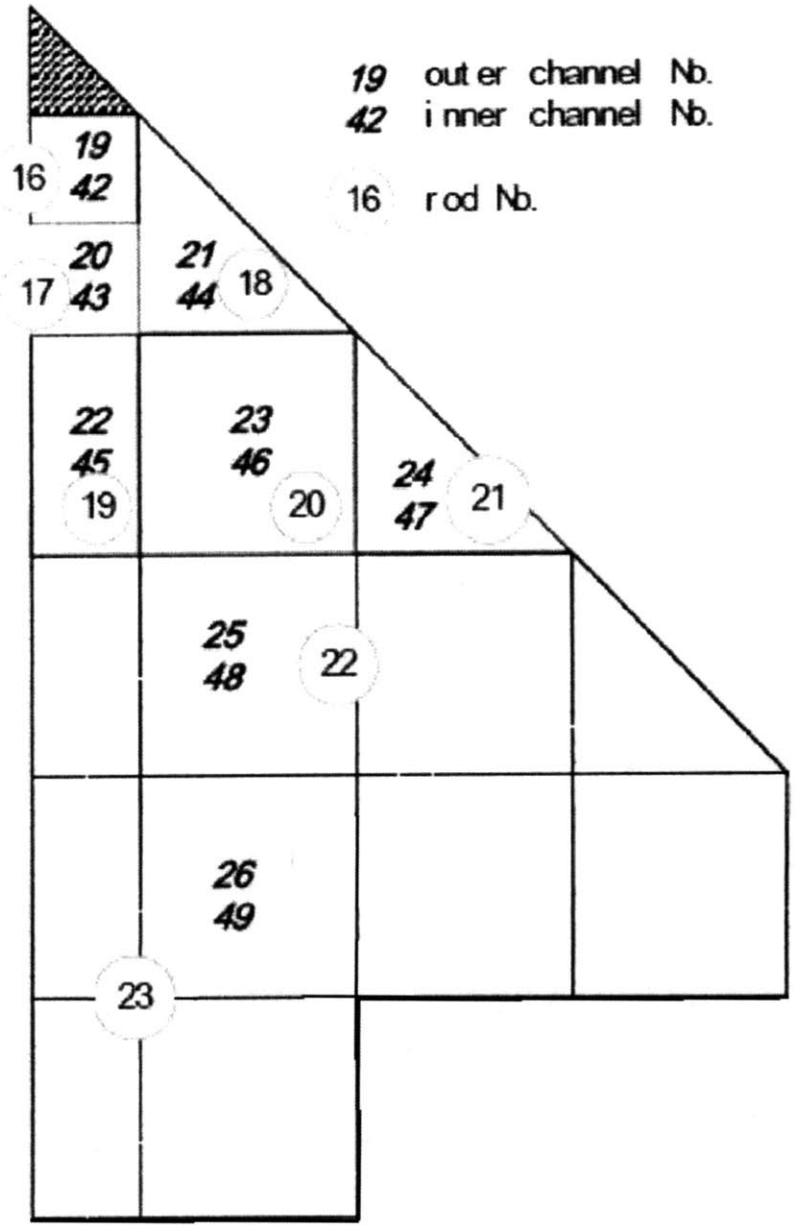
19 outer channel Nb.
42 inner channel Nb.
16 rod Nb.
19
42
16
20
43
17
21
44
18
22
45
19
23
46
20
24
47
21
25
48
22
26
49
23

(b)

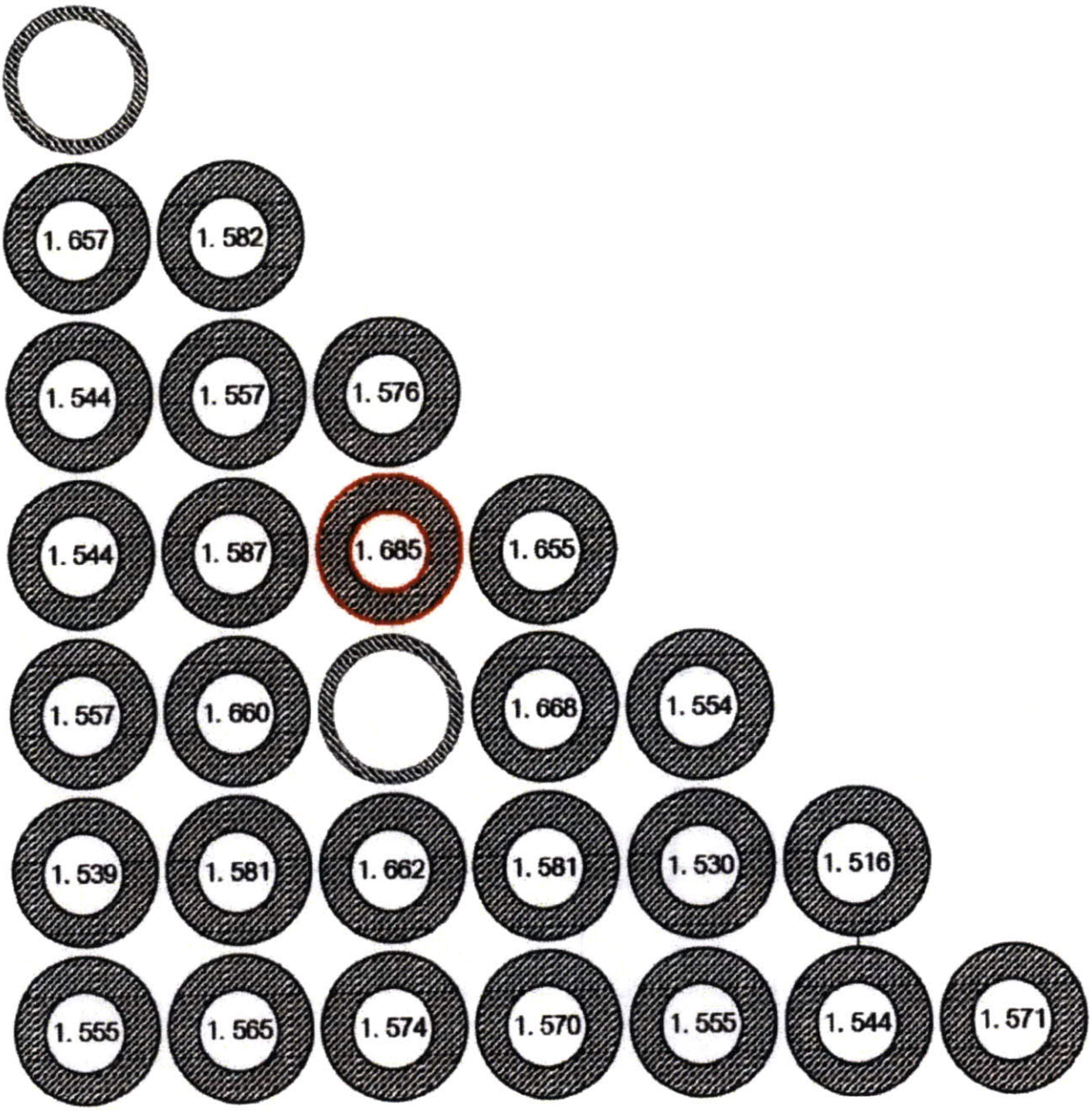
1. 657
1. 582
1. 544
1. 557
1. 576
1. 544
1. 587
1. 685
1. 655
1. 557
1. 660
1. 668
1. 554
1. 539
1. 581
1. 662
1. 581
1. 530
1. 516
1. 555
1. 565
1. 574
1. 570
1. 555
1. 544
1. 571

(c)

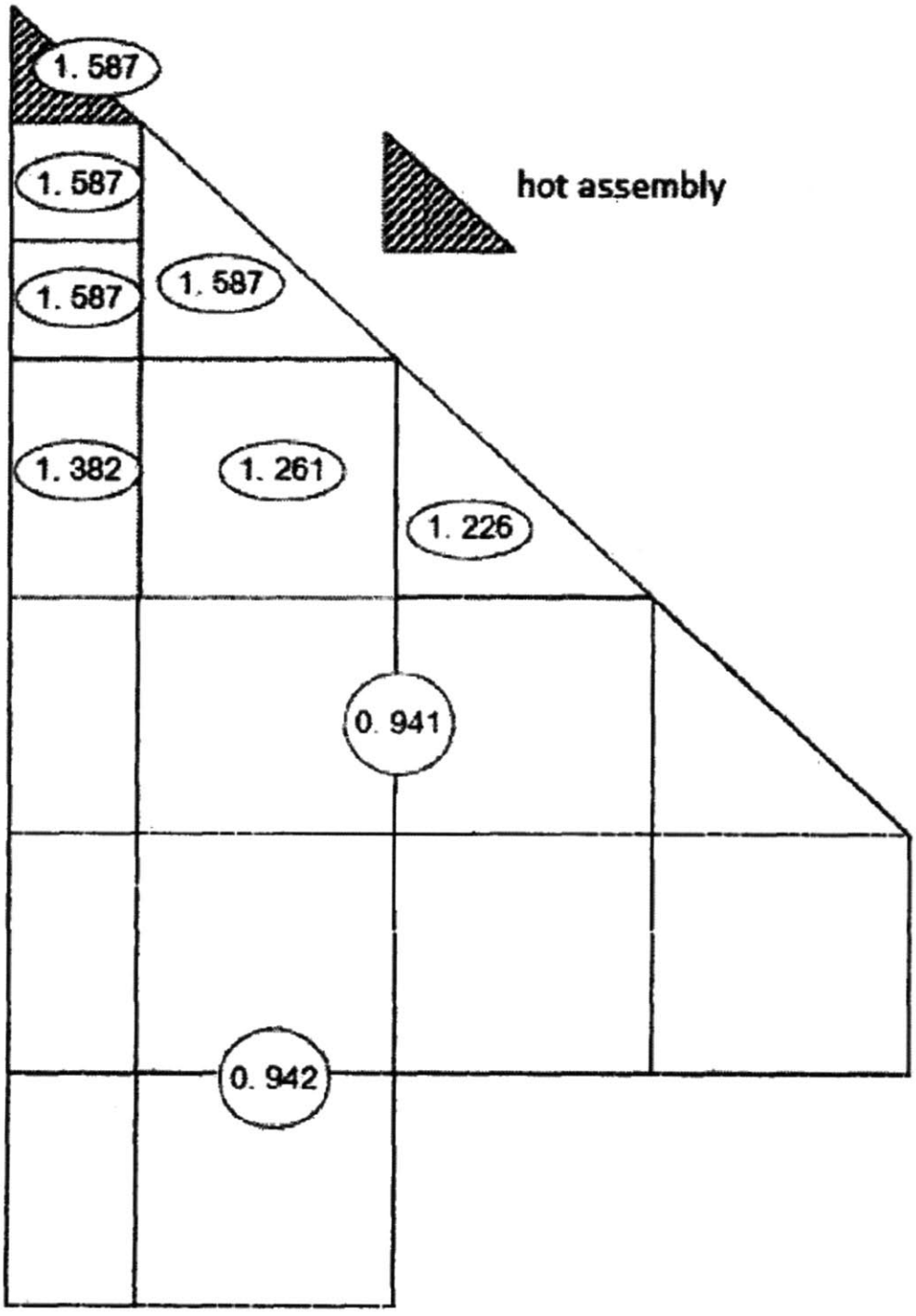

(d)

Figure 5-3 Channel and rod numbering scheme in the 1/8 IXAF core VIPRE model for the IRIS reactor (from Dandong et l., 2007)

The peaking factors were kept the same as the solid fuel core model with a radial factor of 1.55 for the hot assembly. It is noted that the smaller IRIS core might result in higher peaking factors than the larger 3411 MWth core. Also, lower power density helps to keep the power more even compare to a Westinghouse nominal large reactor design.

5.4 IRIS REACTOR DNBR Results

The first case that was considered is a steady state case at overpower conditions. The traditional overpower conditions are selected to cover most operational transients; along with these general model assumptions:

- 118% overpower condition at 100% nominal flow rate
- 2 degree C increase in inlet temperature
- 5% reduced flow rate
- Zero power deposited on the coolant
- Zero for turbulent mixing coefficient
- Chopped Cosine axial power distribution with 1.55 peaking factor for hot assembly
- $1/8^{th}$ core model with individual rods modeled in hot assembly
- 24 channels, 29 rods and 24 axial nodes for solid fuel
- 49 channels, 23 rods and 24 axial nodes for IXAF fuel
- EPRI correlation for void fraction and pressure drop calculation at all flow conditions

- Dittus-Boelter and Thom correlations for single-phase heat transfer and subcooled/saturated nucleate boiling heat transfer, respectively

For MDNBR calculations the W-3L correlation for the external side of the IXAF fuel rods were used. For the inside, it was found that the W-3S provides more accurate results compared to the W-3L [Dandong et al., 2007]. The solid fuel used the W-3L correlation to have comparable results to the IXAF MDNBR. The cases for a 3411 MWth PWR and the IRIS were run and the results are listed in Table 5-1.

Table 5-1 The overpower MDNBR and core pressure drop results for various cases

Core/Fuel Type	MDNBR	DelP (Psi)
Standard PWR Westinghouse 17 X 17 3411 MW	1.484	17.36
14 ft Standard PWR Westinghouse 17 X 17 1000 MW	2.208	9.49
IXAF PWR Westinghouse 13 X 13 5117 MW Inner	1.366	35.2
IXAF PWR Westinghouse 13 X 13 5117 MW Outer	1.902	35.2
IXAF IRIS 13 X 13 1500 MW Inner	1.151	14.5
IXAF IRIS 13 X 13 1500 MW Outer	2.448	14.5
IXAF IRIS 13 X 13 1500 MW Inner, mod.grid	1.442	15.2
IXAF IRIS 13 X 13 1500 MW Outer, mod.grid	1.949	15.2

As seen from Table 5-1, going from 3411 MWth to 1000 MWth XL Westinghouse fuel, increases the MDNBR from 1.484 to 2.208. The IRIS mass flow rate is 4 times smaller, while its power level is only 3.4 times smaller than a typical PWR. Also, the number of rods is only 2.2 times less than the typical PWR. This, along with the extra 2 feet of fuel, gives the IRIS reactor 60 percent the normal PWR power density, hence the larger MDNBR.

For the core with IXAF, the outer channel MDNBR increases by going from a 3411 MWth PWR to the IRIS overpower conditions. However, the inner channel MDNBR decreases to reach below the 1.3 limit. Also, the mass flux in the inner channel of the IRIS reactor was

2.21 Mlbm/ft2-hr compared to 4.3 Mlbm/ft2-hr of the traditional PWR design with IXAF fuel core. However, this is still unacceptable, therefore the spacer grid loss coefficient was increased from 0.6 to 0.85, and hence the "mod.grid" case results in Table 5-1 provide acceptable MDNBR limits. The increase in the loss coefficient will push the flow to the tube center and increase the mass flux, which results in higher MDNBR. The penalty to do this is the higher pressure drop. However, this is a small loss compare to the gain in permissible heat removal. Therefore, from this point on the "mod.grid" version is used to continue the analysis. Additionally, the "CIRIS" refers to use of the "mod.grid" IXAF and PCHE at uprated power of 1500 MWth and this word will be used for the rest of the work reported here.

After the above overpower condition was found to provide sufficient safety margin, IRIS VIPRE input were returned to 100% power and normal conditions and LOFWA and LOFA accidents where calculated. The starting values for the MDNBR can be seen below in Table 5-2.

Table 5-2 The steady state MDNBR values for the IRIS and CIRIS cores at 100% power

Core/Fuel Type (Nominal Values)	MDNBR
IRIS 1000 MW Nominal Design	2.799
CIRIS 1500 MW Inner IXAF channel	3.349
CIRIS 1500 MW Outer IXAF channel	3.588

It was found that for the LOFWA sequence discussed in Chapter 4, after 30 seconds of transient simulation, the MDNBR at nominal condition had the smallest value of the entire transient. This is somewhat opposite to the result shown by Dandong et al. [2007] on MSLBA for a typical PWR. As seen from Figure 5-4, the MDNBR starts increasing as the transient takes place. This is what is expected for the IRIS reactor, since the steam generators are once-through, which increases the inlet temperature of the core and results in negative insertion of reactivity, unlike

the U-Tube steam generators in which MSLBA results in an increase in heat transfer and decrease in core inlet temperature. In Figure 5-4, the faster response of the IXAF due to the higher flow rate was seen in the regular PWR analysis too.

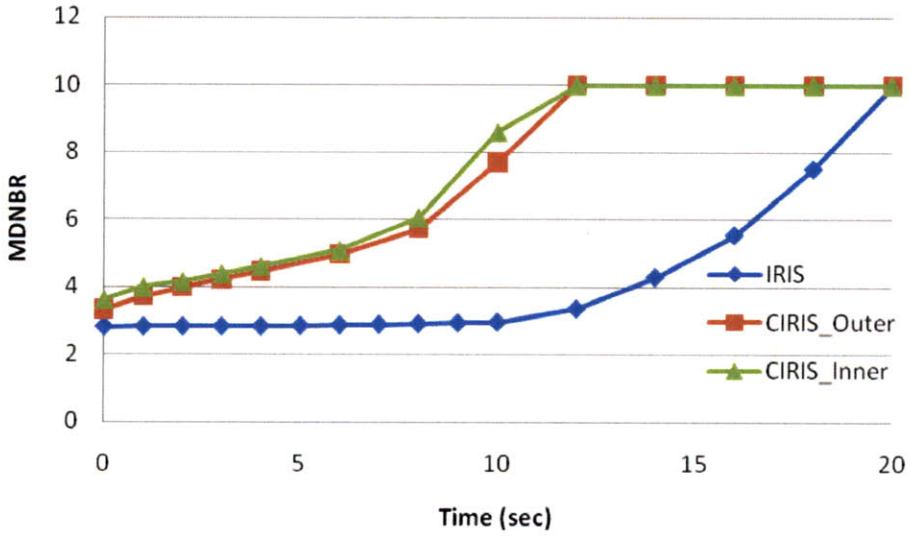

Figure 5-4 The MDNBR vs. Time for the LOFWA at 100% power

For the LOFA case, the previously described RELAP sequence was run and the results for IXAF uprated fuel were not promising, as shown in Table 5-3..

Table 5-3 The MDNBR results for transients

ACCIDENT	MDNBR
LOFA	IRIS
HELICAL	2.029
PCHE	1.998
LOFA	IXAF
HELICAL	**0.462**
PCHE	**0.326**

It is noted that for solid fuel design with PCHE exhibits smaller MDNBR, but it is not a significant effect. But as described before, assuming no flow resistance and coastdown from the pumps, the mass flow rate sharply drops and this results in unacceptable MDNBR value for the IRIS core with the IXAF core at uprated conditions. It is further noted that an MDNBR of 0.9 is reached even with solid fuel of a 3411 MWth PWR with such fast decrease in flow rate. A case where the IRIS with IXAF was run with typical LOFA sequence for 3411 PWR as described in Dandong et al. [2007] as shown in Figure 5-5. For this case, the mass flow rate curves shown for IXAF in Figure 5-5 were inputted into the IRIS RELAP model. Then, the core pressure, power and inlet temperature from the RELAP simulation was used in the IRIS IXAF VIPRE model. If slowing pump coastdown will not be possible, alternative solutions and assumptions are written in the Appendix C.

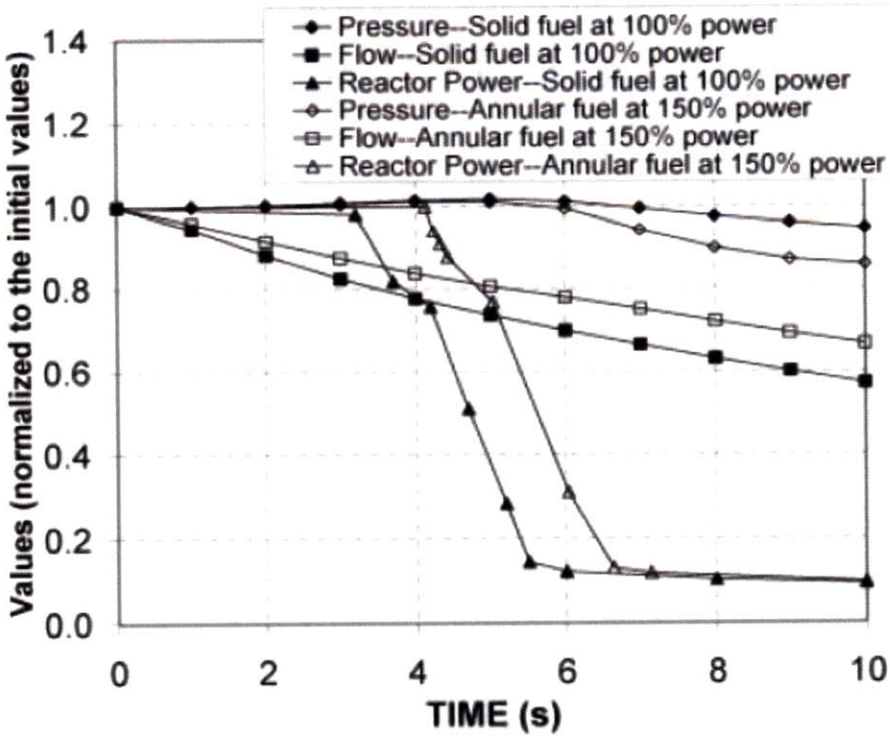

Figure 5-5 A typical LOFA sequence for PWRs (from Dandong et al., 2007)

Figure 5-5 summarizes the total LOFA accident analyzed for a typical PWR Westinghouse design. The accident sequence consists of linearly changing the mass flow rate of the core untill it reached 87% of normal value, when a trip reactor trip signal is generated. This is what Westinghouse considers a LOFA and the sequence has been approved by the NRC. The key difference is that in IRIS, the mass flow rate decreases more dramatically in the MIT RELAP model. As mentioned before, MIT RELAP model does not account for any inertia that the coolant pumps would provide and its results almost match the published result by the IRIS design team.

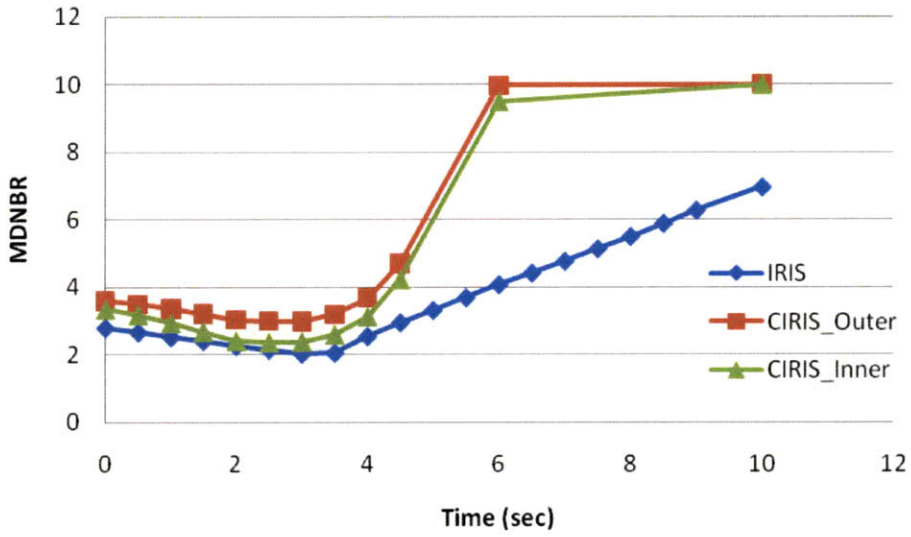

Figure 5-6 The MDNBR vs. Time for the LOFA with fast coastdown for the IRIS and slow coastdown for the CIRIS

The MDNBR was 2.108 for the CIRIS, well above the limit of 1.3, assuming same coastdown rates as shown in Figure 5-5. Clearly, ambiguity in the pump coast down rate is the main problem to decide whether the IRIS reactor safety is not compromised by going to IXAF fuel and uprated conditions. The next Chapter will introduce design modification that can reasonably resolve the above findings. It is noted the solid fuel will also achieve satisfactory

results with the slower coastdown. This is acceptable, however, because of lower maximum fuel temperature and maintenance of the same nominal MDNBR margins under normal operation, the annular fuel was chosen.

Chapter 6 CIRIS OPTIMIZATION

6.1 General model description

The most compact IRIS design needs to meet all safety and reliability criteria for standard nuclear power plants including ASME standards for stress limits of major components. Of course, the main goal of the project is to reduce the cost of the IRIS reactor. As shown in the previous chapters, all preliminary analysis showed promising results and the ideas of using PCHE and IXAF fuel under IRIS conditions and can be further pursued to obtain the optimized results. This optimization study aims not only at meeting safety goals but also improve the economics, and it should take into account how one parameter change affects other parameters.

For example, reducing reactor pressure vessel size seems like an attractive option to reduce the construction cost. However, the smaller vessel size affects the time constant of the transients of IRIS and this will have adverse effects on safety, particularly from the PCHE. Also, reducing the vessel size will result in higher neutron flux on vessel walls, which will require extra shielding and thus increase costs. Similarly, decreasing the vessel height will reduce cost but it will also provide less natural circulation and might result in redesigning all the safety systems. One of the goals of the analysis presented in this chapter is also to try to use the features and designs that have already been modeled for the IRIS and not reinvent the wheel.

There are also questions about the uncertainty within each parameter and how it can affect the final proposed design for CIRIS. For example, the PCHE has never been used in nuclear reactors. In addition, information on PCHE's boiling experiments under any condition and its resistance to corrosion and fouling under IRIS operating conditions could not be found.

Also, the IRIS reactor design uses the spool type pumps that has never been used for nuclear reactors and the size that has not yet been finalized is also troubling. The optimization process will try to avoid too much reliance on the design parameters with large uncertainty and provide room for flexibility while being cost effective.

6.2 Pump optimization

As mentioned above, the pump holds the key to whether one can use annular fuel or not. The more detailed description of the pump can be found in Chapter 4 and its referenced publications. This section focuses on improving pump design and providing enough capacity for the 150% flow case. According to the RELAP results shown in Table 4-10, the head needed for 50% increase in flow rate was 88% higher than the nominal head. This is not surprising, as a regular PWR core behaves in the same fashion [Dandong et al., 2007]. To provide this increase in load and flow rate, the pump geometry has to be modified in one of the two ways given below according to [Nelik, 1999],

$$N_s = \frac{N \cdot Q^{1/2}}{H^{3/4}}, \qquad (6.1)$$

where N_s is the specific speed, N is the speed in rpm, Q is the flow rate in gpm and H is the head in ft. As mentioned, the pump provides specific speeds between 5000-9000. At the same flow rate as the nominal IRIS design and specific speed of 5500, a head of 40 m, which is roughly twice the IRIS nominal head, can be provided. The reduced specific speed will have adverse effect on the PCHE performance, since the steeper the pumping curve (higher N_s), the less

sensitive the impacts of fouling will be on the PCHE [Hesselgreaves, 2001]. However, compared to centrifugal pumps the specific speed of the rotor is still higher.

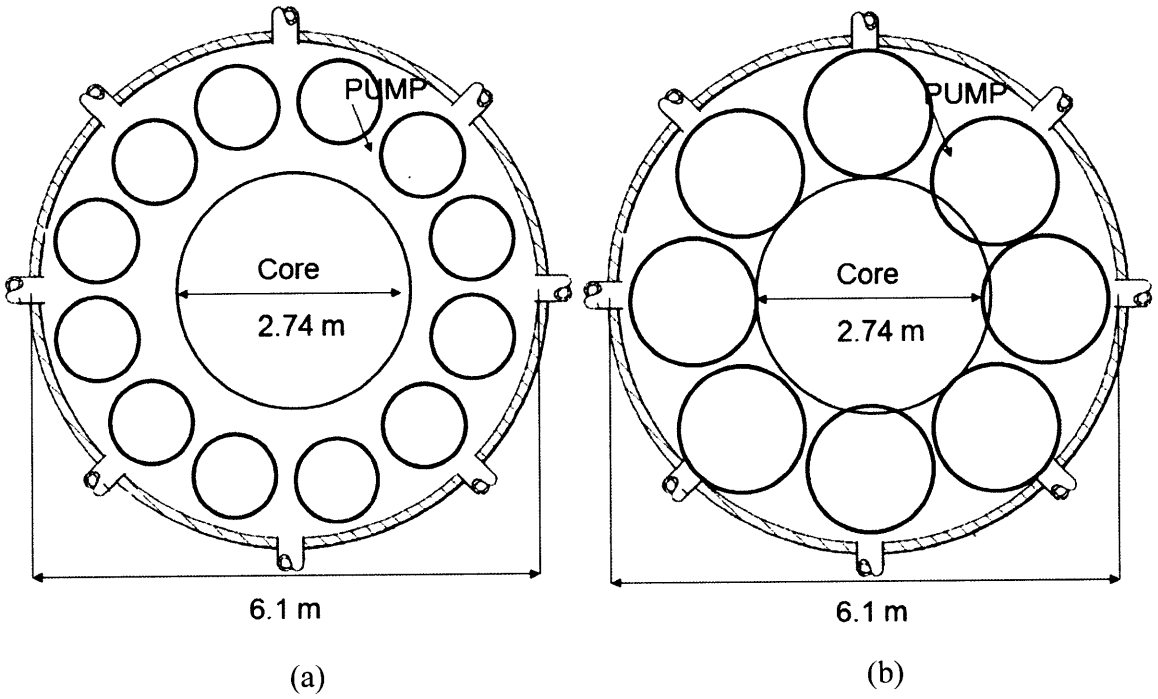

Figure 6-1 The probable cross sectional area needed for the pumps if (a) 12 pumps are used or (b) larger sized 8 pumps are used

The first modification demonstrates that the there is a good possibility of fitting 12 pumps into the current IRIS reactor vessel. As seen in Figure 6-1b, it will be a tight fit to place 8 pumps in the annulus, and there is a potential for pumps hitting each other due to vibration or under maintenance. The size of the pump can be reduced if indeed high temperature materials are used, which eliminates the space for cooling tubes, labeled 141 in Figure 4-8. Figure 6-1b adds to the size of the impeller in each pump. However, the vessel will contain 8 pumps and 12 Steam generators. The PCHE is compact enough so that 8 PCHEs, rated at 150% power, can also easily fit in the IRIS core periphery, unlike the OTHSGs. However, the larger flow rate will have more severe consequences for small break LOCA accidents. At this point, it was decided to

keep the same design conditions, such as the power to flow rate ratio, as the IRIS team concluded. Therefore, Figure 6-1a will be used for the optimized CIRIS design. With that design, there is minimal potential for pump collisions due to vibrations or maintenance, since there is at least 20 cm gap between the pumps and the vessel.

The issue of fast coast down rate is still a problem that needs to be addressed. As seen before, the height of PCHE is 4 m shorter than OTHSG. This will give plenty of space to add a fly wheel for the pump configuration to increase its rotational inertia. The use of fly wheels has been very common with centrifugal pumps in a regular PWR design. The centrifugal pump designs are large and have more room for the addition of flywheels. The reason centrifugal pumps are not being used in the IRIS is due to their large size. Also, the centrifugal pumps are made up of complicated shaft seal system, with the seal protecting it from the containment pressure boundary. Failure of the seal causes a loss of coolant event and it is important to design against such features. Similar to the spool-type pumps, canned pumps have been proposed and used for reactors and there are designs in which they incorporate the flywheel. Canned pumps, just like the IRIS spool type pump, have the entire pump, including rotor and bearings inside to avoid the shaft seal problems.

The flywheel design has to minimize power losses due to friction by the fluid surrounding it. The flywheel will cause significant drag by inhibiting the flow, which is a function of the speed and surface are of the flywheel. At the same time it has to provide enough inertia to the pump to avoid DNB during LOFA accident. One arrangement is discussed by Veronesi et al. [1989], is where a free-wheeling shroud is used. The shroud contains the

flywheel, however, it has passages for the fluid to pass through. This arrangement results in minimum power loss.

From the RELAP manual, the pump speed under coastdown conditions behaves according to:

$$Q(t) = Q_0(\frac{1}{1+\beta \cdot t}) \ , \tag{6.2}$$

where β is the coast down rate (1/sec) and t is the time after the pump trip. The larger the β, the faster the coastdown rate. Using curve fits from the WCAP document released by Westinghouse [Oriani, 2003], the IRIS β is roughly 0.2, almost double the centrifugal pumps in PWR, which have β of 0.09. The pump power is calculated by [Nelik, 1999]:

$$WHP = \frac{Q \times H}{3960}, \tag{6.3}$$

where WHP is power in Watts. Using the uprated H value, the resulting power is 350 kW. The power can be expressed as the multiplication of torque, τ and impellers rotational velocity, ω. At nominal conditions the torque can be expressed as [Nelik, 1999]:

$$WHP = \tau \omega, \tag{6.4}$$

$$\tau = I \frac{d\omega}{dt} \ , \tag{6.5}$$

where I is the moment of inertia. Using the above set of equations, the gain in required inertia can be calculated. As mentioned, the specific speed needed for the pumps for higher head is much lower and that will result in a larger impeller. The current estimate of the pump impeller is

about 0.8 m diameter. Generally, the square of the diameter is proportional to the pump head [Relap, 2001]. The maximum diameter of the impeller that can be reasonably fit in the IRIS is about one meter, roughly the size needed for the new impeller to provide the higher head. Therefore, using above information, the uranium disk of 1 m outer diameter with 25 cm thickness needs to be attached to each pump to reach desirable coast down at inertia of 441 kg-m^2. It is noted that the radius can be decreased if found to be impractical, since there is still 4 m of extra space for the flywheel. The only dimensions of flywheel for canned nuclear reactor namely AP600, was 14.5 inches long with 26 inch outer diameter providing inertia of 170 kg-m^2. Alternatively, the pump impeller itself can be more massive, in which for that case the pump length has to be increase by 3 meters. This is acceptable since there is at least 5 meters extra in the core due to use of the PCHE and the 12-ft IXAF.

6.3 Shielding optimization

Unlike a typical PWR reactors, the IRIS has a very large downcomer that is expected to reduce the dose on the vessel to levels below the D&D limits. Furthermore, there are steel plates inside the down comer to reduce the photon fluence as well [Lombardi et al., 2002]. The simplified MCNP model of the IRIS reactor was created and the dose was calculated. The following is the methodology of the calculations:

- Currently 2D model of IRIS reactor has been designed in MCNP to calculate the Photon and Neutron Doses, the preliminary results matched the IRIS Reference Design.
- The dose conversion factors are taken from the MCNP manual Appendix H.
- The source is a homogenous core in form of a rectangular neutron source with X(E) fission spectrum emitting laterally and down in the vessel.

- The secondary photon and prompt photon are tracked to calculate the photon dose.
- 15 energy bins for neutrons and 20 energy bins for photons are tallied at each section of the Vessel

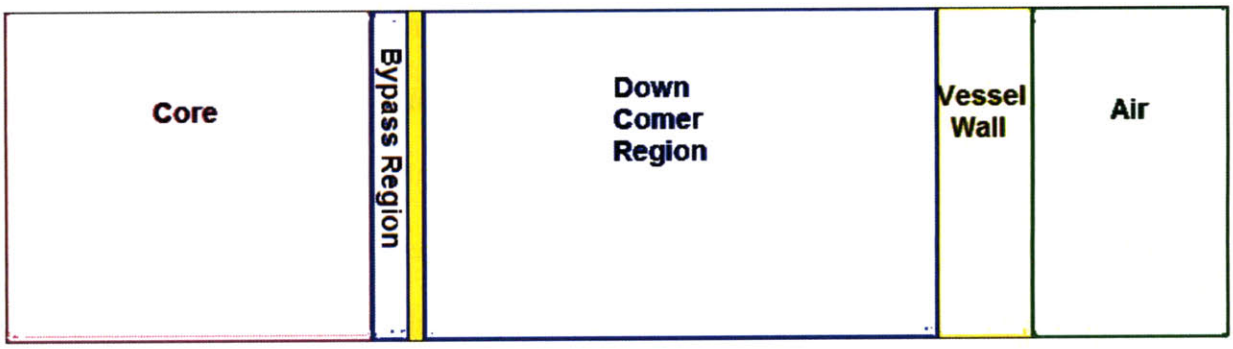

Figure 6-2 The MCNP Model Geometry

The above geometry was ran in MNCP and the total dose from neutrons and photons were calculated and listed in Table 6-1.

Table 6-1 The MCNP5 results for different vessel geometries (all uncertainties were less than 0.1 percent)

Designs	Downcomer	Neutron Dose	Photon Dose
IRIS/OTHSG	1.6 m	2.26 rem/hr	12.6 rem/hr
IRIS/PCHE	0.76 m	1290 rem/hr	69.2 rem/hr
CIRIS/PCHE	0.76 m	1935 rem/hr	103.8 rem/hr

According to Lombardi et al. [2002], the current IRIS total dose is about 26 mrem/h deep into 2 m of concrete. This value is about 2 orders of magnitude less than the U.S regulatory limit for D&D from 10 CFR part 30.70, which will make the relicensing of the IRIS reactor easier. In the same report, the neutron dose is estimated to be roughly the same as the neutron dose calculated for the IRIS with 1.6 m down comer in Table 6-1. The photon dose is far higher since there were not plated shield modeled inside the down comer. It is also shown that if the IRIS

vessel downcomer is shrunk to 0.76 m, because of the smaller PCHE size, the dose will increase by three orders of magnitude and in case of the uprated IRIS, the dose is about 2000 times higher. Since there is only two orders of magnitude margin to get way from extra D&D costs, it was decided to go with the nominal vessel size. The accurate price of a pressure vessel of that size is still unknown. Therefore, if the gain in cost of pressure vessel outweighs its D&D cost, then the option of reducing the vessel size can be used. If the reduced vessel size is used, the RELAP safety analysis does not need to be done again, since the analysis, described in Chapter 4, assumed the downcomer was 0.76 m for conservative calculations.

Five shield plates of 10 cm thick each were added to the MCNP5 Model, and the dose rate can be seen in Figure 6-3. The photon dose virtually is statistically insignificant and the neutron dose is orders of magnitude lower than the current PWR reactors. The Results also matches the IRIS team shielding studies from Lombardi et al. [2002], accounting for 150% higher power due to CIRIS power increase. The dose rate of an empty reactor vessel after irradiation will most likely be higher due to the activation of the plates inside the reactor, however, this analysis was not performed.

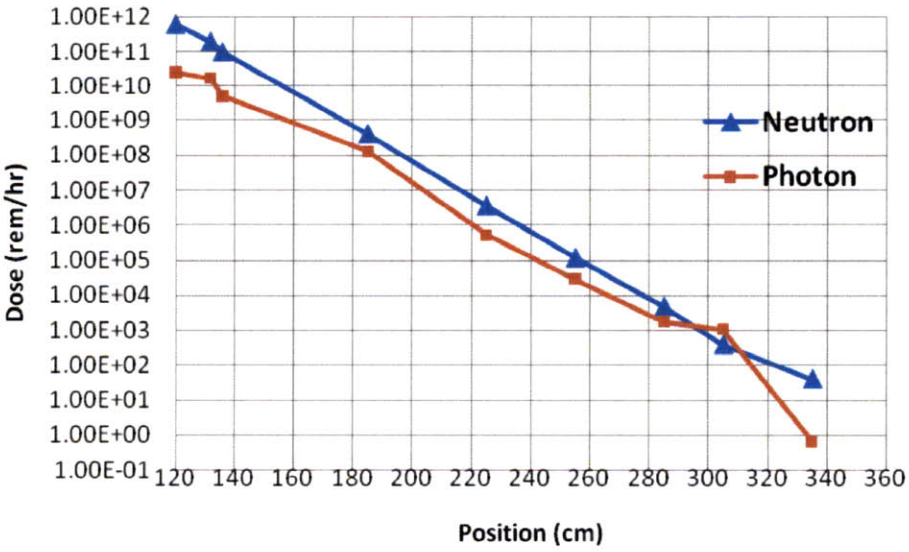

Figure 6-3 Neutron and Photon dose from the core to the outside of the CIRIS reactor vessel (most uncertainties were less than 0.1 percent)

6.4 Economics Optimization

When it comes to design of nuclear power plants, except for safety, economics is arguably the most important factor in design development. In this section, an economic evaluation of the CIRIS is undertaken and a comparison to the IRIS design is done. The analysis considers the fuel cycle cost (which consists of mining, conversion, enrichment, fabrication) along with waste disposal, the capital cost and the O&M costs.

Table 6-2 shows the input parameters for the economic model of the IRIS. The main assumption specific in the project, is to have the same cycle length as the IRIS reactor.

Table 6-2 Input parameters to the economic model

Inputs	IRIS	CIRIS-12ft	CIRIS-14ft	Units
Plant Specifics				
Burnup	38000	73300	62800	MWd/MtU
Uranium Enrichment	4.95	12.5	10	%
Tails Enrichment	0.3	0.3	0.3	%
Uranium Fuel Loaded	48500	37670	43947	kg/cycle
Total Thermal Power	1000	1500	1500	MW-th
Electrical Efficiency	33	33	33	%
Uranium Prices				
Uranium	45	45	45	$/kgU
Conversion	12	12	12	$/kgU
Enrichment	140	140	140	$/kgU
Fabrication	250	250	251	$/kgU
Backend cost				
Waste	1	1	1	mills/kw-hre
Decommission	1	1	1	mills/kw-hre
Shutdown cost	400000	600000	600000	$/day
Storage Cost	200	200	200	$/kgU
Plant Operation Parameters				
Capacity	98	98	98	%
Refueling	15	15	15	day
Recovery	30	30	30	mill/kwr-hre
Cycle length	5.16	5.16	5.16	years
plant life	40	40	40	years
Advance Purchase				
Uranium ore	2	2	2	years
Conversion	1.5	1.5	1.5	years
Enrichment	1.5	1.5	1.5	years
Fabrication	1	1	1	years
Financing Parameter				
Interest rate	10	10	10	%/years
Escalation rate	2	2	2	%/years
Escalation during construction	3	3	3	years
Financing during construction	3	3	3	years
Financing during operation	30	30	30	years

For the more detailed equations, methodology and assumptions, Appendix F can be examined. This is also a similar analysis to that found in Saccherri et al. [2004]. It is noted that a 4 year cycle is chosen for IRIS, however, for simplification it was assumed that the nominal design only contains 4.95% assemblies, which will give a cycle length of about 5 years. The capital cost and O&M cost were taken from the IRIS final technical report [2003]. In the report, the numbers for capital and O&M cost are calculated by assuming there will be three plants built at the same site. As each plant will be constructed, it will provide funds for the other modules. The following levelized costs were calculated using Table 6-2 as inputs. For the total fuel cycle cost including the backend costs from Table 6-2, the following results were obtained:

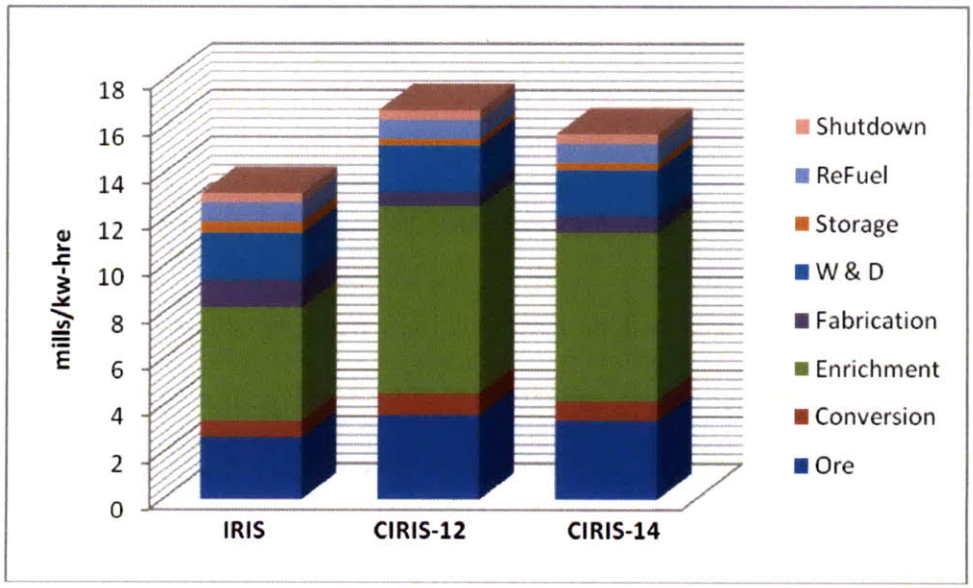

Figure 6-4 The levelized fuel cycle cost of the IRIS and the CIRIS reactor with 12 ft or 14 ft fuel rods

As seen in Figure 6-4, CIRIS-12 refers to the core with 12 ft IXAF and CIRIS-14 refers to the core with 14 ft IXAF. As shown in Figure 6-4, the higher enrichment needed to achieve the same cycle length will imply higher cost. The fabrication requires lower cost, since the actual core loading is less in CIRIS-12 and CIRIS-14. However, the enrichment price dominates

and the CIRIS is less economical than the IRIS reactor. The future development in enrichment technology will provide more economic benefits. If the capital cost and O&M cost are taken into account, then the following and more optimistic results are calculated.

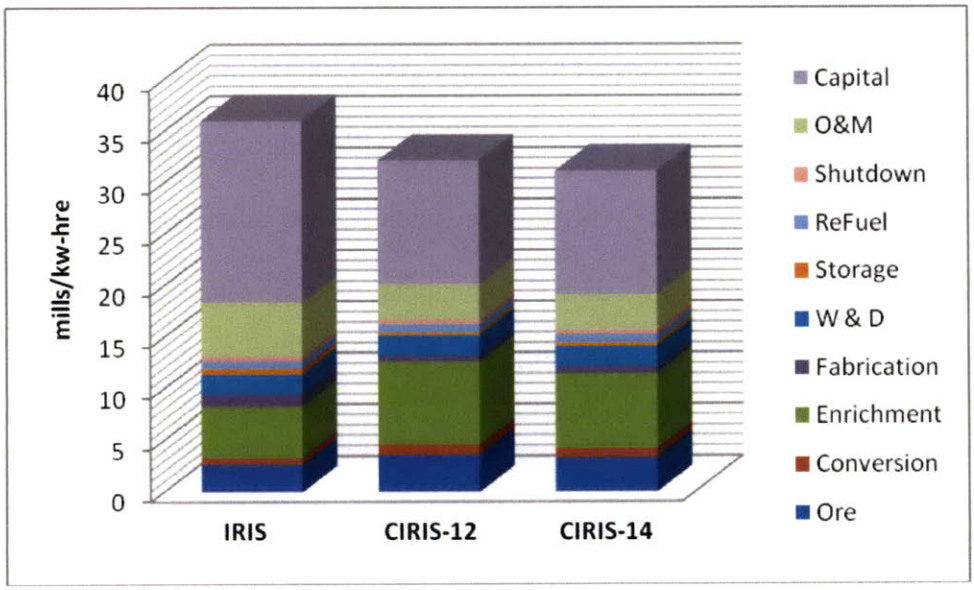

Figure 6-5 The levelized cost of the IRIS and the CIRIS reactor with 12 ft or 14 ft fuel rods

The overall levelized cost will be less for CIRIS reactor concept compared to the IRIS. The only significant difference in the capital cost is the 50% increase in capacity of turbines, which is implemented as seen in Appendix F. The 12 PCHE cost is assumed to be equal to the 8 OTHSG, since the total material needed for PCHE is less, but at the same time the manufacturing will probably be more costly. More specifically, according to Dewson et al. [2003], the PCHE cost will be 132 K$/m^3, which translates to 3.2 million dollars of cost for the CIRIS reactor, which is very small part of the total capital cost. At least 10% decrease in cost can be seen if the CIRIS design is chosen over the current IRIS reactor design, while it will generate 50% more electricity and revenue. If the O&M and Capital costs are taken to be the same value as the current estimated cost of nuclear power plants [Deutch et al., 2009], then even better results can

be achieved and are shown in Figure 6-6. It is shown that choosing the CIRIS design over the IRIS, will result in savings of 20 mills/kw-hre, which is very significant. In another words, the more uncertain the capital and O&M costs, the better the CIRIS will outperform the current IRIS design.

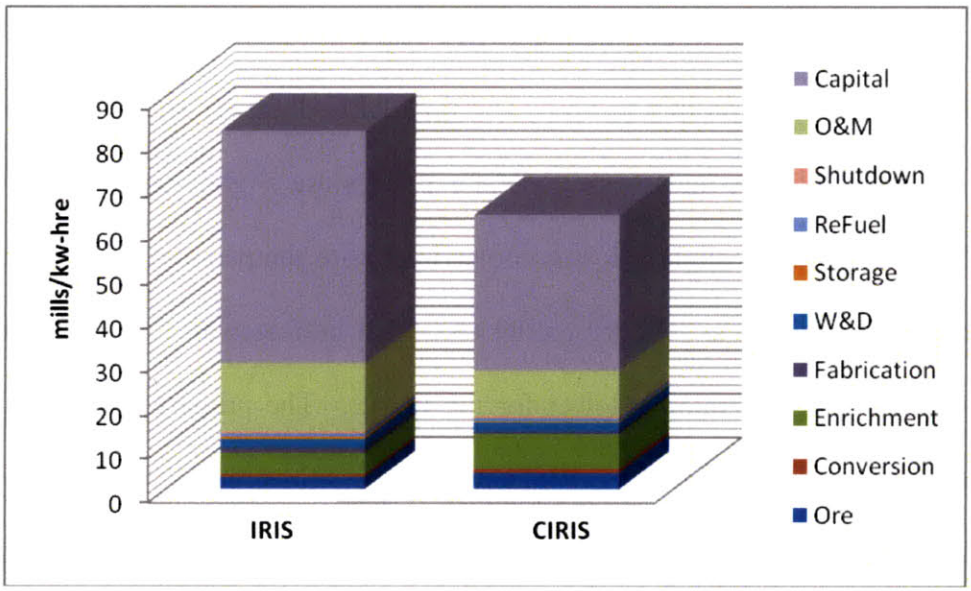

Figure 6-6 The levelized cost of the IRIS and the CIRIS reactor for current PWR capital and O&M levelized costs

Chapter 7 Conclusions and Future Work

7.1 Conclusions

The final design specification of the CIRIS reactor, which includes its geometric and thermal parameters are listed in this section. The final RELAP steady state results are listed in Table 7-1. As seen, the core and steam generator powers are slightly smaller than the 150% power level. This is due to slightly lower cooler inlet core temperature and higher pumping power needed for the pumps as RELAP model takes that into account. The pressure drop on either side of the steam generator is lower for the PCHE. The primary loop circulation is 8 seconds faster than the IRIS design for CIRIS, since the mass flow rate is 50% higher. However, the time that it takes for flow to move from steam generator outlet to core inlet is about 20 seconds for both the IRIS and the CIRIS. Therefore, abnormal conditions in pumps and SGs are propagated at the same rate initially. This is due to the shorter PCHE height, resulting in increase in length of the downcomer, which slows down the fluid flow rate.

Table 7-1 The Final MIT RELAP CIRIS model compare to the IRIS nominal specifications

Parameter	Unit	IRIS	CIRIS	Ratio
Pressurizer pressure	MPa	15.5	15.49	1.00
Core power	MW	1000.0	1498.4	1.50
Total SG power	MW	1001.47	1500.8	1.50
BE vessel flow	kg/s	4707	7060.5	1.50
BE core flow	kg/s	4504	6756.1	1.50
Total steam flow	kg/s	502.8	754.2	1.50
Core inlet temperature	K	565.2	565.1	1.00
Core outlet temperature	K	601.5	601.4	1.00
SG pressure	MPa	5.8	5.8	1.00
Steam exit temperature	K	590.2	591.4	1.00
Dp core	kPa	52.0	70.8	1.36
Dp SG1 prim/sec	kPa	72.0/296	57/32	1.26/9.25
RCP head	m	19.1 (18.3-21.3)	35.2	1.84
Primary Loop Circulation	sec	41.5	33.6	0.81

In terms of accident sequences, the most limiting RELAP model coupled with VIPRE, showed high degree of safety for the IRIS reactor.

The final PCHE specifications compared to the OTHSG are listed in Table 7-2.

Table 7-2 The zigzag PCHE vs. OTHSG specifications

Parameters	Helical	PCHE	
Power	125	125	MW
Primary side:			
Mass Flow rate	589	589	kg/s
Mass Flux	897	957	kg/m2s
Inlet Temperature	328.4	328.4	C
Outlet Temperature	292	291.9	C
Inlet Pressure	15.5	15.5	MPa
Pressure drop(w/headers)	72	69	kPa
H Transfer Coefficient	6843	44249	W/m2k
Secondary side:			
Mass Flow rate	62.5	62.5	kg/s
Mass Flux	693	203	kg/m2s
Inlet Temperature	223.9	223.9	C
Outlet Temperature	317	318.6	C
Outlet Pressure	5.8	5.8	MPa
Pressure drop(w/headers)	296	275	kPa
H Transfer Coefficient	23473	32387	W/m2k
Geometry			
Diameter	variable	0.002	m
Width	-	0.6	m
Height	7.9	4.2	m
Length(core)	-	0.409	m
Volume (no headers)	65	1.031	m3
Volume w/headers	70	1.78	m3
Volume Ratio	39.33	0.03	-
Surface Area Density	44.5	1421	m2/m3
Power Density	1.92	121.24	MW/m3

The PCHE's size uncertainty could arise from uncertainties in correlations (5%), CHF (10%), conduction model (10%) and Fouling (15%). These uncertainties were calculated based

on multiple runs of the Fortran PCHE code. Therefore, Figure 7-1 has the reactor vessel cross-section view with 50% increase in the total length of the PCHE for conservative sizing. There will be at least a gap of 20 cm between each PCHE modules to account space for vibration or maintenance issues.

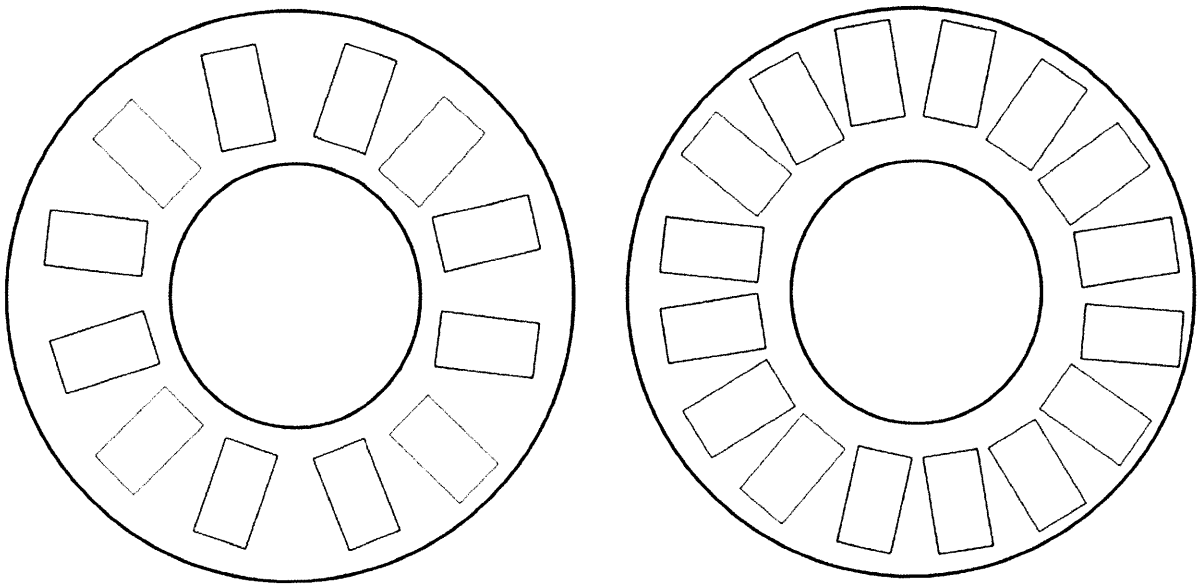

Figure 7-1 The reactor vessel cross-sectional view from top using the PCHE

As seen in Figure 7-1, still up to 16 PCHE can be fitted in the current IRIS vessel, even with the 50% increase in size due to all the possible uncertainty with at least 10 cm gap between the modules. This can add more redundancy which will make the ability to go for longer cycle length without SG maintenance easier.

In conclusion, the complete thermal hydraulics model of the IRIS and CIRIS reactor was performed. In addition, brief studies on stresses, component design, shielding, and economics were performed to optimize the final CIRIS design and provide a more realistic picture. It is

concluded that the CIRIS reactor is cheaper on per kW-hre basis and provides 50% more electricity.

7.2 Recommended Future Work

The rise in interest in the small reactors, led to many integral LWR designs recently. Almost all integral design vessel sizes are limited by size of their heat exchangers. The PCHEs are very beneficial in terms of size and pressure drop for integral type reactors. As of 2009, no recorded data on boiling water with PCHE could be found publically. Their unique channel size, leads them to be characterized somewhere between small tube channels and microchannels. Overall the following recommended work is listed in order of their significance to the reported work:

1. PCHE experiments to evaluate its performance:
    a. Boiling water under high pressure (7 MPa) and low flow rate (100-300 kg/m^2-s)
    b. Corrosion and fouling characteristics
    c. Stress tolerance of large PCHE units
2. Additional detail to IRIS plant model:
    a. Include all the missing safety systems
    b. Model more accidents such as SBLOCA
    c. More detail on shielding and dose calculations during operation or refueling
    d. More detail on pump performance, especially related to coastdown rates and reliability.
3. Maintenance and licensing issues of an integral reactor and PCHE.
4. Compare benefits of placement of the pumps and EHRS inside or outside the vessel.

APPENDECES

Appendix A ANL Benchmarking

The experiments in ANL are the only published work on PCHE with water on one side. There have been two master's theses to figure out a way to model PCHE from Kansas State University. One study uses fluent and the other uses a 3d-finite element analysis to obtain the results on PCHE performance. To make sure the water portion of the code works, the MIT developed PCHE code was benchmarked against ANL experimental data [Meter, 2008].

ANL never released the actual size of the PCHE, however, they released the following information in Table A-1.

Table A-1 The PCHE specification used in the ANL experiments (from Meter, 2008)

	Hot Side	**Cold Side**
Design Pressure, MPa	8.3	21.6
Design Temperature, °C	200	200
Flow Area, mm^2	1047	930
Number of Channels	1176	1050
Hydraulic Diameter, mm	0.92	0.92
Flow Channel Configuration	Semi-circle	Semi-circle
Volumetric Capacity, Liters	2	2
Heat Transfer Area, m^2	5.6	5.6
Total Mass, kg	203	
Outer Dimensions (H x W x L), mm	120 × 200 × 1200	
Design Heat Load, kW	17.5	

The key information missing is the channel pitch and plate thickness. Through trial and error the following PCHE input in Table A-2, was derived based on the given information.

Table A-2 PCHE Input File used to the ANL experiments

zig	Precooler for SNL Loop - zig-zag channel-540kW
1h1c	
20.3	power (kW)
7995	pressure - hot fluid - hot end (kPa)
7995	pressure - cold fluid - cold end (kPa)
87.930d0	temperature - hot fluid - hot end (oC)
31.280d0	temperature - cold fluid - cold end (oC)
0.13906	mass flow rate on hot side (kg/s)
0.19447	mass flow rate on cold side (kg/s)
0.001506	hot channel diameter (m)
0.001506	cold channel diameter (m)
0.00131	hot plate thickness (m)
0.00131	cold plate thickness (m)
3.1375	hot pitch divider
2.124	cold pitch divider (Pitch=channel diameter + (channel diameter)/(pitch divider)
0.0551	HX height (m) - this is total for 4 submodules (actual module H=height/4=5.5)
0.1152	HX width (m)
1	# of modules - how many modules stacked
21	thermal conductivity of the plate (W/mK)
40	# of HX longitudal cells
44.0026	wmh - molar mass
18	wmc - molar mass
co2.fld	hot fluid id (0 co2 else helium)
water.fld	cold fluid water
1.0d-5	pressure iteration precision

The above PCHE specification is different from what the researchers at KSU estimated, which is shown below in Table A-3 [Meter, 2008]:

Table A-3 The Kansas State University calculated dimensions for the ANL experiments (from Meter, 2008)

	Hot	Cold
Channel Diameter, mm	1.506	1.506
Channel Travel Length, mm	1230	1378
Full Bend Angle, degrees	135.8	111.6
Number of Plates	21	21
Channels per Plate	56	50
Thickness between channels, mm	0.48	0.48
Plate Thickness, mm	1.31	1.31
Sidewall Thickness	44.6	
Top and Bottom Wall Thickness, mm	32.5	

For one of the cases, the MIT PCHE code resulted in the hot outlet temperature of 35.9 C as opposed to 35.33 C and the cold outlet temperature of 56.44 C as opposed to 56.22 C in the experiments. The KSU values for the hot and cold outlet were 41.38 C and 41.46 C for this case, respectively, which are less accurate than the MIT code. Same accuracy was found for all the cases in [Meter, 2008], so, it was concluded the MIT PCHE code is works properly for CO2-water cases. The pressure drops could not be compared due to lack of information.

Appendix B RELAP PCHE Benchmarking

In order to successfully model the PCHE in RELAP, first the code itself has to be verfied, due to untraditional geometric parameters of the PCHE. Five different cases were initially run using RELAP and the MIT code. In all cases, the PCHE was physically modeled according to its geometric properties. The first case is the single phase water where the flow on both sides of the PCHE are in the laminar region. As seen in Table B-1, the temperatures and pressure drop are in somewhat close agreement, however, the heat transfer coefficient is off by factor of 3. The standard RELAP heat transfer coefficient recommended by the RELAP manual was used. On the other hand, in turbulent regime, the heat transfer coefficient matches the Fortran code. However, the power is even more different than in the first case, by as much as 45%. The heat flux is also higher for the RELAP case as seen in Figure B-1.

Table B-1 The Fortran vs. RELAP results for single phase laminar flow (Case 1) and single phase turbulent flow (Case 2).

Case 1	Fortran	RELAP	Units	**Case 2**	Fortran	RELAP	Units
Tcold Out	323.16	324.442	k	Tcold Out	61.98	66.5	C
Thot Out	361.28	359.891	k	Thot Out	88.15	82.6	C
Delp cold	1.7	1.27	kPa	Delp cold	146	105.70	kPa
Delp hot	1.6	1.0	kPa	Delp hot	135	97.50	kPa
Cold Htc	2176.87	6.63E+03	W/m2k	Cold Htc	43128	42401	W/m2k
Hot Htc	2766.17	8.24E+03	W/m2k	Hot Htc	54059	51600	W/m2k
Power	100	110	kW	Power	1	1.45	MW
				qppave	3.25E+05	4.2E+05	W/m2

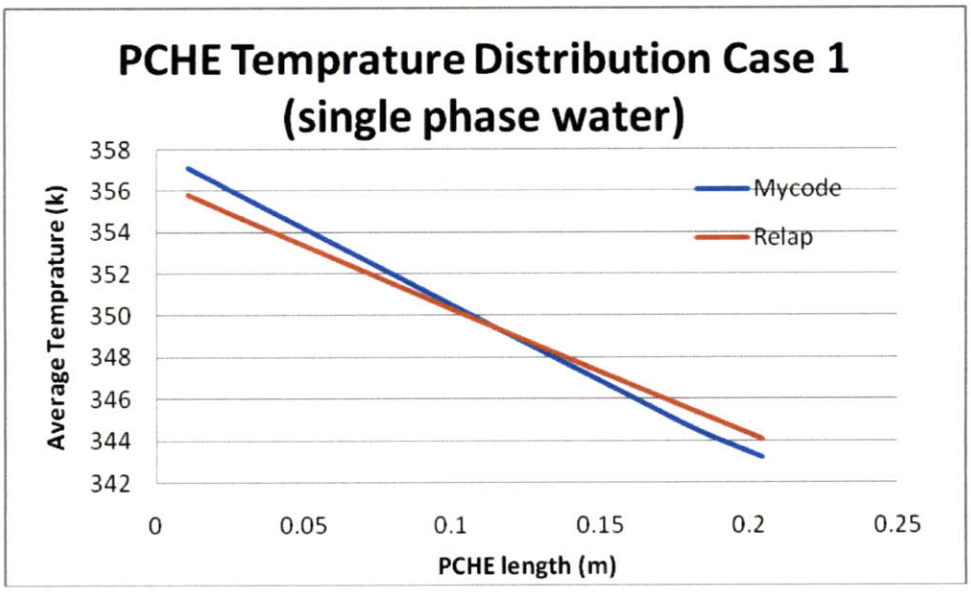

(a)

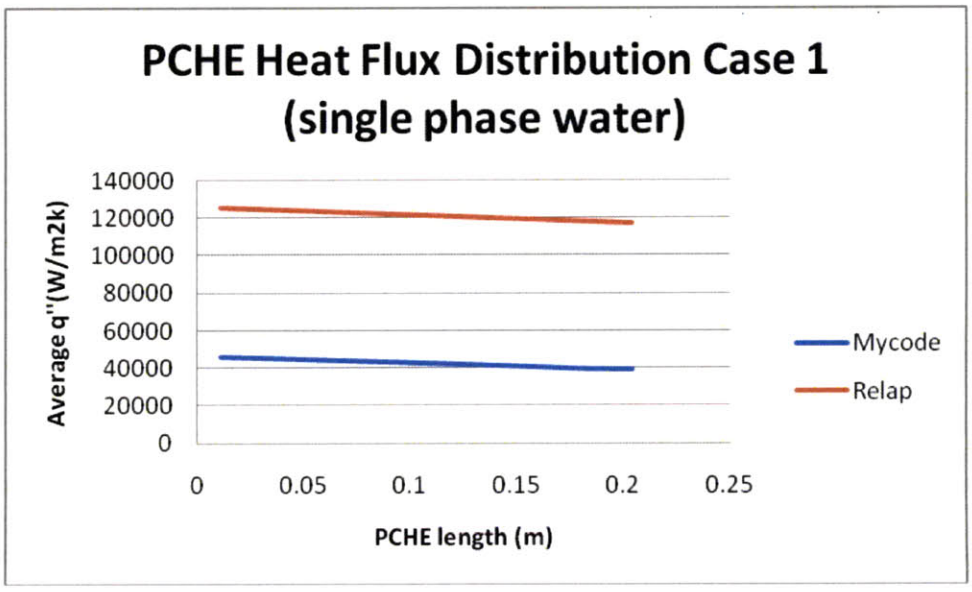

(b)

Figure B-1 The PCHE (a) temperature and (b) heat flux destributions for the single phase laminar flow case.

For the third case, an input deck of a CO2 to Water PCHE RELAP model was run. This input was used by the [Davis et al., 2005] for GFR Precooler design. The INL input uses effective conduction length as the Fortran code uses and also different heat transfer mode that

does not exist in the RELAP5-3D manual. The results were all different as seen in Table B-2, the MIT benchmarked case predicted 325 MW, which is consistent with the goal of the GFR Precooler design. However, their input methodology resulted in 100 MW more power and different temperatures. The Fortran CO2 side heat transfer coefficient did not agree with either RELAP results. The water pressure drop is close but the CO2 side pressure drop is very different between the cases. For the case of CO2 to water, the Fortran code is actually benchmarked against experiments, therefore it was decided the methodology used in RELAP model needs to be changed.

Table B-2 The comparison of PCHE performance for three different models for CO_2 to Water heat transfer as a media.

Case 3: CO2-Water	Fortran	RELAPINL	RELAPMIT	Units
Tcold Out	41.89	48.3585	46.7096	C
Thot Out	41.55	37.1564	39.1889	C
Delp cold	37	30.62	30.2	kPa
Delp hot	53	26	25	kPa
Cold Htc	9997.79	8094.70	7954.8	W/m2k
Hot Htc	2051.18	8276	7894	W/m2k
Power	325	420	395	MW

Case 4 and Case 5 illustrate the RELAP models of single phase to two phase water PCHE with straight and zigzag channels, repectively in Table B-3. The Fortran and PCHE code yielded similar heat transfer coefficients at different regimes including two phase flow. However, the RELAP built-in CHF package which will be described in more detail later, signals the code to move to post-CHF regime very early in the PCHE geometry as seen in Figure B-2.

Table B-3 The Fortran vs. RELAP comparison of the PCHE under IRIS nominal conditions with straight channels (Case 4) and zigzag channels (Case 5).

Case 4	Fortran	RELAP	Straight Units	**Case 5**	Fortran	RELAP	Zigzag Units
Tcold Out	320.27	308.75	C	Tcold Out	319.9	327.97	C
Thot Out	291.96	293.182	C	Thot Out	291.92	291.588	C
Delp cold	6.448	5.83	kPa	Delp cold	38.6	3.7	kPa
Delp hot	16.669	13.8	kPa	Delp hot	61	7.9	kPa
Cold Htc	24504.72	12676	W/m2k	Cold Htc	46523	23260	W/m2k
Hot Htc	20500.56	24816	W/m2k	Hot Htc	56214	74286	W/m2k
Power	125	121.4	MW	Power	125	125.54	MW

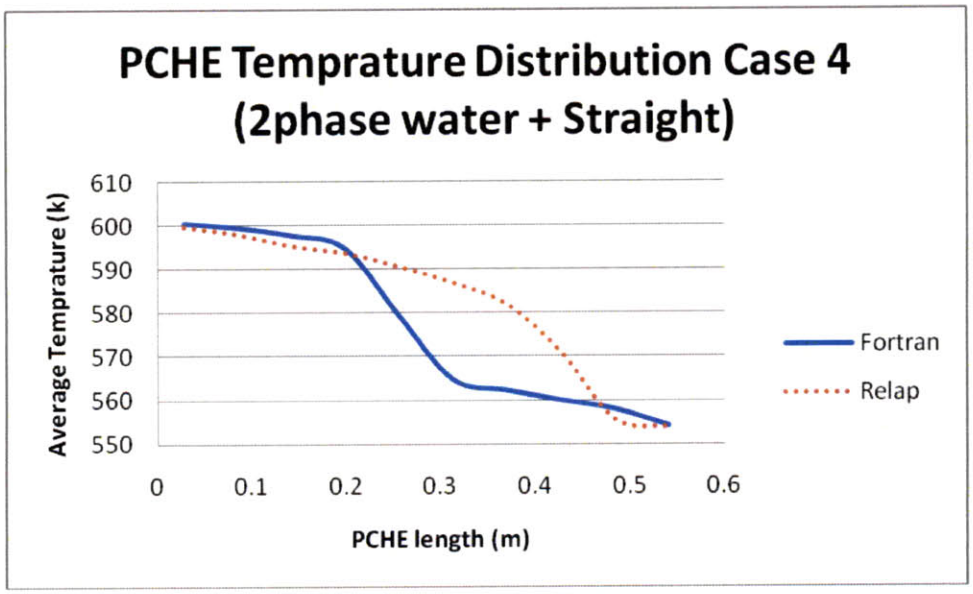

(a)

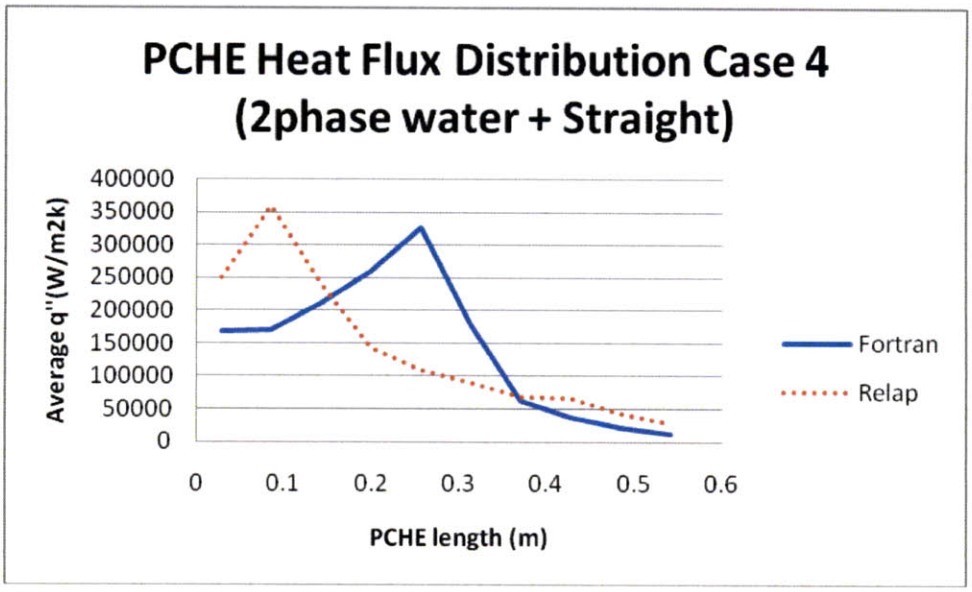

(b)

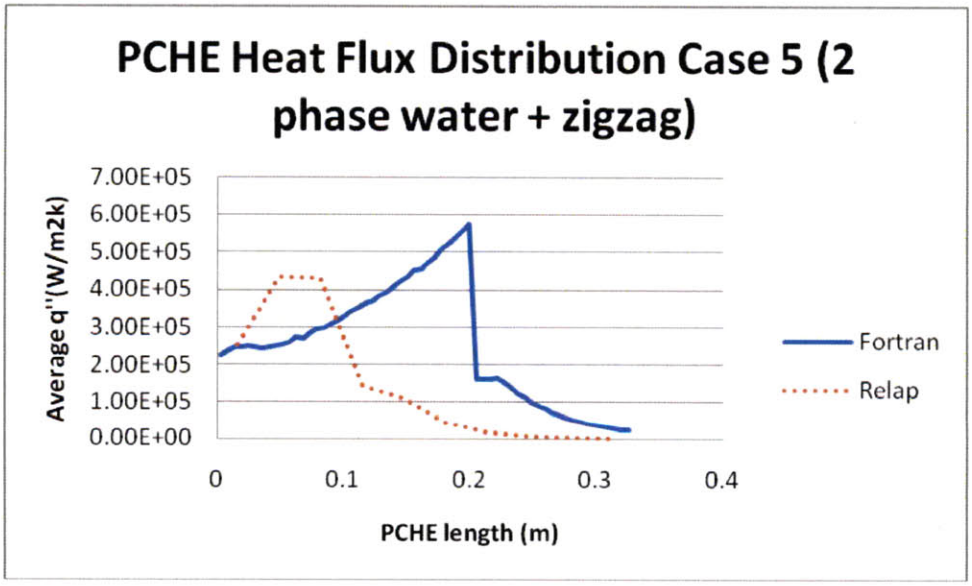

(c)

Figure B-2 The PCHE under nominal IRIS condtions with straight channel's (a) temperature and (b) heat flux distributions and zigzag channel's (c) heat flux distribution.

In summary, the 5 cases showed inconsistancies in laminar heat transfer coefficient, pressure drop, CHF calculation and heat flux. The next few pages will address all of these challenges.

Figure B-3 shows the plot of the heat transfer coefficent using Fortran code, RELAP standard code and the Gnielinski heat trasfer correlation (heat trasnfer mode 160) used by INL as previously mentioned, vs. the Re number.

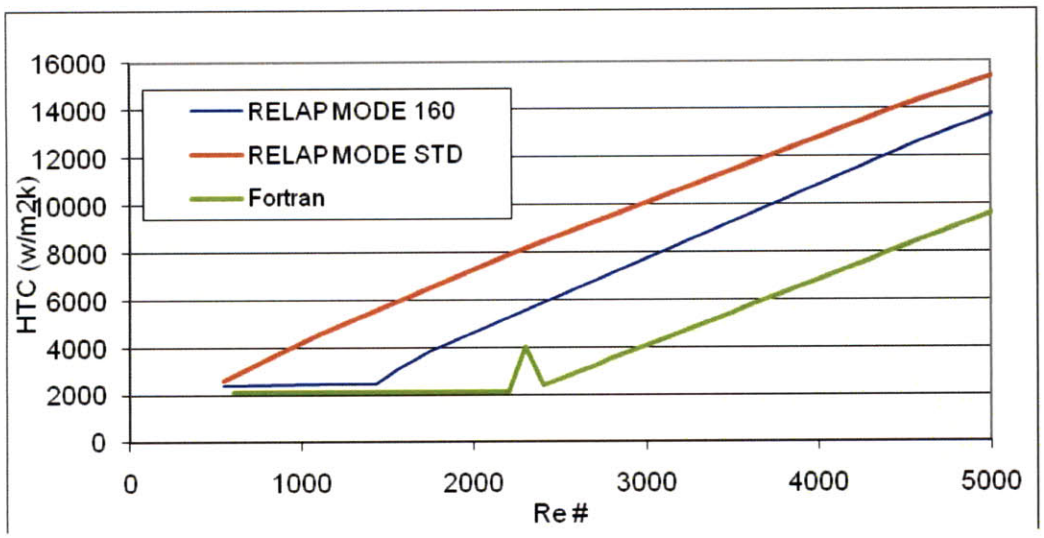

Figure B-3 The Reynalds number vs. the the heat transfer coefficient for the same geometry but different methods.

As can be seen in Figure B-3, the Standard RELAP heat transfer model does not take into acount the laminar flow regime, which contradicts the manual. The INL mode used does take into account laminar regime, however it does not have a transition region. Also, the laminar region in Fortran code is a little bit lower, because Fortran code uses special Nu number for semi-circular channels. Though, not shown in Figure B-3, after Re of 10,000 the differences between the above coefficients is minimal. In conclusion, PCHE will behave as expected at all conditions except for Re # 3000-10,000 at single phase conditions, which will not be experienced under IRIS normal operating conditions and any conditions for the secondary side.

Next, the pressure drop differences in the zigzag geometry are addressed. RELAP can physically model zigzag channels with their specific angles of their bends. However, the manual

mentions that straight tube flow dynamics and physics are used and future RELAP packages will work to improve on this capability.

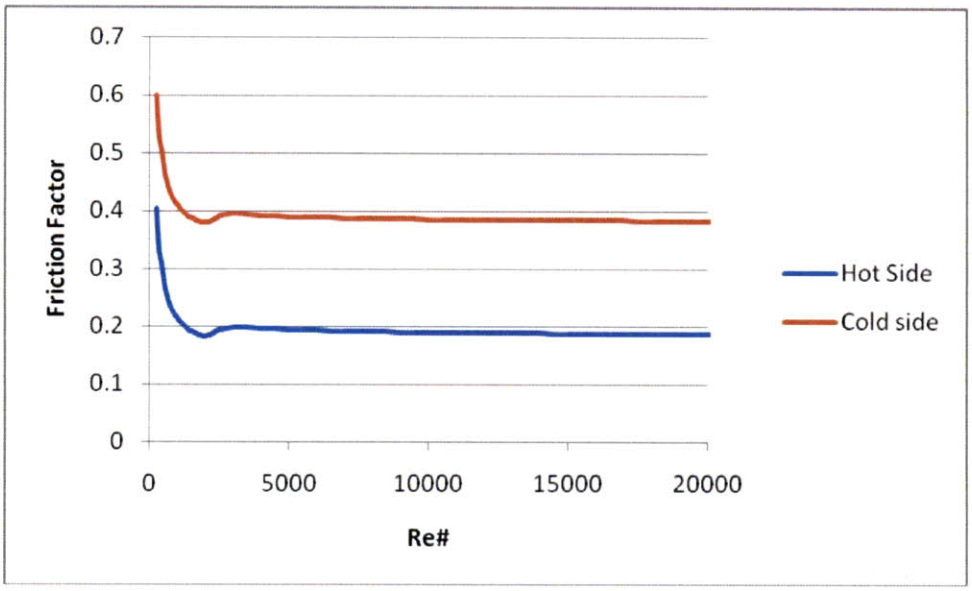

Figure B-4 The friction factor vs. Reynalds number of the zigzag PCHE in Fortran code.

Figure B-4 displays the friction factor as a function of Re, taken from the Fortran code output. This function is then curve fitted and inputted to RELAP as function of Re of the RELAP model. To match cases, the multiplication factor of the model is changed to provide same pressure drops calculated in the Fortran code and the RELAP model as seen in Figure B-5.

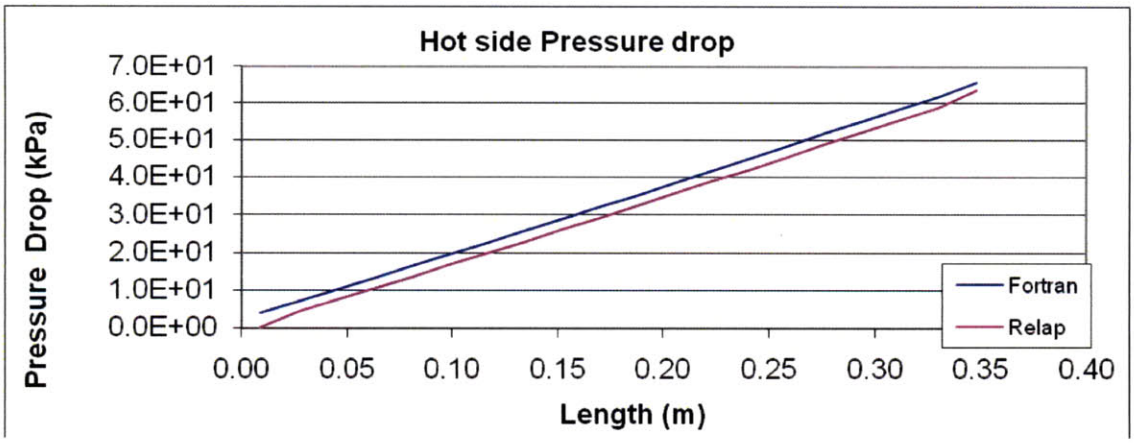

(a)

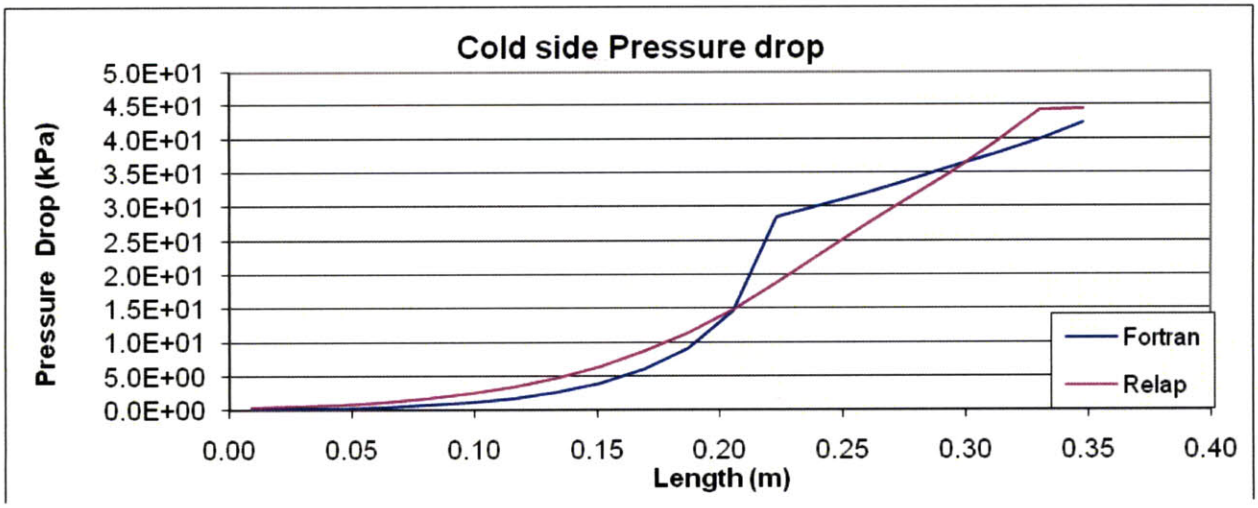

(b)

Figure B-5 The comparison of the Fortran and RELAP PCHE models of pressure drop for (a) hot side and (b) cold side.

As seen in Figure B-5, the overall pressure drop is effectively modeled for the single phase and two phase regions. However, if the same coefficeints is applied to the different Re numbers in RELAP, the results were not successfully extrapolated compared to the Fortran code. In conclusion, the fitted friction function cannot be extrapolated between the different cases. Therefore inlet node of the SGs were given a constant loss coefficient to match nominal pressure drop values.

The CHF in RELAP uses Groeneveld ACLU Tables, however, some inconsistensies were found. The [Groeneveld et al.,1987] recommends multiplying factors that will modify the CHF at different diameters, orientation and conditions. The factors that are definitely not applicable for PCHE modeling are, the bundle factor, grid spacer factor, vertical flow factor, out of range pressure. The detail of the factors that will be used is showed in Table B-4 from RELAP5 manual (2001):

Table B-4 The guidelines for CHF calculation in RELAP5 (from RELAP5 manual, 2001)

k1 = hydraulic factor	$k1 = \left(\frac{0.008}{D}\right)^{0.33}$ for D < 0.016 m $k1 = \left(\frac{0.008}{0.016}\right)^{0.33}$ for D > 0.016 m D = heated equivalent diameter = $\frac{4A}{\text{heated perimeter}}$

k4 = heated length factor	$k4 = \exp\left\{\left(\frac{D}{L}\right)[\exp(2.alp)]\right\}$ $alp = \frac{xlim}{[xlim + (1 - xlim)]}\frac{\rho_g}{\rho_f}$ xlim = min[1, max (0.X_e)] L = heated length from entrance to point in question
k5 = axial power factor	k5 = 1. for X_e < 0 $k5 = \frac{qlocal}{qbla}$; qbla = average flux from start of boiling to point in question
k6 = horizontal factor	k6 = 1 if vertical k6 = 0 if horizontal stratified k6 = 1 if horizontal high flow k6 = interpolate if medium flow

The k6, which accounts for horizontal flow, uses the same method that was used in Chapter 3 of critical heat flux calculations. The nominal mass flux of the PCHE was increased by increasing the flow rate, however at the same pressure and temperature, the critical heat flux in RELAP did not change. This is surprising, since the Groenveld et al. correction factor is in terms of mass flux and the mass flux of the PCHE is higher than the mimimum stratification limit. Another problem with this correlation is that the hydraulic factor is inaccurate as it assumes that all tube diamters below 1.6 cm behave the same way, which it is not true as seen from chapter 3. In fact, the diameter changes are not only function of mass flux but also a function of the pressure and

the flow quality as seen in Table 3-1. Due to these inaccuracies, the boiling factor was used to force CHF behave more like in the Fortran code.

Lastly, the differences in the heat flux were resolved by the same approach that was described in Chapter 2 with the OTHSG RELAP model.

Appendix C RELAP further Transient analysis

The effects of the LOFA without any safety systems can be seen below. Figure C-1 proves that PCHE has little effect on the primary side behavior as the two graphs overlap.

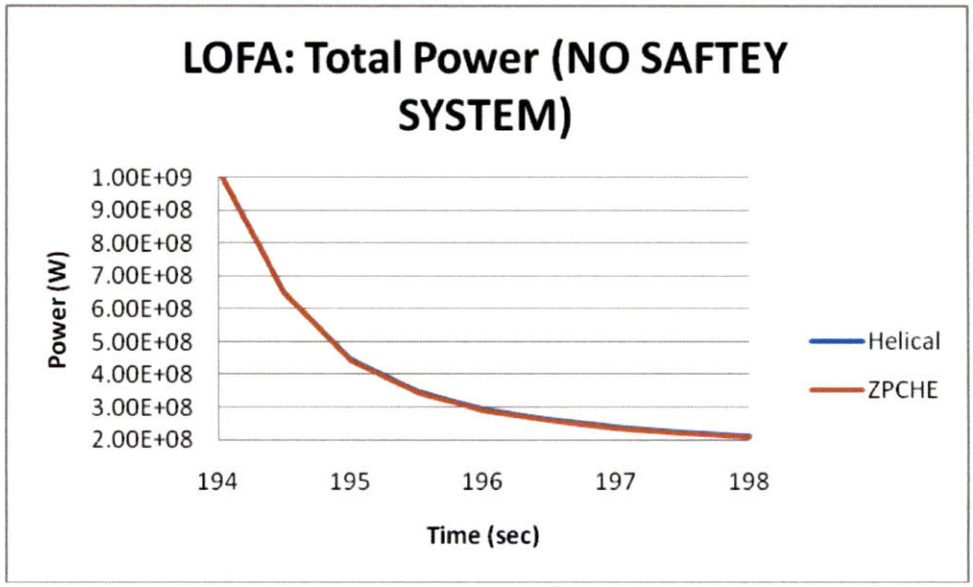

Figure C-1 The behavior of the IRIS during the LOFA, with no safety systems used for OTHSG and the zigzag PCHE.

Unlike the LOFA, the much faster PCHE effect on system response can be clearly seen in Figure C-2.

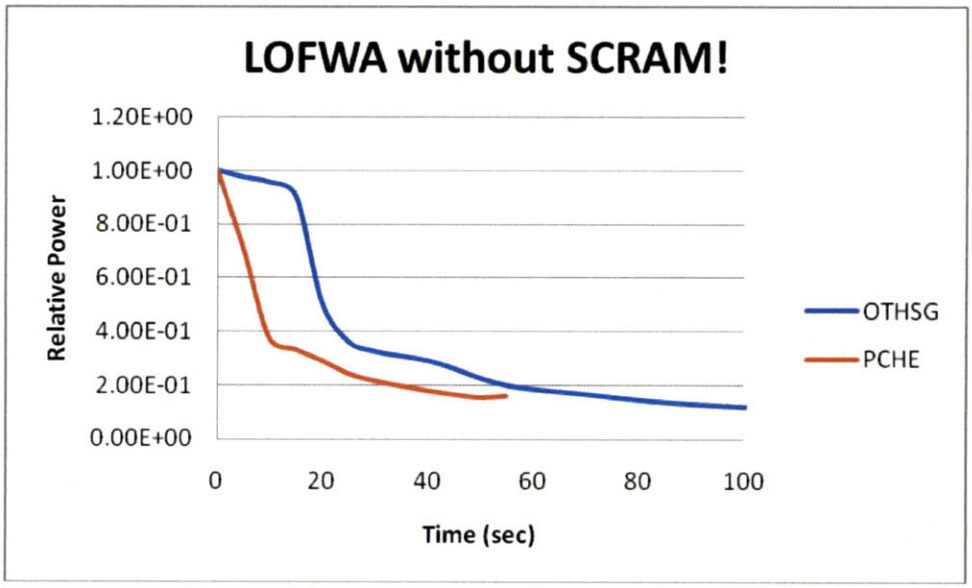

Figure C-2 The behavior of the IRIS during the LOFWA, with no saftey systems used for OTHSG and the zigzag PCHE.

One of the limiting factors of reducing the IRIS reactor vessel size is the pressurizer volume. In IRIS, the pressurizer does not feature a Pressurizer Spray System (PSS), which is needed to be modeled if the volume of the pressurizer is small. As seen in Figure C-3, if the volume of IRIS pressurizer is similar to an ordinary PWR, the system pressure falls very fast and the long term cool-ability of the core will be compromised. The vessel with PCHE almost immediately failed, since the fuel temperature reached temperatures outside of the RELAP model range.

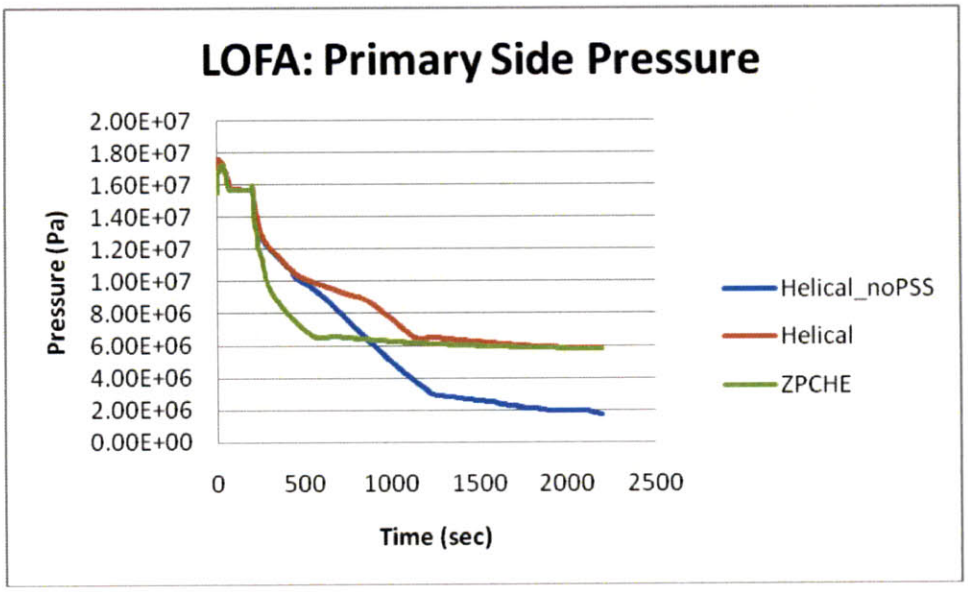

(a)

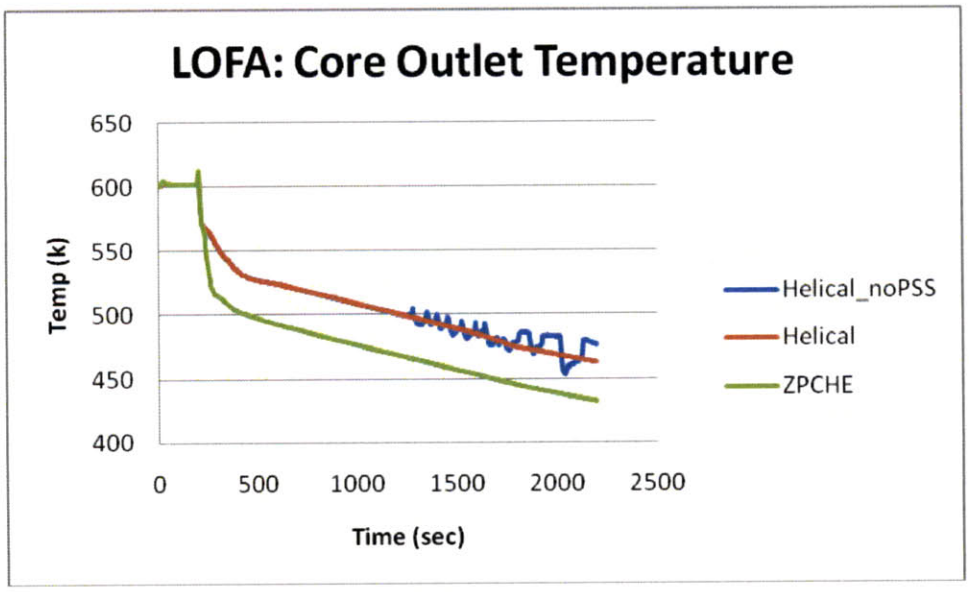

(b)

Figure C-3 The IRIS behavior during the LOFA for No PSS/with PSS cases on (a) primary side pressure and (b) core outlet temperature.

Figure C-3 shows the primary side pressure decreasing as the EHRS is depressurizing the system. As seen, without the PSS discussed previously, the OTHSG can survive up to 1000

seconds of simulation and the core will be uncovered after that time. In case of the PCHE, the core would be uncovered after only 100 seconds of simulation without PSS.

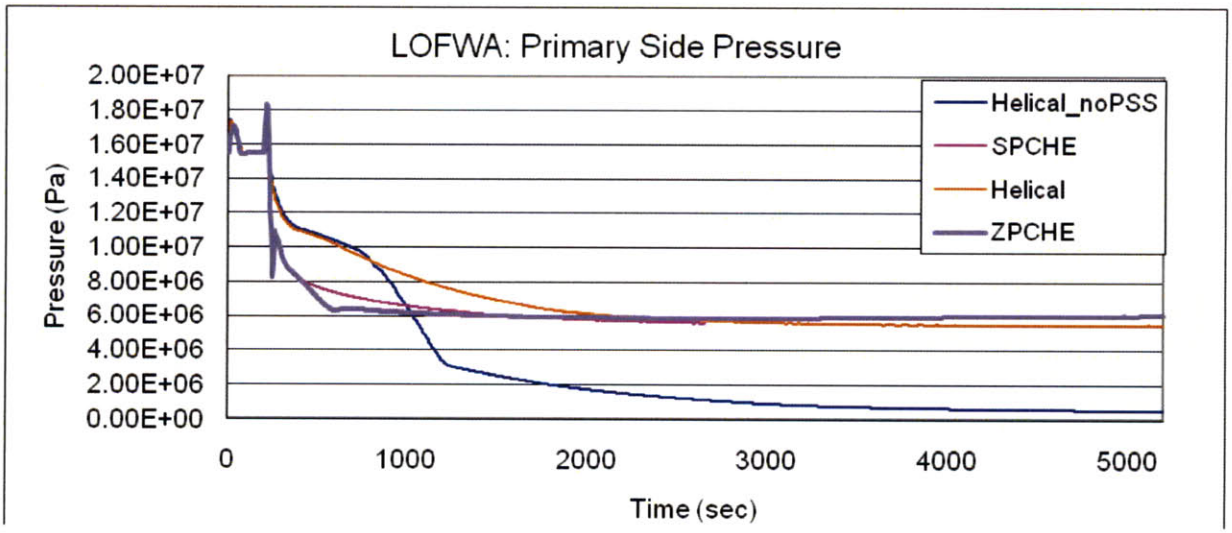

Figure C-4 The IRIS behavior during the LOFWA with PSS and without PSS.

As seen in Figure C-4, the impact the PSS system is again shown. Both straight (0.6 m in length) and zigzag PCHE (0.3 m in length) were modeled and the input was run. It is shown that while the straight PCHE is about twice the size of zigzag PCHE, their behavior is the same in terms of pressure, temperature and core power. Therefore to be conservative, the zigzag PCHE is used for the rest of the analysis and it is assumed that should the final size of PCHE be longer than the above zigzag PCHE, then its saftey implications are inconsequential, assuming the zigzag PCHE meets all the saftey criterion considered in this analysis.

FAST COASTDOWN ISSUES

There are many ways we can approach the problem with the fast coastdown rate such as increasing the inertia of the pumps. This strategy will require more space for the pumps. The pumps are unknown in size and this will work against the idea of increasing the power density of the reactor. Another way is to only increase the reactor power by a minimum percentage that

will assure MDNBR<1.3. The more accurate version of how mass flow rate decreases based on pump specifications was made public in Westinghouse WCAP document [Oriani, 2003] as shown in Figure C-5.

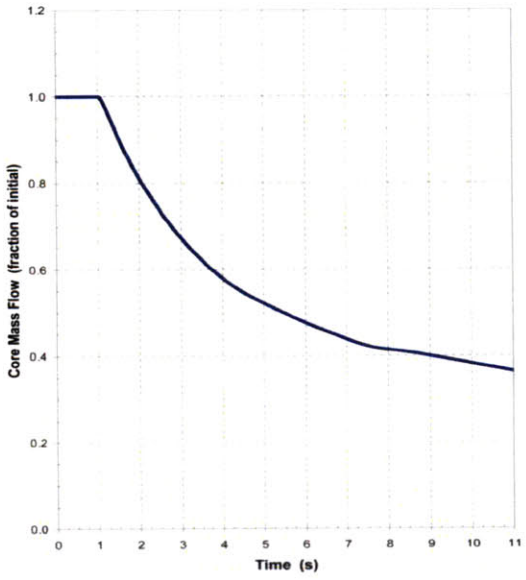

Figure C-5 The coastdown rate during the IRIS LOFA (from Oriani, 2003).

As seen in Figure C-5, this ramp is slower than the assumed no coustdown cases run in RELAP and chapter 4. Three cases were run using the above mass flow rate profile along with the OTHSG and IXAF fuel. These cases were:

1. Using above profile with no neutronic feedback as done by the IRIS team.
2. Using the same sequence as the previous LOFA cases wich SCRAM at 118% core temperature difference compared to the nominal temperature difference.
3. Using the same sequence at in 2, except for the initiation of SCRAM that is 2.5 seconds after the mass flow rate initial decrease.

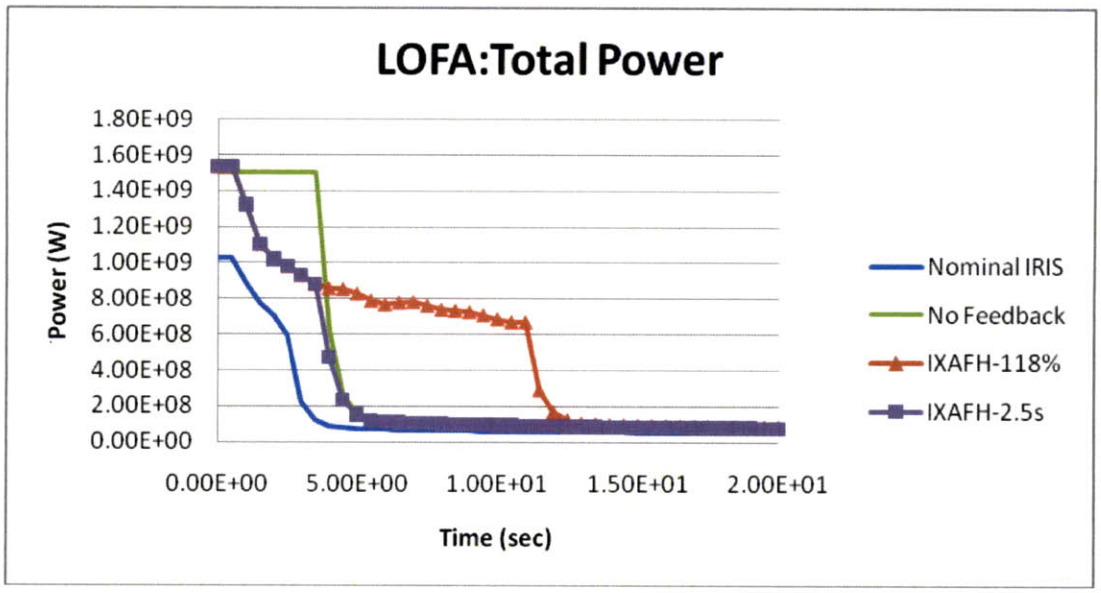

Figure C-6 The IRIS total power during the LOFA assuming different scenarios.

As seen in Figure C-6, in the no feedback case, the total power level stays at 1500 MWth, while feedback plays an important role in the other two cases. For the 1st case MDNBR of 0.2 was reached and for 2nd and 3rd case identical MDNBR of 1.536 were calculated. The conclusion from above is that if no feedback is assumed, the IXAF fuel at 150% uprated power is not safe. However, given the feedback the use of IXAF fuel is considered acceptable. Furthermore, the IRIS core with IXAF fuel passes the 1.3 MDNBR margin, under the assumption of no feedback. However the mass flow rate ramp is slower.

Appendix D PCHE further design

STRESS ANALYSIS

The PCHE much like other SGs are affected by stress and they need to meet the ASME standards. The main key assumptions for this study is to assume that a single channel acts as a pressure vessel. Since the channels are semi-circurular, the pressure boundary is assumed to be rectangular for conservatism, while the channel itself is still semi-circular in calculations. The PCHE uses diffusion bond in plates in which the bond has shown to break after the material itself breaks. The current proposed designs for plates of 1.6 mm and 2 mm channel diameter were in range of the tests performed on the PCHE. In general, creep is factor when considering stress analysis. However, the expected creep should be minimal since the maximum nominal operating temperature is about 320 C. This relatively low temperature compared to temperatures that are being used for gases in PCHE will increase the lifetime of the module. The stainless steel mechanical properties were used to calculate the allowable stresses. Stress rupure strength of stainles steel was used. The allowable stress (σ_a) was calculated using the current design channel pitch (P), channels per meter (N_c) and channel diameter (d_c) and the pressure difference of hot and cold sides ΔP (about 10 and 16 MPa maximum) (Hesselgraves, 2001):

$$\sigma_a = \Delta P \cdot \left(\frac{1}{(P - d_c) \cdot N_c} - 1\right).$$

For 16 MPa, the σ_a is 50 MPa (7250 Psi).

The specific service cycles assuming 18 month of operation minimum will be far less than 10^6 so the fatigue curve for 10^6 was used from the ASME guide book. Using the simplified

stress analysis as mentioned above using the primary general membrane stress intensity, ASME code mandates that $P_m < S_m$. The maximum possible strain on the PCHE will be 0.02% at 50 MPa < 180 MPa at 320 C.

The plate thickness and the channel radius of 1 mm was used to be used in Mohr theory the maximum stress was calculated using the thick cylinder approximation.

$$\tau_{max} = p\frac{\frac{r_o^2 + r_i^2}{r_o^2 - r_i^2} - 1}{2}$$

Using the design pressure of 20 MPa, the maximum allowable stress was calculated to be 12.8 MPa, which will be violated in case of fast depressurization of the cold side. However, since our temperature does not exceed limits, according to Heatric™ website, a general PCHE geometery described in Figure 3-10, should withstand pressures much higher and the design pressure listed as 65.5 MPa, which gives 42 MPa of margin, which will cover the correction of the semi-circular geometery and transients.

CHF CORELATION AND CORRECTION EQUATION

The Duckler Correction factor for Horizontal flow k_{hor}:

- $k_{hor} = 0.0$ if stratified flow ($G<G_1$)
- $k_{hor} = 1.0$ if Nonstratified flow ($G> G_2$)
- $k_{hor} = (G- G_1)/(G_2- G_1)$ if intermediate flow ($G_1 < G < G_2$)

where G_1 is the mass flux boundary between fully startified and intermittent flow defined as:

$$G_1 = \frac{\sqrt{g\,D(\rho_L - \rho_G)}}{X_a}\left(\frac{1}{0.65 + 1.11\,X_{LM}^{0.6}}\right)^2,$$

where g is the gravity, D is the hydraulic diameter, ρ is the density, X_a is the actual quality and X_{LM} is defined as:

$$X_{LM} = \left(\frac{1 - X_a}{X_a}\right)^{0.9}\left(\frac{\mu_L}{\mu_G}\right)^{0.1}\left(\frac{\rho_G}{\rho_L}\right)^{0.5},$$

where μ is the viscosity.

G_2 is the mass flux boundary between intermittent and annular flow calculated by Taitel and Duckler flow regime map [Taitel et al., 1976] as shown:

$$G_2 = \left[\frac{g\,D^{1.2}(\rho_L - \rho_G)}{0.092(1 - X_a)^{1.8}\,\mu_L^{0.2}}\,f_2(X_{LM})^2\right]^{0.556},$$

where f is a function which is defined as:

$$f_2(X_{LM}) = \exp[A + B\ln(X_{LM}) + C\ln^2(X_{LM})],$$

where A = -0.3470, B = +0.2920, C = -0.0556.

Wong Correlation Parameters to calculate

$$T_1 = C_1\,\mathrm{Re}_L^{-0.2}\left(\frac{1 - X_a}{1 - \varepsilon}\right)^2\frac{G^2}{g\,D\,\rho_L(\rho_L - \rho_G)\varepsilon^{0.5}}$$

where $C_1 = 0.046$, ε is the void fraction calculated here by either using drift flux model which is commonly used and referenced in Todreas et al. [1990] or CISE correlations.

The CISE correlation is defined as

$$\varepsilon = \frac{1}{1 + \frac{(1 - X_a)\rho_G S}{X_a \rho_L}},$$

where S is defined as:

$$S = 1 + B_1 \left(\frac{y}{1 + y B_2} - y B_2\right)^{1/2},$$

where $y = \frac{(1-\beta)}{\beta}$, and

$$\beta = \frac{U_G \varepsilon}{[U_G \varepsilon + U_L(1-\varepsilon)]},$$

$$B_1 = 1.578 \mathrm{Re}_L^{-0.19} \left(\frac{\rho_L}{\rho_G}\right)^{0.22}$$

$$B_2 = 0.0273 We_{L0} \mathrm{Re}_{L0}^{-0.51} \left(\frac{\rho_L}{\rho_G}\right)^{-0.08},$$

$$We_{L0} = \frac{G^2 D}{\sigma \rho_L},$$

where σ is the surface tension.

HEADER DESIGN

For every steam generator there is always a header section, in which it is very important part of the steam generator design, since they could acount for large pressure drop. In the PCHE case the headers are unique and in Figure D-1 represention [Hejzlar et al., 2006].

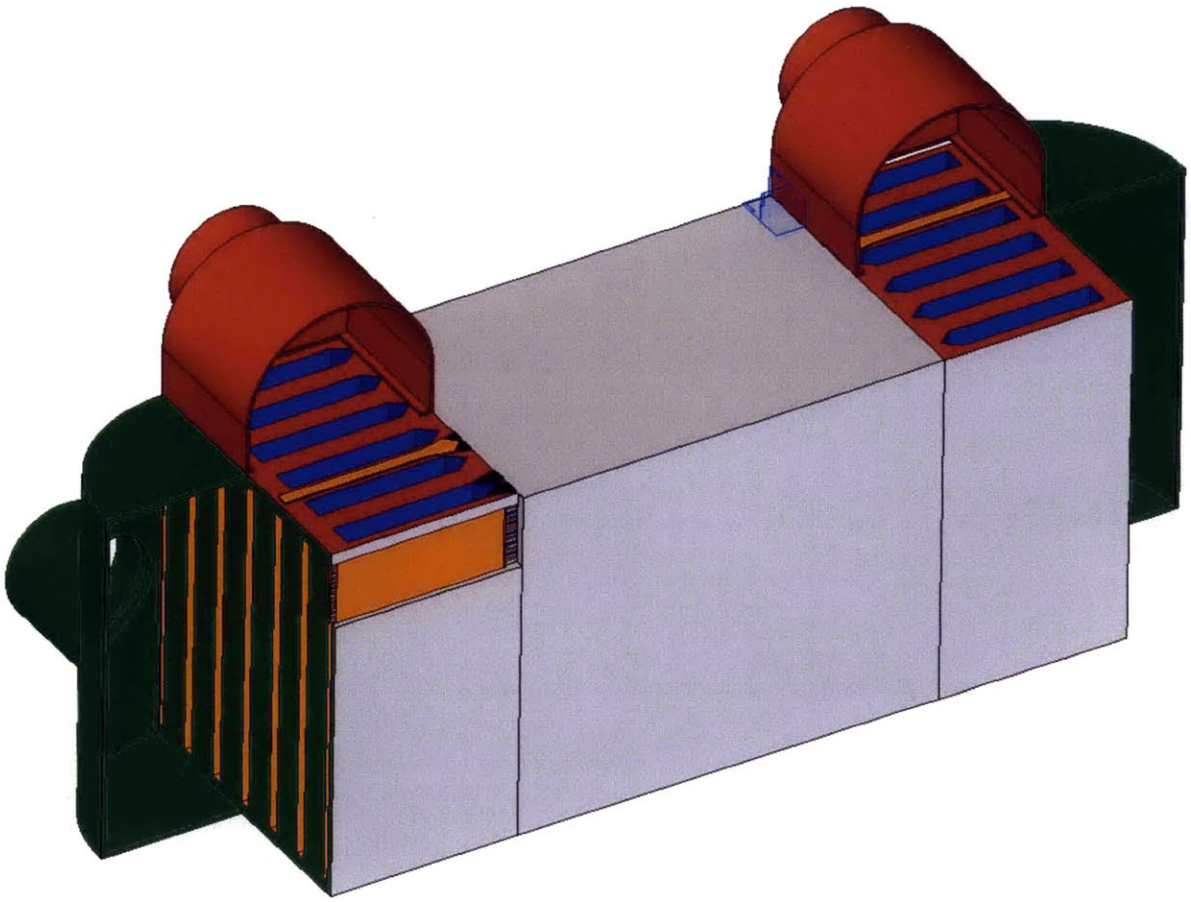

Figure D-1 The PCHE header and distributor design (from Hejzlar et al., 2006).

For the more specific IRIS design, Figure D-2 was sketched to scale:

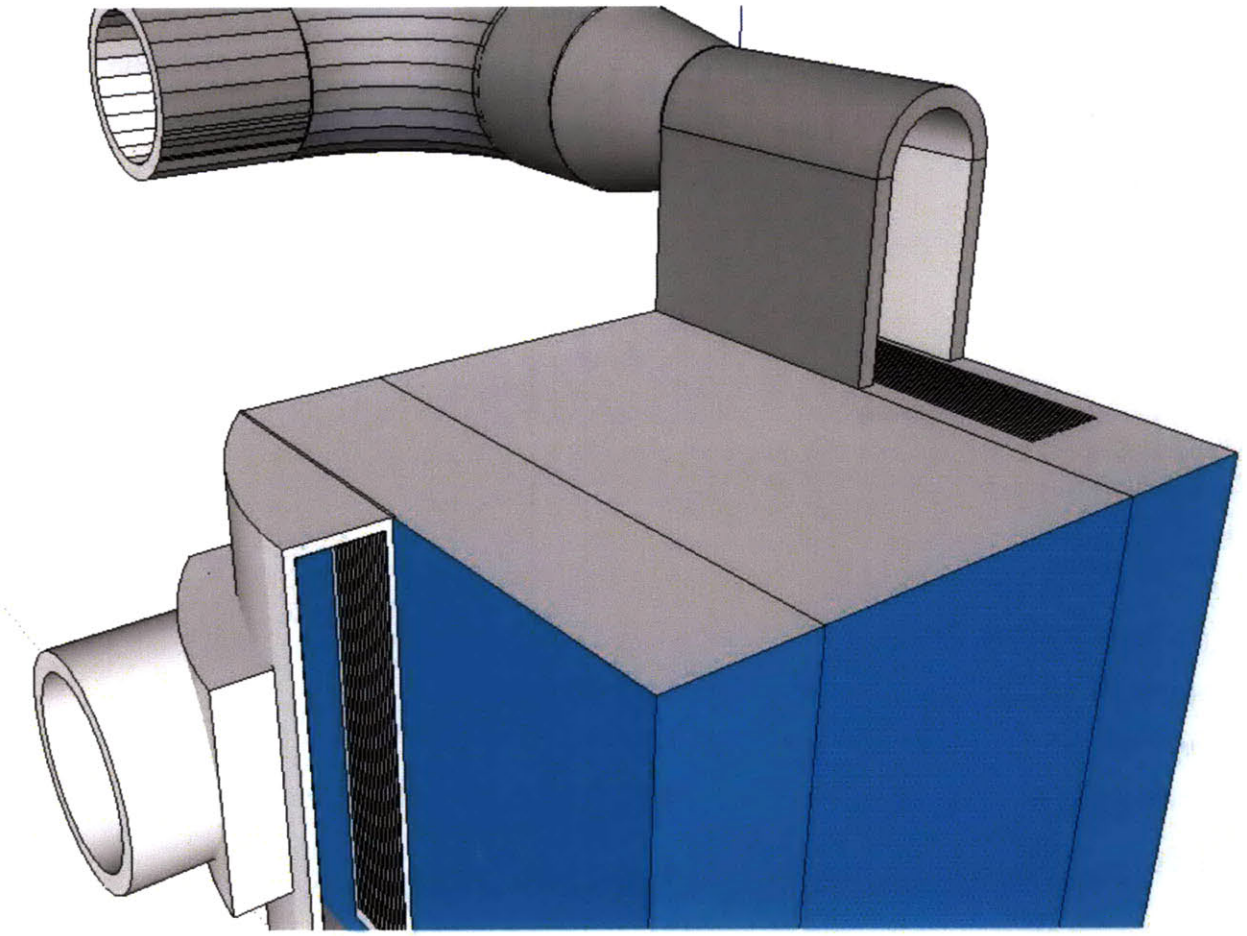

Figure D-2 The PCHE detailed sketch of headers and distributors.

While the entrance and exit loss coefficient for the PCHE are modeled in the Fortran code, they do not include any headers or distributors. It was decided to keep the headers and distributors separate from the code since for different cases, different headers can be assumed. As seen from above Figure for primary and secondary side, there are eight stages of pressure drop, four headers for inlet and outlet of each side and four distributers to evenly distribute to the flow in the PCHE flow channels. Each header and distributor has been modeled in the Tk-solver and the primary pressure drop was calculated to be 20 kPa, while the Secondary was calculated to be 120 kPa. The model is shown below:

Header Pressure Drop Calculations

Rules Sheet

Rules

;h means Header

;s means Secondary

;p means Primary

;# means which header design

;i/o means inlet and outlet respectively

$\Delta ppg = -\rho p \cdot g \cdot H$

$\Delta psg = (\rho si + \rho so) \cdot g \cdot H$

$$Ah1 = \frac{\pi \cdot hD1^2}{4}$$

$$Gph1 = \frac{mp}{Ah1 \cdot Nph1}$$

$$Reph1 = \frac{Gph1 \cdot hD1}{\mu p}$$

$Ahp2 = phw2 \cdot phh2$

$$Gph2 = \frac{mp}{Ahp2 \cdot Nph1}$$

$$hpD2 = \frac{4 \cdot Ahp2}{(phw2 + phh2) \cdot 2}$$

$$Reph2 = \frac{Gph2 \cdot hpD2}{\mu p}$$

$Ah3 = hw3 \cdot hh3$

$Aph3 = hpw3 \cdot hh3$

$$Gph3 = \frac{mp}{Aph3 \cdot hp3N}$$

$$hpD3 = \frac{4 \cdot Ah3}{2 \cdot (hw3 + hh3)}$$

$$Reph3 = \frac{Gph3 \cdot hpD3}{\mu p}$$

$$Gsh1 = \frac{ms}{Ah1}$$

$$Resh1i = \frac{Gsh1 \cdot hD1}{\mu si}$$

$$Resh1o = \frac{Gsh1 \cdot hD1}{\mu so}$$

$$Ahs2 = \frac{\pi \cdot shD2^{2}}{4}$$

$$Gsh2 = \frac{ms}{Ahs2}$$

$$Resh2i = \frac{Gsh2 \cdot shD2}{\mu si}$$

$$Resh2o = \frac{Gsh2 \cdot shD2}{\mu so}$$

$$Gsh3 = \frac{ms}{Ah3 \cdot h3N}$$

$$Resh3i = \frac{Gsh3 \cdot hpD3}{\mu si}$$

$$Resh3o = \frac{Gsh3 \cdot hpD3}{\mu so}$$

$$impnum = \frac{(Gsh3)^{2}}{\rho p}$$

$$\Delta pph2i = \frac{\left[1 - \left[\frac{Ah1}{Ahp2}\right]\right]^{2} \cdot Gph1^{2}}{2 \cdot \rho p}$$

$$\Delta pph3i = \frac{0.15 \cdot \left[1 - \left[\frac{Aph3}{Ahp2}\right]\right] \cdot Gph2^{2}}{2 \cdot \rho p}$$

$$\Delta pph2o = \frac{0.15 \cdot \left[1 - \left[\frac{Ah1}{Ahp2}\right]\right] \cdot Gph2^{2}}{2 \cdot \rho p}$$

$$\Delta pph3o = \frac{\left[1 - \left[\frac{Aph3}{Ahp2}\right]\right]^{2} \cdot Gph3^{2}}{2 \cdot \rho p}$$

$$\Delta psh2i = \frac{\left[1 - \left[\frac{Ah1}{Ahs2}\right]\right]^{2} \cdot Gsh1^{2}}{2 \cdot \rho si}$$

$$\Delta psh2o = \frac{0.15 \cdot \left[1 - \left[\frac{Ah1}{Ahs2}\right]\right] \cdot Gsh2^{2}}{2 \cdot \rho so}$$

$$\Delta psh3o = \frac{\left[1 - \left[\frac{Ah3}{Ahs2}\right]\right]^{2} \cdot Gsh2^{2}}{2 \cdot \rho si}$$

Rules

$$\Delta psh3i = \frac{0.15 \cdot \left[1 - \left[\frac{Ah3}{Ahs2}\right]\right] \cdot Gsh3^{2}}{2 \cdot \rho so}$$

$$\Delta pfh3p = \frac{0.184 \cdot Reph3^{-0.2} \cdot 0.5 \cdot \left[\frac{hL3}{hpD3}\right] \cdot Gph3^{2}}{\rho p}$$

$$\Delta pph2iL = \frac{\left[1 - \left[\frac{Ah1L}{Ahp2L}\right]\right]^{2} \cdot Gph1^{2}}{2 \cdot \rho p}$$

$$ratio = \frac{Ah1L}{Ahp2L}$$

$$\Delta psh2oL = \frac{0.15 \cdot (1 - (ratios)) \cdot Gsh1^{2}}{2 \cdot \rho so}$$

$$\Delta PSTotal = \Delta psh2i + \Delta psh2o + \Delta psh3i + \Delta psh3o + \Delta psg$$

$$\Delta PPTotal = \Delta pph2i + \Delta pph2o + \Delta pph3i + \Delta pph3o + \Delta ppg$$

Variables Sheet

Input	Name	Output	Unit	Comment
.004	hw3		m	Header dimensions
4.2	hh3		m	Header dimensions
12	h3N		m	Header dimensions
.15	hL3		m	Header dimensions
.0016	hpw3		m	Header dimensions
48	hp3N		m	Header dimensions
	Aph3	.00672	m2	Header Area
.085	phw2		m	Header dimensions
.085	phh2		m	Header dimensions
5	Nph1			Number of Primary pipes
.08	hD1		m	Primary Pipe Outer Diameter
589	mp		kg/s	Primary Mass Flow rate
	Δppg	-28812	Pa	Gravitational Primary Pressure drop
700	ρp		kg/m3	Primary Density
9.8	g		m/s2	Gravity
4.2	H		m	PCHE overall Height
	Δpsg	35603.4	Pa	Gravitational Secondary Pressure drop
.366	shD2		m	Header dimensions
840	ρsi		kg/m3	Inlet Secondary Density
25	ρso		kg/m3	Oulet Secondary Density
	Reph1	18748452.296225		Reynolds #
	Gph1	23435.565370	kg/m2s	Mass Flux
.0001	μp		kg/sm	Primary Fluid Viscosity

Input	Name	Output	Unit	Comment
.00012	μsi		kg/sm	Secondary Inlet Fluid Viscosity
.00002	μso		kg/sm	Secondary Outlet Fluid Viscosity
	Ah1	0.005027	m2	Header Area
	Reph2	13858823.529412		Reynolds #
	Gph2	16304.498270	kg/m2s	Mass Flux
	Ahp2	.007225		Header Area
	hpD2	.085	m	Header dimensions
	Reph3	145942.356486		Reynolds #
	Gph3	1826.016865	kg/m2s	Mass Flux
	hpD3	0.007992	m	Header dimensions
	Ah3	.0168	m2	Header Area
	Resh1i	8289319.952703		Reynolds #
	Gsh1	12433.979929	kg/m2s	Mass Flux
	Resh1o	49735919.716217		Reynolds #
62.5	ms		kg/s	Secondary Mass Flow Rate
	Resh2i	1811873.213706		Reynolds #
	Gsh2	594.056791	kg/m2s	Mass Flux
	Resh2o	10871239.282233		Reynolds #
	Ahs2	0.105209	m2	Header Area
	Gsh3	310.019841	kg/m2s	Mass Flux
	Resh3i	20648.324347		Reynolds #
	Resh3o	123889.946083		Reynolds #
	impnum	137.303289	Pa	Head
	Δpsh2i	83442.726135	Pa	Pressure Drop
	Δpsh2o	1008.128532	Pa	Pressure Drop
	Δpsh3i	242.294558	Pa	Pressure Drop
	Δpsh3o	148.331538	Pa	Pressure Drop
	Δpfh3p	762.566591	Pa	Pressure Drop
	Δpph2i	36322.941422	Pa	Pressure Drop
	Δpph3i	1990.818318	Pa	Pressure Drop
	Δpph2o	8666.768363	Pa	Pressure Drop
	Δpph3o	11.635595	Pa	Pressure Drop
	Δpph2iL	150.828177	Pa	Pressure Drop
.05	Ah1L		m2	Header Area
.051	Ahp2L		m2	Header Area
	ratio	0.980392		For sensitivity
.9	ratios			For sensitivity
	Δpsh2oL	46381.157063	Pa	Pressure Drop
	ΔPSTotal	120444.880762	Pa	Total Header Pressure Drop Secondary
	ΔPPTotal	18180.163697	Pa	Total Header Pressure Drop Primary

IRIS PCHE SAMPLE INPUT

zig ! Precooler for SNL Loop - zig-zag channel-540kW

1h1c

125000.0 ! power (kW)

15500.0 ! pressure - hot fluid - hot end (kPa)

5810.0 ! pressure - cold fluid - cold end (kPa)

328.4 ! temperature - hot fluid - hot end (oC)

223.9 ! temperature - cold fluid - cold end (oC)

589.0 ! mass flow rate on hot side (kg/s)

62.5 ! mass flow rate on cold side (kg/s)

0.002 !hot channel diameter (m)

0.002 !cold channel diameter (m)

0.0016 !hot plate thickness (m)

0.0016 !cold plate thickness (m)

3.1 !hot pitch divider

3.1 !cold pitch divider (Pitch=channel diameter + (channel diameter)/(pitch divider)

4.200 !HX height (m) - this is total for 4 submodules (actual module H=height/4=5.5)

.600 !HX width (m) - this is maximum size of photo etching (2x0.6 submodules separated by chamber)

1.0 ! # of modules - how many modules stacked, hence total H=H/4* # of mudules

21.0 !thermal conductivity of the plate (W/mK)

60.0 ! # of HX longitudal cells

18.0026 !wmh - molar mass

18.0026 !wmc - molar mass

water.fld !hot fluid id (0 co2 else helium)

Water.fld !cold fluid water

1.0d-5 !pressure iteration precision

40

IRIS PCHE SAMPLE OUTPUT

OPERATING CONDITIONS

125000.00 power (kW)

15500.00 pressure - hot fluid - hot end (kPa)

5810.00 pressure - cold fluid - cold end (kPa)

60966.8376 hot side pressure drop (Pa)

-38619.7063 cold side pressure drop (Pa)

589.0000 mass flow rate on hot side (kg/s)

62.5000 mass flow rate on cold side (kg/s)

0.11 cold mass flow rate over hot mass flow rate

291.92 temperature - hot fluid cold end (oC)

224.01 temperature - cold fluid cold end (oC)

328.40 temperature - hot fluid hot end (oC)

319.93 temperature - cold fluid hot end (oC)

1507.62 enthalpy - hot fluid - hot end (kJ/kg)

1295.45 enthalpy - hot fluid - cold end (kJ/kg)

2963.17 enthalpy - cold fluid - hot end (kJ/kg)

963.68 enthalpy - cold fluid - cold end (kJ/kg)

0.1625 cold side inlet velocity (m/s)

1.7210 hot side outlet velocity (m/s)

19008.48 Reynolds number - hot fluid average (-)

1721.36 Reynolds number - cold fluid average (-)

56036.13 Heat transfer coef. - hot fluid average (W/m2/K)

92209.62 Heat transfer coef. - cold fluid average (W/m2/K)

11002.16 Total heat transfer coeff. - average (W/m2/K)

HX GEOMETRY

0.82754 Total HX volume - all modules (m3)

0.82754 1 Module HX volume (m3)

4.20000 HX height (m)

0.60000 HX width (m)

0.32839 HX length (m)

0.27696 HX length (m)

2.00 Channel diameter on hot side (mm)

2.00 Channel diameter on cold side (mm)

2.65 Channel pitch on hot side (mm)

2.65 Channel pitch on cold side (mm)

293888. Number of channels on hot side per 1 module

293888. Number of channels on cold sideper 1 module

1.60 Plate thickness on hot side (mm)

1.60 Plate thickness on cold side (mm)

1312.00 Number of hot plates

1312.00 Number of cold plates

1.00 Number of HX modules

OTHERS

25.00 HX material conductivity (W/mK)

1.56 Conduction length (mm)

60 Number of nodes

0.10D-04 Pressure iteration precision

Appendix E VIPRE

19 X 19 ANALYSIS

There is still high degree of uncertainty in how large is the pumps for IRIS reactor and whether they will fit in the reactor vessel or not. Another way of increasing the power density of the core without having to change pumps is through having smaller diameter tubes and packing more fuel rods in the core. The low mass flux of IRIS makes the 19 x 19 design more attractive to pass stability tests such as vortex and fluid elastic stability compared to the use of such design in a typical 3411 MWth PWR cores. The input file for 19 x 19 PWR already exists, however, the modifications need to be done in order to obtain IRIS MDNBR. The following diagrams describe the peaking factors and the IRIS specific modeling scheme [Dandong et at. 2007].

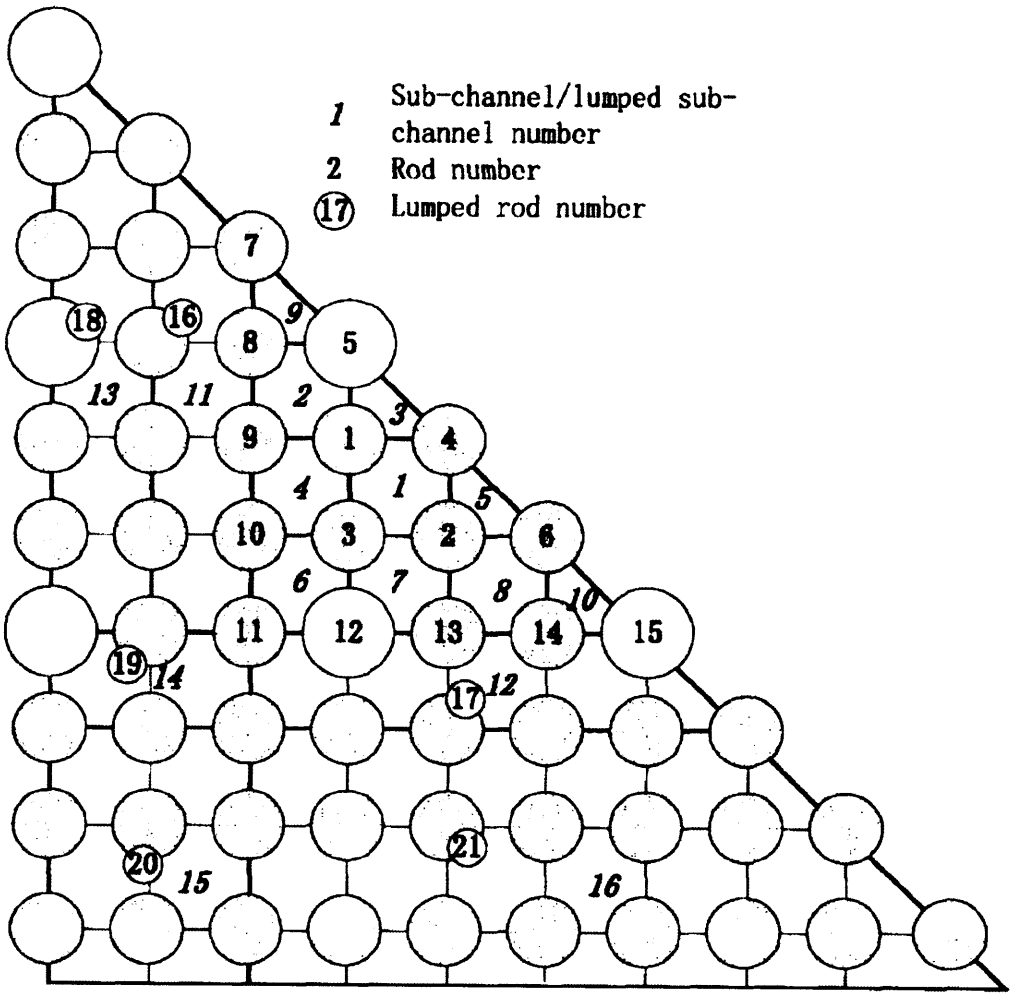
1 Sub-channel/lumped sub-channel number
2 Rod number
17 Lumped rod number

(a)

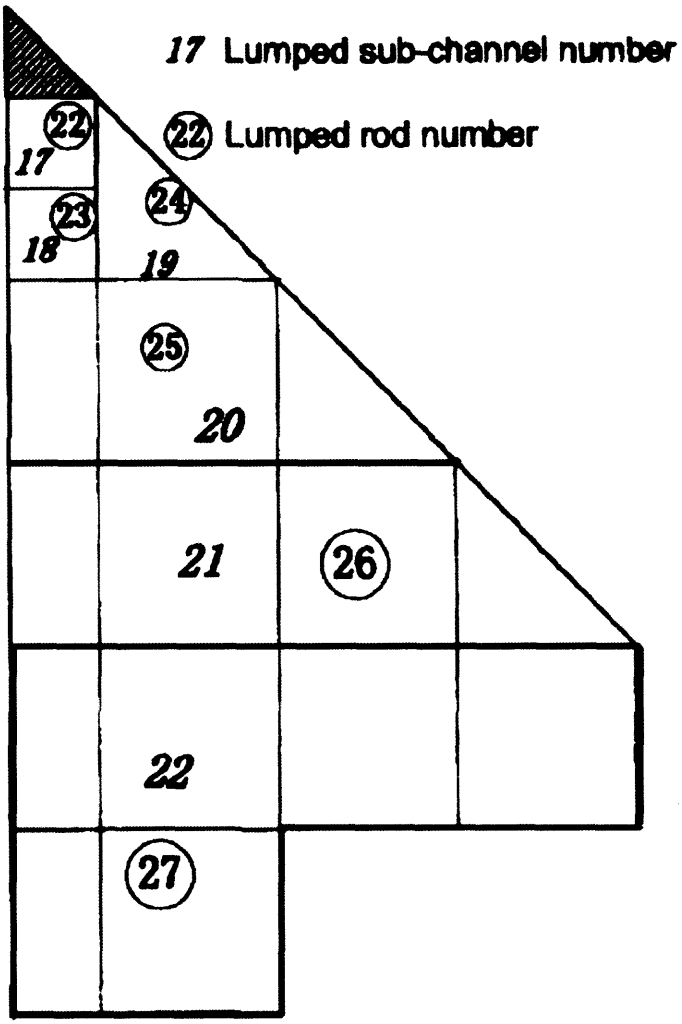

(b)

Figure E-1 The VIPRE 19 x 19 modeling scheme of the hot assembly and 1/8th core (from Dandong, 2007)

The same overpower conditions, as described in Chapter 5, were used with the 19 x 19 array. The MDNBR results were less than 1, which is not acceptable. The problem arises due to the fact that since the same P to D ratio was used, the small mass flux will dominate more than the reduced heat flux due to having more heat transfer area.

Also, 12x12 and 14x14 IXAF array sizes were used to see if the MDNBR will be improved under nominal IRIS conditions. The Figure E-2 shows that while there are

improvements, under the overpower condition, the MDNBR of the inner channel is still most limiting and is a weak function of the array size.

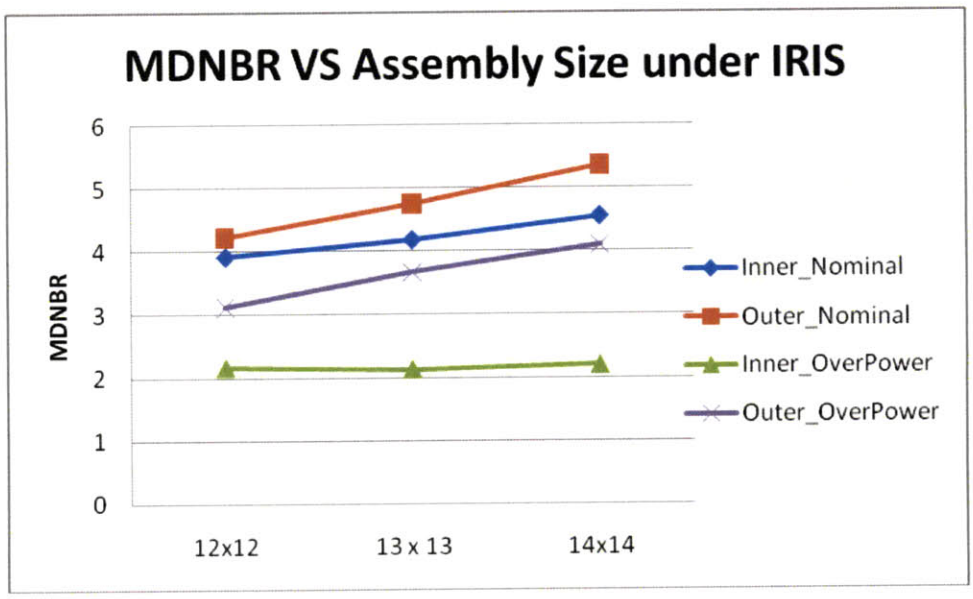

Figure E-2 The MDNBR vs. IXAF array size under IRIS overpower conditions.

SHORTENING THE CORE

As previously mentioned, the current IRIS specification has lower power density than AP1000. Therefore, one way to take advantage of this margin is by shortening the core, while keeping the same nominal mass flow rate, power, and inlet flow temperature. While, the LOFA is the limiting case for MDNBR, the MDNBR under the overpower conditions while shortening the fuel rods is calculated. Since, IRIS uses "spool-type" pumps, the pump impeller acts as a flywheel and its size can be increased to increase its inertia and lessen the LOFA MDNBR consequences. MDNBR of 1.45 is taken as a limit, which is about the same as a typical PWR under over power conditions. Under IRIS conditions, the fuel height can be decreased from 168 inches to 96 inches, which increases the power density of the core by 75%. This 96 inch core will require additional 72 kg-m^2 of impeller inertia to achieve a MDNBR of 1.5, which translates

to 0.5 m increase in the pumps' impeller. If the rotational inertia of the pumps is not increased, then the core can be only shortened by one foot.

VIPRE INPUT FILES:

```
* 17 x 17 Westinghouse XL Fuel for 1000 MWth IRIS reactor
*
*Vipre Input of PWR
*Summer 2007
1,0,0
1/8 PWR channel
*geom.1: Nchal, Ncard, NDX, NAzone, NcTyp, MBWR  page 35
geom,21,21,48,0
*geom.2: length, Vert, s/l  page 36
168., 0., 2.
*geom.4: #, FA, WP, HP, G#, C#, GW, Discentroid   page 45
1,.0590,.6300,.4406,2,2,.068,.496,7,.122,.744
2,.1180,1.260,0.8812,3,3,.068,.496,4,.122,.496,7,.122,.744
3,.0590,.6300,.4406,1,5,.122,.496
4,.1362,1.175,1.175,3,5,.122,.496,7,.122,.744,8,.122,.496
5,.1362,1.175,1.175,2,6,.122,.496,9,.122,.496
6,.0590,.6300,.4406,1,10,.068,.496
7,1.2983,12.0465,10.7215,2,8,.122,.744,12,.19,1.984
8,.1180,1.260,.8812,2,9,.068,.496,12,.068,.744
9,.1180,1.260,.8812,2,10,.122,.496,13,.068,.744
10,.1180,1.260,.8812,2,11,.068,.496,13,.122,.744
11,.0590,.6300,.4406,1,13,.122,.744
12,1.103,8.9818,8.2247,2,13,.268,1.736,14,.366,2.976
13,1.4731,12.5688,12.1902,1,14,0.61,2.976
14,9.527,87.01,77.55,2,15,1.054,3.968,16,1.054,4.464
```

15,9.527,87.01,77.55,2,16,1.054,6.448,17,1.054,6.448

16,19.05,174.,155.1,1,18,2.108,8.432

17,19.05,174.,155.1,2,18,2.108,6.432,20,1.054,8.432

18,38.11,348.,310.2,2,19,2.108,8.432,20,2.108,8.432

19,19.05,174.,155.1,1,20,2.108,8.432

20,114.32,1044.,930.6,1,21,7.378,12.648

21,190.54,1740.,1551.

* flag, Nprop, Isteam, Nfprop, ipvar (no superheat) page 84

prop,0,0,2,0

*----------

*

* Rods page 91

*rods.1: axialprofile,#,Cond,geom,#,gapcond,from,cpr,forcefunc

*Inglag,Naxp,Nrod,NC,Nfuelt,Nmat,lgpff,Ngpff,nopt,ipwv,icpr,irff

rods,1,23,1,2,0,0,0,0,

*rods.2: zzh,zstrt,ndals,nodalt page 97

0.0,0.0,0

*rods.3: Naxn page 98

-1 *symmetric ocsine

*rods.5: PSTAR page 99

1.55 *peaktoaverage ratio

*rods.9: I,IDfuel, radial, iap,lrdum,phidum page 108

1,2,1.605,1, 1,.125,7,.375

2,2,1.641,1, 1,.25,2,.25,7,.5

3,2,1.607,1, 2,.25,4,.25,7,.5

4,2,1.650,1, 2,.25,3,.25,4,.25,5,.25

5,2,1.631,1, 3,.125,5,.25,6,.125

6,2,1.603,1, 4,.25,7,.5,8,.25

7,2,1.648,1, 4,.25,5,.25,8,.25,9,.25

8,2,1.650,1, 5,.25,6,.25,9,.25,10,.25

9,1,1.617,1, 7,7.

10,2,1.620,1, 7,.25,8,.25,12,.5

11,2,1.624,1, 9,.25,10,.25,13,.5

12,2,1.601,1, 10,.25,11,.25,13,.5

13,2,1.541,1, 11,.125,13,.375

14,1,1.557,1, 12,6.5

15,1,1.510,1, 13,9.0

16,1,1.578,1, 14,66.0

17,1,1.578,1, 15,66.0

18,1,1.578,1, 16,132.0

19,1,1.382,1, 17,132.0

20,1,1.261,1, 18,264.0

21,1,1.226,1, 19,132.0

22,1,.94093,1, 20,792.0

23,1,.94268,1, 21,1320.0

0

*rod.62: I,Ftype,Drod,Dfuel,Nfuel,Dcore, Tclad (rod dimensions) page 148

2,nucl,.374,.3715,6,0.,0.022

*rod.63: IRAdp,imatf,imatc,igpc,igforc,hgap,ftdens,fclad page 148

0,0,0,0,0,2000.,.94,0.

*rods.68 for dummy rod page 155

1,dumy,.374

*----------

*

*Operation page 178

*oper.1: flag,IH,IG,ISP,NPOWR,NDND,IRUN,IFCVR,LUF,IHBAL (inlet G)

oper,1,1,0,0,0,1,0

*oper.2: DPS,DNBRL,FCOOL,DNBRC,IHROD PAGE 180

0.0,0.0,2.6,0.0

*oper.5: PREF HIN GIN PWRINP HOUT page 181

2250.0,557.7,1241.2,3.584

*OPER.12: FORCING FUNCTION PAGE 189

0

*---

*

*cORRELATIONS PAGE 208

*corr.1 FLAG,NCOR,NHTC,IXCHF

corr,1,1

*corr.2 NSCVD,NBLVDD,NFRML,NHTWL PAGE 209

levy,homo,homo,none,

*corr.6 NFCON,NSUBC,NSATB,NCHFC,NTRNB,NFLMB page 216

ditb,thsp,thsp,w-3l,

*Corr.9: nchf page 222

w-3l

*corr.11: TDCL,SPK,FLGRD (GRID STUFF) page 223

.042,.066,1.000

*---

*

*MIX GROUP CONTROL DATA PAGE 232

*MIXX.1: FLAG,NSCBC,NBBC,MXK (MIXIN CORRELATION)

mixx,0,0,1

*mixx.2: FTM,ADETA,BBETA PAGE 233

0.0,0.038

*MIX.3: ADETA,BBETA (MIXING COEFF) PAGE 233

0.0380,0.0, 0.0250,0.0, 0.0380,0.0, 0.0380,0.0,

0.0250,0.0, 0.0380,0.0, 0.0250,0.0, 0.0380,0.0,

0.0380,0.0, 0.0380,0.0, 0.0380,0.0, 0.0380,0.0,

0.0250,0.0, 0.0095,0.0, 0.0380,0.0, 0.0250,0.0,

0.0380,0.0, 0.0250,0.0, 0.0380,0.0, 0.0250,0.0,

0.0250,0.0, 0.0042,0.0, 0.0063,0.0, 0.0063,0.0,

0.0048,0.0, 0.0042,0.0, 0.0029,0.0, 0.0029,0.0,

0.0022,0.0, 0.0029,0.0, 0.0015,0.0, 0.0029,0.0,

0.0015,0.0, 0.0015,0.0, 0.0009,0.0

*---

*

*DRAG DATA PAGE 241

*DRAG.1: FLAG,NCHTP,NGPTP,KIJOPT

drag,1,1,4

*drag.2: atf,btf,ctf,alf,blf,clf page 242

0.184,-0.2,0., 64.,-1.,0.

*drag.7: ddok ppitch page 243

0.374,0.496

*dfrag.8: atg,btg,ctg,alg,blg,clg page 244

3.15,-0.2,0., 3.15,-0.2,0.

*---

*

*Grids dat page 252

*grid.1: flag,kopt,nkcor

grid,0,1

*grid.2: cdk

0.8

*grid.4: nci,nlev (local loss coef) page 253

-1,7

*grid.6: axj,kor page 254

15.0,1,38.0,1,61.0,1,84.0,1,?

107.0,1,130.0,1,153.0,1,

```
0
*-------------------------------------------------------------
*
*steady state computaional method page 278
cont
*cont.2: ttdum,ndtdum,ntrydm,itry,itrym,idrect,itstep,itmod
0.,0,20,0,0,1
*cont.3: werrx,werry,ferror,terror,htcerr,dampng,accely,accelf
0.,0.,0.01,0.,0.,0.8
*cont.6-11   page 282-285
0,5,6,3,5,0,1,1,0,0,0,1
1000.0,0.,0.,0.,0.,0., *max time
2,3,4,5,6            *printed channels
3,4,6,7,10,11        *printed gaps
4,5,8               *printed rods
2,3,4,5,6            *printed chf info
*-------------------------------------------------------------
*
endd
0
*                                                              *
* 1/8 core, 13x13 annular pins, using PWR power distribution   *
* IRIS REACTOR CONDITIONS                                      *
****************************************************************
1,0,0                                    *vipre.1
1/8 core, 13x13 PQN02 annular pins,PWR power distribution      *vipre.2
geom,49,49,20,0,0,0  *normal geometry input                    *geom.1
144.0,0.0,0.5                            *geom.2
1,0.0675,0.9503,0.7127,1,2,0.045,0.542,
```

2,0.1350,1.9007,1.9007,2,3,0.045,0.542,4,0.045,0.650,

3,0.0675,0.9503,0.9503,1,5,0.045,0.542,

4,0.1350,1.9007,1.9007,2,5,0.045,0.650,7,0.045,0.650,

5,0.1350,1.9007,1.9007,2,6,0.045,0.542,8,0.045,0.650,

6,0.0675,0.9503,0.9503,1,9,0.045,0.542,

7,0.1350,1.9007,1.9007,2,8,0.045,0.650,11,0.045,0.650,

8,0.1350,1.9007,1.4255,2,9,0.045,0.650,12,0.045,0.650,

9,0.1350,1.9007,1.4255,2,10,0.045,0.542,13,0.045,0.650,

10,0.0675,0.9503,0.9503,1,14,0.045,0.542,

11,0.1350,1.9007,1.9007,2,12,0.045,0.650,16,0.045,0.650,

12,0.1350,1.9007,1.4255,2,13,0.045,0.650,16,0.045,0.650,

13,0.1350,1.9007,1.4255,2,14,0.045,0.650,16,0.045,0.650,

14,0.1350,1.9007,1.9007,2,15,0.045,0.542,17,0.045,0.650,

15,0.0675,0.9503,0.9503,1,17,0.045,0.542,

16,0.4051,5.7020,5.7020,2,17,0.045,1.842,18,0.135,0.657,

17,0.3376,4.7517,4.7517,1,18,0.135,0.657,

18,0.9440,12.35430268,12.3543,1,19,0.300,2.282,

19,5.294,74.126,69.849,2,20,0.300,4.232,21,0.270,4.938,

20,5.766,80.303,76.026,2,21,0.300,4.938,22,0.300,6.348,

21,11.514,160.368,151.815,1,23,0.600,7.054,

22,11.533,160.606,152.053,2,23,0.600,6.348,25,0.300,7.054,

23,23.066,321.212,304.106,2,24,0.600,7.054,25,0.600,7.054,

24,11.533,160.606,152.053,1,25,0.600,6.500,

25,69.195,963.635,912.317,1,26,2.098,10.581,

26,115.33,1606.06,1520.53,

27,0.0454,0.5339,0.5339,

28,0.0454,0.5339,0.5339,

29,0.0454,0.5339,0.5339,

30,0.0907,1.0678,1.0678,

```
31,0.0454,0.5339,0.5339,
32,0.0454,0.5339,0.5339,
33,0.0907,1.0678,1.0678,
34,0.0907,1.0678,1.0678,
35,0.0454,0.5339,0.5339,
36,0.0454,0.5339,0.5339,
37,0.0907,1.0678,1.0678,
38,0.0907,1.0678,1.0678,
39,0.0454,0.5339,0.5339,
40,0.4536,5.3388,5.3388,
41,0.5444,6.4066,6.4066,
42,3.629,42.711,42.711,
43,3.629,42.711,42.711,
44,7.258,85.422,85.422,
45,7.258,85.422,85.422,
46,14.517,170.843,170.843,
47,7.258,85.422,85.422,
48,43.553,512.527,512.527,
49,72.584,854.216,854.216                    *geom.4
prop,0,0,2,1   *internal EPRI functions                    *prop.1
rods,1,46,1,1,4,0,0,0,0,0,0  *three material types,one type of geo. *rods.1
0.0,0.0,0,0                                  *rods.2
-1                                           *rods.3
1.55  *chopped cosine, with peak to average=1.55           *rods.5
******rods geomatry input                              *rods.9
1,1,1.657,1,1,0.25,2,0.25,
-1,1,1.657,1,27,0.5,
2,1,1.582,1,1,0.125,2,0.25,3,0.125,
-2,1,1.582,1,28,0.5,
```

3,1,1.544,1,2,0.25,4,0.25,

-3,1,1.544,1,29,0.5,

4,1,1.557,1,2,0.25,3,0.25,4,0.25,5,0.25,

-4,1,1.557,1,30,1,

5,1,1.576,1,3,0.125,5,0.25,6,0.125,

-5,1,1.576,1,31,0.5,

6,1,1.544,1,4,0.25,7,0.25,

-6,1,1.544,1,32,0.5,

7,1,1.587,1,4,0.25,5,0.25,7,0.25,8,0.25,

-7,1,1.587,1,33,1,

8,1,1.685,1,5,0.25,6,0.25,8,0.25,9,0.25,

-8,1,1.685,1,34,1,

9,1,1.655,1,6,0.125,9,0.25,10,0.125,

-9,1,1.655,1,35,0.5,

10,1,1.557,1,7,0.25,11,0.25,

-10,1,1.557,1,36,0.5,

11,1,1.66,1,7,0.25,8,0.25,11,0.25,12,0.25,

-11,1,1.66,1,37,1,

12,1,1.668,1,9,0.25,10,0.25,13,0.25,14,0.25,

-12,1,1.668,1,38,1,

13,1,1.554,1,10,0.125,14,0.25,15,0.125,

-13,1,1.554,1,39,0.5,

14,1,1.586,1,11,0.5,12,0.5,13,0.25,16,2.5,18,1.25,

-14,1,1.586,1,40,5,

15,1,1.554,1,13,0.25,14,0.5,15,0.375,16,0.5,17,2.5,?

18,1.875

-15,1,1.554,1,41,6,

16,1,1.587,1,18,3.25,19,36.75,

-16,1,1.587,1,42,40,

17,1,1.587,1,20,40,

-17,1,1.587,1,43,40,

18,1,1.587,1,18,0.125,21,79.875,

-18,1,1.587,1,44,80,

19,1,1.382,1,22,80,

-19,1,1.382,1,45,80,

20,1,1.261,1,23,160,

-20,1,1.261,1,46,160,

21,1,1.226,1,24,80,

-21,1,1.226,1,47,80,

22,1,0.941,1,25,480,

-22,1,0.941,1,48,480,

23,1,0.942,1,26,800,

-23,1,0.942,1,49,800, *rods.9

0 *rods.9

1,tube,0.605,0.339882,5 *rods.68

2,1,0.0224921,0.0,? *inner cladding *rods.69

2,2,0.0024488,0.0,? *inner gap *rods.69

8,3,0.0826772,1.0,? *fuel ring *rods.69

2,4,0.0024409,0.0 *outer gap *rods.69

2,1,0.0225000,0.0 *outer cladding *rods.69

*2,tube,0.605,0.339882,1 *rods.68

*3,1,0.132559,1.0, *rods.69

1,17,409.0,clad *rods.70

0.0,0.0671,7.3304509,?

25,0.0671,7.3304509

50,0.0671,7.33045093,?

65,0.0671,7.33045093

80.33,0.0671,7.33045093,?

260.33,0.07212,8.11585329

692.33,0.07904,9.80167423,?

1502.33,0.08955,13.2923001

1507.73,0.11988,13.3211893,?

1543.73,0.14089,13.5166505

1579.73,0.14686,13.717249,?

1615.73,0.1717,13.9231981

1651.73,0.1949,14.1347101,?

1687.73,0.18388,14.3519980

1723.73,0.1478,14.5752746,?

1759.73,0.112,14.804753

1786.73,0.085,14.9810589

*2240.33,0.085,18.5665964

2,1,0.025,igap *rods.70

1,1.240834,0.2156263 *Cp=5195J/kg-K *gap=6000 *rods.71

3,22,650.617,FUO2 *rods.70

86,0.05677357,4.73275874,?

176,0.06078589,4.29917259

266,0.06366347,3.93877428,?

356,0.06581210,3.63454049

446,0.06747631,3.37435643,?

536,0.06880819,3.1493668

626,0.06990545,2.95294976,?

716,0.07083283,2.78005572

806,0.07163441,2.62676801,?

896,0.07234099,2.49000319

986,0.07297458,2.36730189,?

1076,0.07355124,2.25667975

1166,0.07408294,2.1565193,?

```
1256,0.07457886,2.06549023
1346,0.07504628,1.98248979,?
1436,0.07549123,1.90659753
1526,0.0759191,1.83704065,?
1616,0.07633503,1.77316713
1706,0.0767443,1.7144247,?
1796,0.07715268,1.66034425
1886,0.07756663,1.61052668,?
1976,0.07799351,1.5646323                    *rods.71
4,1,0.025,ogap                               *rods.70
1,1.240834,0.2149314   *Cp=5195J/kg-K *gap=6000        *rods.71
oper,1,1,0,1,0,1,0,0,0                       *oper.1
-1.0,1.3,0.0,0.005,                          *oper.2
0                                            *oper.3
*27,39,52,53,54,55,56,57,58,59
2250.0,557.7,1861.8,105.337,0.0              *oper.5
0          *no forcing functions             *oper.12
corr,2,2,0                                   *corr.1
epri,epri,epri,none                          *corr.2
0.2                                          *corr.3
ditb,thsp,thsp,w-3l,cond,g5.7   *correlation for boiling curve   *corr.6
w-3s,w-3l          *dnb analysis by w-3l          *corr.9
0.0          *w-3s input data                 *corr.10
0.042,0.066,0.986  *w-3l input data           *corr.11
drag,1,1,4                                   *drag,1
0.32,-0.25,0.0,64.0,-1.0,0.0                 *drag.2
0.605,0.65                                   *drag.7
7.333,-0.2,0.0,7.333,-0.2,0.0
grid,0,3                                     *grid.1
```

```
0.6,0.4,1.0,                                    *grid.2
26,9                                           *grid.4
1,2,3,4,5,6,7,8,9,10,11,12,13,14,15,16                  *grid.5
17,18,19,20,21,22,23,24,25,26                          *grid.5
0.0,2,12.007874,1,32.007874,1,52.007874,1,?
72.007874,1,92.007874,1,112.007874,1,132.007874,1
144.0,3                  *grid loc.          *grid.6
23,2
27,28,29,30,31,32,33,34,35,36,37,38,39,40,41,42,
43,44,45,46,47,48,49,
0.0,2,144.0,3
0
cont                                           *cont.1
0.0,0,150,50,3,1,   *iterative solution                 *cont.2
0.0,0.0,0.001,0.0,0.0,0.9,1.5,1.0                      *cont.3
5,0,0,0,0,0,1,1,0,0,0,1,0,0                           *cont.6
1000.,0.0,0.0,0.0,0.0,0.0,0.0                         *cont.7
endd
*
*end of data inpu
```

Appendix F Economics

The following is the printout of the TK solver model used for economic analysis.

TKSolver REPORT

Total IRIS Economics

Rules Sheet

Rules

$$BUdischarge = \frac{Bubatch \cdot (2 \cdot N)}{N + 1}$$

$$Ucostt = \frac{F \cdot Ucost \cdot (1 + x \cdot \Delta Tup)}{P}$$

$$\frac{F}{P} = \frac{xp - xw}{xf - xw}$$

$$Ccostt = \frac{F \cdot Ccost \cdot (1 + x \cdot \Delta Tuc)}{P}$$

$$Ecostt = \frac{SWU \cdot CSWU \cdot (1 + x \cdot \Delta Tue)}{P}$$

$$SWU = P \cdot Vxp + W \cdot Vxw - F \cdot Vxf$$

$$Vxw = V(xw)$$

$$Vxf = V(xf)$$

$$Vxp = V(xp)$$

$$SF = Vxp + WdP \cdot Vxw - FdP \cdot Vxf$$

$$WdP = \frac{xp - xf}{xf - xw}$$

$$FdP = \frac{xp - xw}{xf - xw}$$

$$F = \frac{xp \cdot P + xw \cdot W}{xf}$$

$$F = P + W$$

$$fcostt = fcost \cdot (1 + x \cdot \Delta Tuf)$$

$$Tcost = fcostt + Ccostt + Ecostt + Ucostt$$

$$rate = \frac{Tcost \cdot 1000 \cdot P}{Time \cdot pe}$$

$$Ifcc = Ifccu + IfccC + IfccE + Ifccf$$

$$Ifccu = \frac{\dfrac{Ucostt \cdot e^{(x \cdot \Delta Tup)} \cdot x}{8.77 \cdot p \cdot \eta \cdot L \cdot \left[1 - e^{\left[\frac{-x \cdot TC}{365.25}\right]}\right]}}{1 + x \cdot \Delta Tup}$$

Rules

$$IfccC = \frac{Ccostt \cdot e^{(x \cdot \Delta Tuc)} \cdot x}{8.77 \cdot p \cdot \eta \cdot L \cdot \left[1 - e^{\left[\frac{-x \cdot TC}{365.25}\right]}\right]} \cdot (1 + x \cdot \Delta Tuc)$$

$$IfccE = \frac{Ecostt \cdot e^{(x \cdot \Delta Tue)} \cdot x}{8.77 \cdot p \cdot \eta \cdot L \cdot \left[1 - e^{\left[\frac{-x \cdot TC}{365.25}\right]}\right]} \cdot (1 + x \cdot \Delta Tue)$$

$$Ifccf = \frac{fcost \cdot e^{(x \cdot \Delta Tuf)} \cdot x}{8.77 \cdot p \cdot \eta \cdot L \cdot \left[1 - e^{\left[\frac{-x \cdot TC}{365.25}\right]}\right]}$$

$$BUD = \frac{p \cdot L \cdot Time}{24}$$

$$pe = pth \cdot \eta$$

$$p = \frac{pth}{P}$$

$$L = Lp \cdot \left[1 - \frac{TR}{TC}\right]$$

$$BUC = \frac{BUdischarge}{N}$$

$$BUd = p \cdot Lp$$

$$TC = \frac{BUC}{BUd} + TR$$

$$REC = er \cdot (1 - L)$$

$$Cshut = \frac{Cshutd \cdot TR \cdot 1000}{pe \cdot L \cdot Time}$$

$$FuelCycleCost = Cshut + REC + Waste + Ifcc + Wstor$$

$$Wstor = \frac{e^{(x \cdot Twaste)} \cdot x}{8.77 \cdot p \cdot \eta \cdot L \cdot \left[1 - e^{\left[\frac{-x \cdot TC}{365.25}\right]}\right]} \cdot wstor$$

$$Icc = Iic + Ireact \cdot \left[\left[\frac{Kcc}{Kic}\right]^{mreact} - 1\right] + Iturb \cdot \left[\left[\frac{Kcc}{Kic}\right]^{mturb} - 1\right]$$

$$PVCFesc = Iic \cdot \left[\frac{g \cdot (1 + g)^{Tesc} \cdot Tesc}{(1 + g)^{Tesc} - 1} - 1\right]$$

Rules

$$PVCFfin1 = PVCFesc \cdot \left[\frac{d \cdot (1+d)^{Tcons} \cdot Tcons}{(1+d)^{Tcons} - 1} - 1 \right]$$

$$PVCFfin2 = PVCFfin1 \cdot \left[\frac{x \cdot (1+x)^{Tfinop} \cdot Tfinop}{(1+x)^{Tfinop} - 1} - 1 \right]$$

$$PVCFtot = lic + PVCFesc + PVCFfin1 + PVCFfin2$$

$$PVCFtotr = \frac{PVCFtot}{Kic \cdot \eta \cdot \Delta Tplife \cdot 365.25 \cdot 24}$$

$$OTHSGM = \left[\frac{\pi \cdot \left[Dco^2 - Dci^2 \right] \cdot Lc \cdot Ntube}{4} + \frac{\pi \cdot \left[\left[Dhoo^2 - Dhoi^2 \right] + \left[Dhio^2 - Dhii^2 \right] \right] \cdot Lh}{4} \right] \cdot pothsg \cdot NTothsg$$

$$PCHEM = PH \cdot PW \cdot PL \cdot ppche \cdot NTpche$$

$$TotalCost = PVCFtotr + FuelCycleCost + OMcost$$

Functions Sheet

Name	Type	Arguments	Comment
V	Rule	x;V	
Pn	Rule	P,n;Pn	

Rule Function: V

Comment

Parameter Variables

Argument Variables x

Result Variables V

Rule

$$V = (2 \cdot x - 1) \cdot \ln\left[\frac{x}{1-x} \right]$$

Rule Function: Pn

Comment

Parameter Variables

Argument Variables P,n

Result Variables Pn

Rule

$$Pn = P \cdot (1 + 0.125)^{n}$$

Variables Sheet

Input	Name	Output	Unit	Comment
38000	Bubatch		MWD/MT	Single Batch Burnup

Input	Name	Output	Unit	Comment
1	N			Number of Batches
250	fcost		$/kgU	Fabrication Cost
.1	x			Discount Rate
2	ΔTup		yrs	Uranium ore purchase time
.0495	xp			The Target enrichment
.0071	xf			The Ore enrichment
45	Ucost		$/kgU	Uranium Ore cost
12	Ccost		$/kgU	Conversion Cost
1.5	ΔTuc			Conversion Purchase Time
	Ucostt	612.439024	$/kgU	Uranium Ore cost
	Ccostt	156.512195	$/kgU	Conversion Cost
	F	550060.975610	kg	Uranium Ore needed
	Ecostt	1144.539681	$/kgU	Enrichment cost
	SWU	344783.692626	SWU	Total SWU
140	CSWU		$/SWU	Specific SWU
1.5	ΔTue		yrs	Enrichment Purchase Time
48500	P		kg	Core Loading
	Vxp	2.662469		
	W	501560.975610		
	Vxw	5.771302		
	Vxf	4.870380		
.003	xw			Tailing Enrichment
	SF	7.108942		
	WdP	10.341463		
	FdP	11.341463		
	fcostt	275	$/kgU	Fabrication Cost
1	ΔTuf			Fabrication Purchase Time
	Tcost	2188.490900	$/kgU	Total unadjusted fuel cylcle cost
	rate	7.069876	mill/kw-hre	Uadjusted Fuel Cycle cost
	Time	45494.693878	hours	Cycle length
	lfcc	9.425917	mill/kw-hre	Total Fuel Cycle Cost
	p	20.618557	kW/kg	Specific Power
	L	0.972245		Availability Factor
.33	η			Electric Efficiency
	pe	330000	kWe	Electric Power
1000000	pth		kW	Thermal Power
.98	Lp			Capacity Factor
15	TR		days	Refueling Period
	TC	1895.612245	days	Total Cycle length
	BUC	38000	MWD/MT	Cycle Burnup
	BUdischarge	38000	MWD/MT	Discharge Burnup
	BUd	20.206186	MWD/MT/day	Burnup per day

Input	Name	Output	Unit	Comment
38000	BUD		MWD/MT	Burnup
	REC	0.832643	mill/kw-hre	Recovery Cost
30	er		day	Forced Outage Time
	Cshut	0.411056	mill/kw-hre	Shutdown Cost
400000	Cshutd		$	Shutdown Cost
	FuelCycleCost	13.155969	mill/kw-hre	Cycle Total cost
2	Waste		mill/kw-hre	Waste and Decontamination Cost
5.16	TFL		yrs	Total Fuel Cycle length
38	BU		MWD/kg	Burnup
	lfccu	2.653797	mill/kw-hre	Adjustted Ore cost
	lfccC	0.673165	mill/kw-hre	Adjustted Conversion cost
	lfccE	4.922712	mill/kw-hre	Adjustted Enrichment cost
	lfccf	1.176242	mill/kw-hre	Adjustted Fabrication cost
	Wstor	0.486354	mill/kw-hre	Storage Cost
200	wstor		$/kg	Storage Cost
-5.6	Twaste		yrs	Waste time
	Icc	2000931019.37822	$	CIRIS capital cost
1960465509.68911	Iic		$	Iris capital cost
9000000	Ireact		$	Iris reactor cost
1500	Kcc		MW	CIRIS Power
1000	Kic		MW	IRIS Power
.8	mreact			
134400000	Iturb		$	Turbine Cost
.6	mturb			Turbine cost increase
	PVCFesc	78936218.130282	$	Eslcaltion cost
.02	g			Esclation interest
3	Tesc			Esclation Period
	PVCFfin1	17161010.572696	$	1st Finance period cost
.1052	d			Interest rate
3	Tcons		yrs	Finance period
	PVCFfin2	37451802.451516	$	2nd Finance period cost
30	Tfinop		yrs	Total operation time
	PVCFtot	2094014540.8436	$	Total Capital cost
	PVCFtotr	18.096905	mill/kw-hre	Total Capital cost
40	ΔTplife		yrs	Plant Lifetime
.01746	Dco		m	OTHSG Tube outer diamter
.01324	Dci		m	OTHSG Tube inner diamter
32	Lc		m	OTHSG Tube length
655	Ntube			Number helical tubes
1.64	Dhoo		m	OTHSG outer inner diameter
1.6	Dhoi		m	OTHSG outer inner diamter
.61	Dhio		m	OTHSG inner outer diameter

Input	Name	Output	Unit	Comment
.57	Dhii		m	OTHSG inner inner diamter
9	Lh		m	OTHSG Height
	OTHSGM	230005.678296	kg	OTHSG mass
8500	pothsg		kg/m3	OTHSG material density
	PCHEM	188697.6	kg	PCHE mass
4.2	PH		m	PCHE height
.6	PW		m	PCHE Width
.8	PL		m	PCHE Length
7800	ppche		kg/m3	PCHE material Density
8	NTothsg			Number of OTHSG
12	NTpche			Number of PCHE
	TotalCost	36.452873	mill/kw-hre	Final Total cost
5.2	OMcost		mill/kw-hre	O & M costs

Lists Sheet

Name	Elements	Units	Comment
PVCFesc	6		
Iic	6		
PVCFfin1	6		
PVCFfin2	6		
PVCFtot	6		
PVCFtotr	6		
Kic	6		
P	6		
xp	6		
Bubatch	6		
pe	6		
pth	6		
BUD	6		
Cshutd	6		
BU	6		
Ifcc	6		
FuelCycleCost	6		
OMcost	6		
TotalCost	6		
fcost	6		
Ifccu	6		
IfccC	6		
IfccE	6		
Ifccf	6		
Wstor	6		
REC	6		
Cshut	6		

List: PVCFesc

Comment

Format

Display Unit

Calculation Unit

Element	Value
1	77306914.128867
2	78936218.130282
3	78936218.130282
4	231920742.386601
5	233550046.388016
6	78936218.130282

List: Iic

Comment

Format

Display Unit

Calculation Unit

Element	Value
1	1.92E9
2	1960465509.68911
3	1960465509.68911
4	5.76E9
5	5800465509.68911
6	1960465509.68911

List: PVCFfin1

Comment

Format

Display Unit

Calculation Unit

Element	Value
1	16806794.170432
2	17161010.572696
3	17161010.572696
4	50420382.511296
5	50774598.913559
6	17161010.572696

List: PVCFfin2

Comment

Format

Display Unit

Calculation Unit

Element	Value
1	36678768.563653
2	37451802.451516
3	37451802.451516
4	110036305.690959
5	110809339.578822
6	37451802.451516

List: PVCFtot

Comment

Format

Display Unit

Calculation Unit

Element	Value
1	2050792476.86295
2	2094014540.8436
3	2094014540.8436
4	6152377430.58886
5	6195599494.56951
6	2094014540.8436

List: PVCFtotr

Comment

Format

Display Unit

Calculation Unit

Element	Value
1	17.723371
2	12.064603
3	12.064603
4	53.170112
5	35.695764
6	12.064603

List: Kic

Comment

Format

Display Unit

Calculation Unit

Element	Value
1	1000
2	1500
3	1500
4	1000
5	1500
6	1500

List: P

Comment

Format

Display Unit

Calculation Unit

Element	Value
1	48500
2	37668.8
3	43946.93
4	48500
5	37668.8
6	37668.8

List: xp

Comment

Format

Display Unit

Calculation Unit

Element	Value
1	.0495
2	.125
3	.1
4	.0495
5	.125
6	.0495

List: Bubatch

Comment

Format

Display Unit

Calculation Unit

Element	Value
1	38000
2	73305
3	62833
4	38000
5	73305
6	38000

List: pe

Comment

Format

Display Unit

Calculation Unit

Element	Value
1	330000
2	495000
3	495000
4	330000
5	495000
6	495000

List: pth

Comment

Format

Display Unit

Calculation Unit

Element	Value
1	1000000
2	1500000
3	1500000
4	1000000
5	1500000
6	1500000

List: BUD

Comment

Format

Display Unit

Calculation Unit

Element	Value
1	38000
2	73305
3	62833
4	38000
5	73305
6	38000

List: Cshutd

Comment

Format

Display Unit

Calculation Unit

Element	Value
1	400000
2	600000
3	600000
4	400000
5	600000
6	600000

Comment

Format

Display Unit

Calculation Unit

Element	Value
1	38
2	73.305
3	62.833
4	38
5	73.305
6	38

List: Ifcc

Comment

Format

Display Unit

Calculation Unit

Element	Value
1	9.425917
2	13.206262
3	12.153604
4	9.425917
5	13.206262
6	8.393578

List: FuelCycleCost

Comment

Format

Display Unit

Calculation Unit

Element	Value
1	13.155969
2	16.702750
3	15.692098
4	13.155969
5	16.702750
6	12.666557

List: OMcost

Comment

Format

Display Unit

Calculation Unit

Element	Value
1	5.23
2	5.23
3	3.47
4	15.6
5	10.41
6	3.47

List: TotalCost

Comment

Format

Display Unit

Calculation Unit

Element	Value
1	36.109339
2	32.237353
3	31.226701
4	81.926080
5	62.808514
6	28.201160

List: fcost

Comment

Format

Display Unit

Calculation Unit

Element	Value
1	250
2	250
3	251
4	250
5	250
6	250

List: Ifccu

Comment

Format

Display Unit

Calculation Unit

Element	Value
1	2.653797
2	3.608334
3	3.347069
4	2.653797
5	3.608334
6	2.363150

List: IfccC

Comment

Format

Display Unit

Calculation Unit

Element	Value
1	0.673165
2	0.915294
3	0.849022
4	0.673165
5	0.915294
6	0.599439

List: IfccE

Comment

Format

Display Unit

Calculation Unit

Element	Value
1	4.922712
2	8.073056
3	7.243496
4	4.922712
5	8.073056
6	4.383570

List: Ifccf

Comment

Format

Display Unit

Calculation Unit

Element	Value
1	1.176242
2	0.609577
3	0.714017
4	1.176242
5	0.609577
6	1.047418

List: Wstor

Comment

Format

Display Unit

Calculation Unit

Element	Value
1	0.486354
2	0.252049
3	0.294056
4	0.486354
5	0.252049
6	0.433088

List: REC

Comment

Format

Display Unit

Calculation Unit

Element	Value
1	0.832643
2	0.832909
3	0.832909
4	0.832643
5	0.832909
6	1.046017

List: Cshut

Comment

Format

Display Unit

Calculation Unit

Element	Value
1	0.411056
2	0.411530
3	0.411530
4	0.411056
5	0.411530
6	0.793875

REFERENCES

Bajs T., Oriani L., Ricotti M., Barroso A., "Transient Analysis of the IRIS Reactor", International Conf. Nuclear Energy for New Europe, Kranjska Gora, Slovenia, 2002.

Bayless P., "A Performance Model for a Helically Coiled Once-Through Steam Generator Tube," M.S Thesis, MIT-NSE, 1979.

Bergles A., Lienhard J., Kendall G., Griffith P., "Boiling and Evaporation in Small Diameter Channels," Heat Transfer Engineering, 24:1, 18 — 40, 2003.

Bergles A. , Rohsenow M., "The Determination of Forced Convection Surface Boiling Heat Transfer," Vol. 86C, p. 365, 1964.

Carelli M., "IRIS: A global approach to nuclear power renaissance", Nuclear News, September 2003.

Carelli M., Conway L., Oriani L., Lombardi C., Ricotti M., Brroso A., Collado J., Cinotti L., Moraes M., Kozuch J., Grgic D., Nonokata H., Boroughs R., Ingersoll D., Oriolo F., "The Design and Safety Features of the IRIS Reacotr," 11th International Conference on Nuclear Engineering, Tokyo, Japan, 2003.

Carelli M., Petrovic P., Ricotti M. , "IRIS: Reliable SMRs for a Wide Range of Energy Needs", ANS Annual meeting, 2009.

Cho Y., "Use of Electronic Descaling Technology to Control Precipitation Fouling in Compact Heat Exchangers for the Process Industries," Begell House, New York, 1997.

Cinotti L., Bruzzone M., Meda N., Corsini G., Lombardi C., Ricotti M., Conway L., "Steam Generator of the International Reactor Innovative and Secure," Proc. ICONE10, Arlington, Virginia, American Society of Mechanical Engineers, 2002.

Cioncolini A., Cammi A., Cinotti L., Castelli G., Lombardi C., Luzzi L., Ricotti M., "Thermal Hydraulic Analysis of IRIS Reactor Coiled Tube Steam Generator," Politecnico di Milano, 2003.

Cornwell K., Kew P., "Compact Evaporators in Convective Flow and Pool Boiling, "Proceedings of the International Eng. Foundation 3rd Conf., Irsee Germany, Taylor and Francis, 1999.

Dangdong F., Morra P., Sundaram R., Lee W., Saha P., Hejzlar P., Kazimi M., "Safety Analysis of High-Power Density Annular Fuel For PWRs," Nuclear Technology, Vol. 160, Oct, 2007.

Dandong F., Hejzlar P., Kazimi M., "Thermal-Hydraulic design of high-power-density Annular Fuel in PWRs," Nuclear Technology Vol. 160, Oct, 2007.

Davis C., Marshal T., Weaver K., "Modeling the GFR with RELAP5-3D", Idaho national lab, sept. 2005

Dostal V., "A Supercritical Carbon Dioxide Cycle for Next Generation Nuclear Reactors", MIT PhD Thesis, Jan 2004.

Deutch J., Forsberg C, Kadak A., Kazimi M., Moniz E., Parsons J., "Update of the MIT 2003 Future of Nuclear Power Study", MIT, 2009.

Dewson S., Grady C., HEATRIC Workshop at MIT, Cambridge, Ma, USA, October 2nd, 2003.

Edenius M., Eckberg B., Forssen B., Knott D., "CASMO-4, A Fuel Assembly Burnup Program, User's Manual," Studsvik/SOA-95/1, Studsvik of America, Inc. 1995.

"FINAL TECHNICAL PROGRESS REPORT," DOE project # 99-0027, 2003.

Gnielinski V., "Heat Tranfsfer and Pressure Drop in Helically Coiled Tubes," Proc. 8th INt. Heat Transfer Conf., Vol. 6, pp. 2847-2854, Washington D.C., 1986.

Groeneveld D. , Cheng S. , Doan T., "AECL-UO critical heat flux lookup table," Heat Transfer Eng. 7, 46—62, 1986.

Groeneveld D., Leunff L., Kirillov P., Bobkov V., Smogalev I., Vinogradov V., Huang X., Royer E., "The 1995 look-up table for critical heat flux in tubes," Nuclear Eng. Design 163, 1996.

HEATRIC™, <www.heatric.com>, accessed in December 2008

Hejzlar P., Driscoll M., Gibbs J., Gong Y., Kao S., "Supercritical CO2 Brayton Cycle for Medium Power Applications," MIT-ANP-PR-117, 2006.

Helalizadeh A., Müller-Steinhagen H., Jamialahmadi M., "Crystallisation Fouling Of Mixed Salts During Convective Heat Transfer And Sub-Cooled Flow Boiling Conditions," ECI Conf. on HE Fouling & Cleaning: Fund. & Apps, Santa Fe, New Mexico, 2003.

Henry J., "Headers, nozzles, and turnarounds", Heat Exchanger Design Handbook, Section 2.2.7-5, Begell House Inc., New York, 1987.

Hesselgreaves J., "Compact Heat Exchangers", K. LAMBERT, Ed., Elsevier Science, Oxford, United Kingdom, 2001.

Hewitt G., "Gass-liquid flow," Heat Exchanger Design Handbook, Section 2.3.2-1, Begell House Inc., New York, 1987.

Holt A. J., Azzopardi B., Biddulph M., "Two-Phase pressure drop and void fraction in channels," 5th UK national Conf. On Heat Transfer, Ichem E, London, 1997.

IAEA Final Technical Report, "Innovative small and medium sized reactors: Design Features, Safety approaches and R&D trends", May 2005.

Idelchick I., "Handbook of Hydraulic Resistance", 2nd edition, Hemisphere Publishing Corporation, 1986.

ISHIZUKA T., KATO Y., MUTO Y., NIKITIN K., TRI N., HASHIMOTO H., "Thermal Hydraulic Characteristics of Printed Circuit Heat Exchanger in a Supercritical CO2 Loop," Proc. NURETH 11, Avignon, France, 2005.

Kakac S., "Boilers, evaporators, and condensers," New York, Wiley, 1991.

Kazimi M., Hejzlar P., "High Performance Fuel Design For Next Generation PWRs: Final Report," MIT-NFC-PR-082, Center for Advanced Nuclear Energy Systems, MIT (Jan 2006).

Kitch D., Kujawski J., Farruggia D., Matos J., Farr C., "Nuclear Reactor submerged high temperature Spool Pump," Curtiss-Wright Electro-Mechanical, PA, Patent: US 6,813,328,B2, 2004.

Kujawski J., Kitch D., Conway L., "The IRIS Spool-Type Reactor Coolant Pump," 10th international Conference on Nuclear Engineering, Arlington, VA, 2002.

Lahoda E., Feinroth H., Salvatore M., Russo O., Hamilton H., "High-Power Density Annular Fuel for Pressurized Water Reactors: Manufacturing Costs and Economic Benefits", Nuclear Technology, Vol 160, Pages 112-134, October 2007.

Lombardi C., Bucholz J., Petrovic B., "Internal Shield Design in the IRIS Reactor and its Implications on Maintenance and D&D Activities," 4th International Conference on Nuclear, Croatia, 2002.

"MCNP-a General Monte Carlo N-Particle Transport Code, Version 5", Volume I, X-5 Monte Carlo Team, 2003.

Meter J. , "Experimental Investigation of a Printed Circuit Heat Exchanger using Supercritical Carbon Dioxide and Water as Heat Transfer Media", Master's Thesis, Kansas State University, 2008.

Nelik L., "Centrifugal and Rotary Pumps fundamentals with Applications", CRC Press, Florida, 1999.

Oriani L., "IRIS Preliminary Safety Assessment," WCAP-16082-NP, 2003.

"RELAP5/MOD3.3 Beta Code Manual", NUREG/CR-5535/Rev 1, INROMATION Systems Laboratoris, Inc. 2001.

Ricotti M., Cammi A., Cioncolini A., Cipollaro A., Oriolo F., Lombardi C., Conway L., Barroso A., "Preliminary Safety Analysis of the IRIS Reactor," 10th International Conference on Nuclear Engineering, Arlington, Va, 2002.

Saccheri J., Todreas N., Driscoll M., "A Tight Lattice, Epithermal Core Design for the Integral PWR", ICAPP, Pittsburg, 2004.

Santini L., Cioncolini A., Lambardi C., Ricotti M., "Two-phase pressure drops in a helically coiled steam generator," Int. Journal of Heat and Mass Transfer, Issue 51, pp. 4926–4939, 2008.

Southall D., "Diffusion Bonding in Compact Heat Exchangers", *Proceedings of ICAPP '09*, p. 9069-9074, Tokyo, Japan (2009).

Stewart C., "VIPRE-01: A Thermal-Hydraulic Code for Reactor Cores. Vol 2 User's Manual," August 1989.

Tanasea A., Cheng S., Groenevelda D., Shan J., "Diameter effect on critical heat flux," Nuclear Engineering and Design, 5189, 2008.

Taitel Y., Duckler A., "A Model for Predicting Flow Regime Transitions in Horizontal and Near Horizontal Gas-Liquid Flow", AlChe J., vol. 22, pp. 47-55, 1976.

"TK Solver 5 User's Guide", Universal Technical Systems, Inc., 2003.

"The Future of Nuclear Power", An interdisciplinary MIT Study, http://web.mit.edu/nuclearpower/, 2003.

Todreas N., Kazimi M., "Nuclear Systems I: Thermal Hydraulic Fundamentals," New York, Taylor & Francis, 1990.

Tong W., Bergles A., Jensen M., "Pressure Drop with Highly Subcooled Flow Boiling in Small-Diameter Tubes," International Symposium on Two-Phase Flow Modeling and Experimentation, Vol 15, 1997.

Triplett K., Ghiaasiaan S., Abdel-Khalik S., LeMouel A., McCord B., "Gas-liquid two-phase flow in microchannels Part II: void fraction and pressure drop", Int. J. of Multiphase Flow 25, 395-410, 1999.

Veronesi L., Raimondi A., "Canned Pump having a high Inertia Flywheel," Patent 4,886,430, 1989.

Wong Y., Groeneveld D., Cheng S., "CHF Prediction for Horizontal Tubes", Int. J. Multiphase Flow Vol. 16, No. 1, pp. 123-138, 1990.

Zhang W., Hibiki T., Mishima K., "Correlation for Flow Boiling Heat Transfer at Low Liquid Reynolds Number in Small Diameter Channels," Heat Transfer 127, 1214, 2005.

Zhao L., Guo L., Bai B., Hou Y., Zhang X., "Converctive boiling heat transfer and two-phase flow characteristics inside a small horizontal helically coiled tubing once-through steam generator," International Journal of Heat and Mass Transfer 46, 4779-4788, 2003 .

Zhiwen X., Otsuka, Y., Hejzlar P., and. Kazimi M.S, Driscoll, J., "High-Performance Annular Fuel Reactor Physics and Fuel Management"," Nuclear Technology, Vol. 160 No. 1, October 2007.

Yu W., France D., Wambsganss M., Hull J., "Two-phase pressure drop, boiling heat transfer, and critical heat flux to water in a small-diameter horizontal tube," International Journal of Multiphase Flow, Volume 28, Issue 6, Pages 927-941, June 2002.